DTIC
ELECTE
JAN 03 1995
S D
B

19941228 035

lation of the Optimal Trajectory for an Air-Breathing Medi Air-to-Air Missile

THESIS

Timothy Zadzora
Captain, USAF

AFIT/GAE/ENY/94D-23

DISTRIBUTION STATEMENT A
Approved for public release;
Distribution Unlimited

DEPARTMENT OF THE AIR FORCE
AIR UNIVERSITY
AIR FORCE INSTITUTE OF TECHNOLOGY

Wright-Patterson Air Force Base, Ohio

AFIT/GAE/ENY/94D-23

Formulation of the Optimal Trajectory for an Air-Breathing Medium Range Air-to-Air Missile

THESIS

Timothy Zadzora
Captain, USAF

AFIT/GAE/ENY/94D-23

DTIC QUALITY INSPECTED 2

Approved for public release; distribution unlimited

AFIT/GAE/ENY/94D-23

Formulation of the Optimal Trajectory for an Air-Breathing Medium Range Air-to-Air Missile

THESIS

Presented to the Faculty of the School of Engineering

of the Air Force Institute of Technology

Air University

In Partial Fulfillment of the

Requirements for the Degree of

Master of Science in Aeronautical Engineering

Accession For

NTIS GRA&I ☑

DTIC TAB ☐

Unannounced ☐

Justification

By

Distribution/

Availability Codes

Dist | Avail and/or Special

A-1

Timothy Zadzora, B.S.

Captain, USAF

December, 1994

Approved for public release; distribution unlimited

Acknowledgements

Foremost, I would like to thank my advisor, Dr. (Major) Brian L. Jones for all his guidance and assistance. His methodical approach to the thorough examination of problems and his unwavering perseverance was as educational to me as the master's program itself. I would also like to thank my committee members for their input, suggestions and accommodations.

I must also mention the gratitude I have for my family. They always seem to provide the support I need in all my pursuits. It would be difficult to imagine where I would be without them.

Finally, but most of all, thank you Cristina. AFIT will always remind me of the beginning of my life with you.

Timothy Zadzora

Table of Contents

	Page
Acknowledgements	ii
List of Figures	v
List of Tables	vii
List of Symbols	viii
Abstract	xii
I. Introduction	1-1
1.1 Background	1-1
1.2 Previous Work	1-2
1.3 Project Scope	1-3
1.4 Sequence of Presentation	1-4
II. Basic Equations for the Simulation	2-1
2.1 Atmosphere	2-1
2.2 Coordinate Systems	2-7
2.2.1 Inertial Axis	2-7
2.2.2 Velocity Axis	2-7
2.2.3 Stability Axis	2-9
2.2.4 Body Axis	2-10
2.3 Force Equations	2-11
2.4 Aerodynamic Forces	2-20
2.5 Engine	2-21
2.5.1 Rocket Boost Phase	2-21

Page

2.5.2 Air-Breathing Boost Phase 2-22

2.5.3 Coast Phase 2-24

III. Guidance and Control 3-1

3.1 Guidance 3-1

3.2 Control 3-11

3.2.1 Fuel Flow Rate Control 3-11

3.2.2 Roll Control 3-11

3.2.3 Pitch Control 3-15

IV. Analysis of Simulation 4-1

V. The Optimal Control Problem 5-1

5.1 Necessary Conditions For a Minimum 5-1

5.2 Shooting Method 5-7

5.3 Shooting Method Example Problem 5-13

5.4 Three-Dimensional Pursuit 5-23

5.5 Two-Dimensional Pursuit 5-28

VI. Conclusions and Recommendation 6-1

Bibliography BIB-1

Vita VITA-1

List of Figures

Figure		Page
2.1.	Standard Atmosphere Relation Between Temperature and Altitude	2-4
2.2.	Density and Pressure as Percent of Sea Level Value	2-6
2.3.	Inertial Axis System	2-8
2.4.	Rotation Sequence From Earth to Velocity Axis	2-8
2.5.	Rotation from Velocity to Stability Axis	2-9
2.6.	Rotation Sequence from Stability to Body Axis	2-10
2.7.	Body Fixed Axis System	2-11
2.8.	Free Body Diagram of the Missile in Flight	2-12
2.9.	Forces on Missile in Stability Axis System	2-16
2.10.	Rocket Engine Control Volume	2-22
2.11.	Features of the General RAMJET Engine	2-23
3.1.	Typical Missile-Target Intercept Scenario	3-2
3.2.	Line of Sight Geometry for the $x_{LOS} - y_{LOS}$ Plane	3-4
3.3.	Line of Sight Geometry for the $x_{LOSE1} - z_{LOS}$ Plane	3-6
3.4.	Block Diagram of Roll Control	3-12
3.5.	Roll Response to a 5 Degree Step Command	3-14
3.6.	Block Diagram of Pitch Control	3-15
3.7.	Angle of Attack Response to 1g Command	3-17
4.1.	Initial Conditions of Baseline Simulation	4-1
4.2.	x_E, y_E, z_E and V Simulation Comparisons for Flight 1	4-2
4.3.	γ, ψ, α and σ Simulation Comparisons for Flight 1	4-3
4.4.	x_E, y_E, z_E and V Simulation Comparisons for Flight 2	4-4
4.5.	γ, ψ, α and σ Simulation Comparisons for Flight 2	4-5

Figure		Page
4.6.	Density as a Function of Altitude	4-6
4.7.	Percent Error in the Density Value	4-7
4.8.	Percent Error in $\dot{\gamma}_{LOS}$	4-9
5.1.	Relationship Between $\tilde{\delta}\boldsymbol{x}_f$, $\delta\boldsymbol{x}_f$, and $\dot{\boldsymbol{x}}_f\delta t$	5-5
5.2.	Lunar Launch Example Problem	5-13
5.3.	Quadrant Problem for Lunar Launch Control	5-17
5.4.	Time Histories of States for Lunar Launch	5-22
5.5.	Control History for Lunar Launch	5-22

List of Tables

Table		Page
2.1.	Properties of the Atmosphere at the Isothermal Gradient Boundaries	2-6
4.1.	Initial Conditions and Results for Baseline Simulations	4-2
5.1.	Iteration History of $\boldsymbol{\lambda}_o$ for Shooting Method Example Problem .	5-21
5.2.	Iteration History of t_f and $\|\boldsymbol{h}\|$ for Shooting Method Example Problem	5-21
5.3.	Summary of $\boldsymbol{x}(t_f)$ for Shooting Method Example Problem	5-21

List of Symbols

Symbol	Page
g_{loft} = Loft Command	1-1
$g_{alt_{cmd}}$ = Altitude Command	1-1
R_{LOS} = Line of Sight Range	1-1
R_{LOS_o} = Initial Line of Sight Range	1-1
τ_{loft} = Loft Decay Constant	1-1
MW_{air} = Molecular Weight of Air	2-1
R_u = Universal Gas Constant	2-1
P = Total Pressure	2-1
T = Total Temperature	2-1
ρ = Density	2-1
R_{air} = Gas Constant for Air	2-1
h_G = Geometric Height Above Surface of the Earth	2-2
$\tilde{g}$ = Gravity as a Function of Altitude	2-2
h = Geopotential Altitude	2-2
R_E = Radius of the Earth	2-2
g = Acceleration Due to Gravity at Earth's Surface	2-3
T_b = Reference Temperature	2-5
h_b = Reference Geopotential Altitude	2-5
ρ_b = Reference Density	2-5
a = Speed of sound	2-7
Q_o = Dynamic Pressure	2-7
γ_{air} = Specific Heat Ratio of Air	2-7
x_E = Down Range Distance	2-7
y_E = Cross Range Distance	2-7
z_E = Altitude	2-7

Symbol	Page
ψ = Heading Angle	2-7
x_{E1} = Intermediate x During Earth to Body Rotation	2-7
y_{E1} = Intermediate y During Earth to Body Rotation	2-7
z_{E1} = Intermediate z During Earth to Body Rotation	2-7
γ = Flight Path Angle	2-8
$x_V = x$, Velocity Axis	2-8
$y_V = y$, Velocity Axis	2-8
$z_V = z$, Velocity Axis	2-8
V = Velocity	2-9
$\mathbf{T_{EV}}$ = Rotation Matrix, Earth to Velocity	2-9
σ = Roll angle	2-9
$x_S = x$, Stability Axis	2-9
$y_S = y$, Stability Axis	2-9
$z_S = z$, Stability Axis	2-9
$\mathbf{T_{VS}}$ = Rotation Matrix, Velocity to Stability	2-10
β = Side slip Angle	2-10
α = Angle of Attack	2-10
$x_B = x$, Body Axis	2-11
$y_B = y$, Body Axis	2-11
$z_B = z$, Body Axis	2-11
$\mathbf{T_{SB}}$ = Rotation Matrix, Stability to Body	2-11
W = Missile Weight	2-13
F_a = Axial Force	2-13
F_n = Normal Force	2-13
F_y = Lateral Force	2-13
F_T = Thrust	2-13
D = Drag Force	2-15

Symbol	Page
S = Side Force	2-15
L = Lift Force	2-15
m = Mass of Missile	2-17
C_a = Coefficient of Axial Force	2-20
M = Mach Number	2-20
ΔC_a = Coefficient of Axial Force Correction Factor	2-20
A_{ref} = Aerodynamic Reference Area	2-20
C_n = Coefficient of Normal Force	2-21
T_{sl} = Thrust at Sea Level	2-21
A_{exit} = Exit Area of the Nozzle	2-22
p_{sl} = Pressure at Sea Level	2-22
$\dot{w}_f$ = Fuel flow Rate	2-22
$I_{sp_{sl}}$ = Specific Impulse at Sea Level	2-22
V_o = Velocity of Free-stream Air	2-22
$\dot{w}_a$ = Air Flow Rate	2-22
A_o = Capture Area	2-22
V_{exit} = Velocity of Gases Exiting the Nozzle	2-23
p_{exit} = Pressure of Gases Exiting the Nozzle	2-23
A_{exit} = Exit Area of the Nozzle	2-23
D_i = Induced Drag Due to Inlet	2-24
C_{d_i} = Coefficient of Induced Drag	2-24
$\boldsymbol{\omega}_{LOS}$ = Angular Rate of the Line of Sight Vector	3-1
N = Proportional Navigation Ratio	3-1
$\mathbf{a_m}$ = Acceleration Vector	3-1
x_{LOS} = Line of Sight Distance Along x_V	3-3
y_{LOS} = Line of Sight Distance Along y_V	3-3
z_{LOS} = Line of Sight Distance Along z_V	3-3

Symbol	Page
$V_{x_{LOS}}$ = Relative Velocity Along x_V	3-3
$V_{y_{LOS}}$ = Relative Velocity Along y_V	3-3
$V_{z_{LOS}}$ = Relative Velocity Along z_V	3-3
V_{close} = Closing Velocity	3-3
t_{go} = Time to Go	3-3
$\dot{\psi}_{LOS}$ = Cross Range Angular Velocity of the LOS	3-3
$\dot{\gamma}_{LOS}$ = Angle Along LOS from the Horizontal	3-3
g_{mach_x} =Mach Command	3-8
M_{cmd} = Desired Mach Number	3-9
M = Actual Mach Number	3-9
ΔM = Delta Mach Number	3-9
$\dot{\sigma}$ = Roll Rate	3-12
σ_{cmd} = Roll Command	3-12
C_σ = Feedforward Gain in the Roll Control	3-12
F_σ = Feedback Gain in the Roll Control	3-12
J = Performance Index	5-1
$\boldsymbol{\lambda}(t)$ = Lagrange Multipliers	5-2
J' = Augmented Performance Index	5-2
$\boldsymbol{\Phi}$ = State Transition Matrix	5-9

AFIT/GAE/ENY/94D-23

Abstract

The Air Breathing Medium Range Air-to-Air Missile (ABMRAAM) represents developmental technology which incorporates both a rocket engine and a RAMJET engine. Such a missile uses proportional navigation guidance plus an additional trajectory loft command. This thesis examines the optimal trajectory, and hence the optimal lofting command, for an ABMRAAM. A numerical simulation of the missile is presented and the necessary conditions for the optimal trajectory are derived. From these conditions, the problem can be numerically solved for the optimal loft command.

Formulation of the Optimal Trajectory for an Air-Breathing Medium Range Air-to-Air Missile

I. Introduction

1.1 Background

The United States Air Force (USAF) is investigating the feasibility of air-to-air missiles that incorporate both a rocket engine and a variable throttle RAMJET engine. The missile with both a rocket engine and a variable throttle RAMJET has been termed a Variable Flow Ducted Rocket (VFDR). The goal is to improve the performance of the missile for the same preflight weight as a purely rocket-propelled version. Currently, these missiles incorporate proportional navigation guidance plus a loft command, g_{loft}. Generally, the loft command is related to the ratio of the current line of sight distance to the original line of sight distance between the missile and the target and an altitude command. As the range between the two decreases, the magnitude of the command decays exponentially:

$$g_{loft} = g_{alt_{cmd}} \left(\frac{R_{LOS}}{R_{LOS_o}} \right)^{\tau_{loft}} \tag{1.1}$$

where

$g_{alt_{cmd}} =$ the altitude command,

$R_{LOS} =$ the current range along the line of sight vector,

$R_{LOS_o} =$ the initial range along the line of sight vector, and

$\tau_{loft} =$ the loft decay constant.

Due to the short duration of propulsion and near constant thrust, commanding a loft according to Eq. (1.1) has proven to be effective in rocket-propelled missiles as a method of increasing the potential energy of the vehicle. Attempting to gain altitude, thus increasing potential energy, may or may not be the most effective guidance implementation for a variable throttle RAMJET. Therefore, the optimal trajectory of this missile is being investigated in an effort to determine the correct loft command for the VFDR to minimize intercept time.

The RAMJET engine compresses the incoming air without the mechanical compressor associated with most air-breathing engines (4). The pressure of the incoming air is increased by passing through standing shock waves. To ensure appropriate pressure increase, the incoming air flow must remain relatively undisturbed. To prevent disturbances, the sideslip angle must be approximately zero for the VFDR due to the configuration of the RAMJET inlet. Hence, the missile equipped with a RAMJET must fly a bank to turn (BTT) profile to maintain zero sideslip angle. Therefore, the VFDR utilizes coordinated turning to alter its cross range position, rather than the skid to turn (zero roll angle) profile of the typical rocket propelled missile.

1.2 Previous Work

The model for the simulation is based on the simulation ENGAGE (10). ENGAGE was created for use with personal computers and simulates a one-on-one aircraft pursuit and evasion. Each aircraft is capable of launching one missile at the other aircraft. The algorithms are versatile and permit extensive variations of guidance and control algorithms for both the aircraft and the missiles they fire. However, ENGAGE is not useful as a tool to optimize a given performance criterion; whether the criterion is minimum time, maximum range, etc. Parameters such as feedback gains, loft command cutoff values, and altitude commands can be varied by the user in an attempt to achieve improved performance. This type of optimization is ad hoc

at best. The variable throttle RAMJET complicates performance evaluation even further by greatly increasing the variation of the missile's performance based upon the trajectory flown (6:319). Paris et. al. evaluated the optimal trajectory for an air-breathing missile problem but only for the RAMJET phase of boost. ENGAGE simulates the full flight of the missile but is not designed to allow the application of the calculus of variations to determine optimal loft command.

1.3 Project Scope

The scope of this project is to first recreate a simulation for the VFDR using MATLAB^{TM}. During the course of recreating the missile portion of ENGAGE, a few errors were discovered so an analysis of the impact is presented. Second, the necessary conditions for the optimal loft control are developed. The minimum time optimal loft control for the three-dimensional interception problem is shown to be most interesting when the engagement is in a vertical plane. Therefore, the emphasis is shifted to determining the optimal control assuming missile flight is restricted to the vertical plane. Third, a numerical shooting method is developed to solve the two-point boundary-value problem that is derived as a result of optimizing the loft command. The discussion so far has frequently referred to "optimal control;" however, optimal performance is never complete until a measure of performance is presented. The goal of this analysis is to find the optimal control for loft to minimize the final time of rendezvous with the target. Hence, the performance index can be stated as

$$\text{minimize } J = t_f \tag{1.2}$$

where

$J =$ the performance index, and

$t_f =$ the final time.

1.4 Sequence of Presentation

The first step in solving this problem is to develop a simulation for the VFDR. Chapters two and three describe the model that is simulated in ENGAGE. The description includes the coordinate systems, the atmospheric model, the equations of motion, the engines and the guidance and control. Chapter four analyzes the simulations and discusses the errors discovered. Chapter five presents the derivation of the necessary conditions for an extremal solution for the free final time problem. The shooting method is presented as a numerical technique for solving the two-point boundary-value problem formulated from the necessary conditions for an extremal solution. An example problem and the numerical results accompany the discussion. The formulation for the optimal trajectory is presented for the three-dimensional intercept. An interesting situation occurs when flight is restricted to the vertical plane. Therefore, the two-dimensional intercept is examined and the formulation for the optimal trajectory two-point boundary-value problem is presented.

II. Basic Equations for the Simulation

2.1 Atmosphere

The atmosphere is modeled using the U.S. Standard Atmosphere, 1962 (1). The model assumes that the atmosphere is comprised of ideal air that contains no moisture or dust and can be characterized by the ideal gas law. An ideal gas is a gas in which the molecules are sufficiently far apart so that intermolecular forces are negligible; the gas acts as a continuous material in which the properties are determined by statistical average of the particle effects (8:48). Up to altitudes of 80 kilometers (km), air is assumed to be homogeneously mixed with a relative volume composition that leads to a constant molecular weight, MW_{air}. Applying the ideal gas law to air yields

$$P = \frac{\rho R_u T}{MW_{air}}, \tag{2.1}$$

where

R_u = the universal gas constant,

P = the total pressure of air,

T = the total temperature, and

ρ = density.

However, since the molecular weight of air is assumed constant,

$$\begin{aligned} R_{air} &= \frac{R_u}{MW_{air}}, \\ &= \text{constant}. \end{aligned}$$

Therefore, the ideal gas law for air becomes,

$$P = \rho R_{air} T. \tag{2.2}$$

To 80 km, the modeled atmosphere is also assumed to be in equilibrium which means that the pressure is related to the geometric altitude by the differential relation

$$dP = -\rho \tilde{g} dh_G \tag{2.3}$$

where

h_G = the geometric height above the earth's surface, and

$\tilde{g}$ = gravity as a function of altitude.

Equation (2.3) is the hydrostatic equation. The customary approach in standard atmosphere calculations is to eliminate the variation of gravity with altitude from the hydrostatic equation. To effectively eliminate the dependence, geopotential altitude h is introduced. Before the geopotential altitude can be defined, the variation of gravity with geometric altitude is examined.

Consider two small elements of the atmosphere, where one is just at the surface of the earth ($h_G = 0$) and the other is at some geometric altitude, h_G, above the surface of the earth. The inverse square law of gravitation expresses the attractive force between each element and the earth as

$$m_1 \tilde{g} = G \frac{M_E m_1}{R_E^2}, \tag{2.4}$$

$$m_2 \tilde{g} = G \frac{M_E m_2}{(R_E + h_G)^2} \tag{2.5}$$

where

R_E = the radius of the earth,

G = the gravitational constant,

m_1 and m_2 = the mass of the elements, and

$$M_E = \text{the mass of the earth.}$$

Defining g as the acceleration due to gravity at the earth's surface, it is noted that $\tilde{g} = g$ when h_G is zero. Also noting that the mass of each element cancels from the expressions above, Eqs. (2.4) and (2.5) become

$$g = G\frac{M_E}{R_E^2}, \tag{2.6}$$

$$\tilde{g} = G\frac{M_E}{(R_E + h_G)^2}. \tag{2.7}$$

An expression for $\tilde{g}$ as a function of geometric altitude is obtained by forming the ratio of the above equations,

$$\frac{\tilde{g}}{g} = \frac{R_E^2}{(R_E + h_G)^2}, \tag{2.8}$$

$$\tilde{g} = g\frac{R_E^2}{(R_E + h_G)^2}. \tag{2.9}$$

The hydrostatic equation, Eq. (2.3), can be expressed either as

$$dP = -\rho\tilde{g}dh_G \tag{2.10}$$

or noting that if $\tilde{g} \equiv g$, then dh_G is equal to an arbitrarily small change in geopotential height, dh, and the hydrostatic equation can be expressed as

$$dP = -\rho g dh. \tag{2.11}$$

Equating Eqs. (2.10) and (2.11) and solving for dh yields

$$dh = \frac{\tilde{g}}{g}dh_G. \tag{2.12}$$

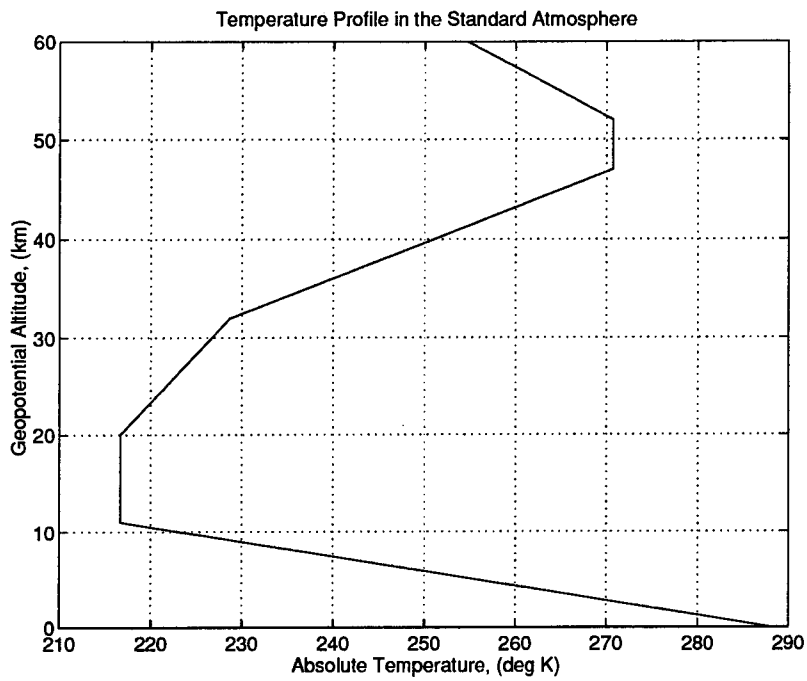

Figure 2.1 Standard Atmosphere Relation Between Temperature and Altitude

Substituting the relation obtained in Eq. (2.8) and then performing the integration an expression for h is

$$dh = \frac{R_E^2}{(R_E + h_G)^2} dh_G$$
$$h = \frac{R_E}{(R_E + h_G)} h_G \tag{2.13}$$

Equation (2.13) is the geopotential altitude, an altitude that assumes gravity is constant and equal to its sea level value. The variation of temperature with altitude was determined experimentally for the U.S. Standard Atmosphere, 1962 and is shown in Fig. 2.1. For the atmosphere in which air-breathing flight takes place, there are two noticeable traits. There is a temperature gradient region and an isothermal region. The temperature in the gradient region varies linearly. Therefore, the temperature

at a given h is expressed by

$$T = T_b + \frac{dT}{dh}(h - h_b) \tag{2.14}$$

where

T_b = the reference temperature at the start of the region of interest, and

h_b = the associated reference geopotential altitude.

Dividing Eq. (2.3) by Eq. (2.1)and performing the integration, two expressions for density are formed. The first expression is valid for the region that temperature varies linearly with h. The second expression is applicable in the isothermal region.

$$\rho = \rho_b \left(\frac{T}{T_b}\right)^{-\left(1+\frac{g}{R_{air}\frac{dT}{dh}}\right)} \text{ for } \frac{dT}{dh} \neq 0, \tag{2.15}$$

$$\rho = \rho_b \exp\left\{-\frac{g(h - h_b)}{R_{air}T_b}\right\} \text{ for } \frac{dT}{dh} = 0. \tag{2.16}$$

where,

ρ_b = the reference density at the start of the region of interest.

Equations (2.15) and (2.16) are two expressions for ρ, depending upon whether the altitude is in an isothermal region or a temperature gradient region. Table 2.1 gives the corresponding reference values for h, T_b, ρ_b, and $\frac{dT}{dh}$.

The above atmospheric model allows the determination of T, ρ, and P solely as a function of geopotential altitude up to 80 km. Figure 2.2 shows the variation of density and pressure as a function of geopotential altitude for the atmospheric model. The values for density and pressure are normalized by the respective sea-

Reference Altitude, h, km	Reference Temperature, T_b, K	Reference Density, ρ_b, kg/m^3	$\frac{dT}{dh}$, K/km
0	288.15	1.225	-6.5
11	216.65	3.639×10^{-1}	0
20	216.65	8.803×10^{-2}	1
32	228.65	1.332×10^{-2}	1
47	270.65	1.427×10^{-3}	2.8
52	270.65	7.594×10^{-4}	0
61	252.65	2.511×10^{-4}	-2

Table 2.1 Properties of the Atmosphere at the Isothermal Gradient Boundaries

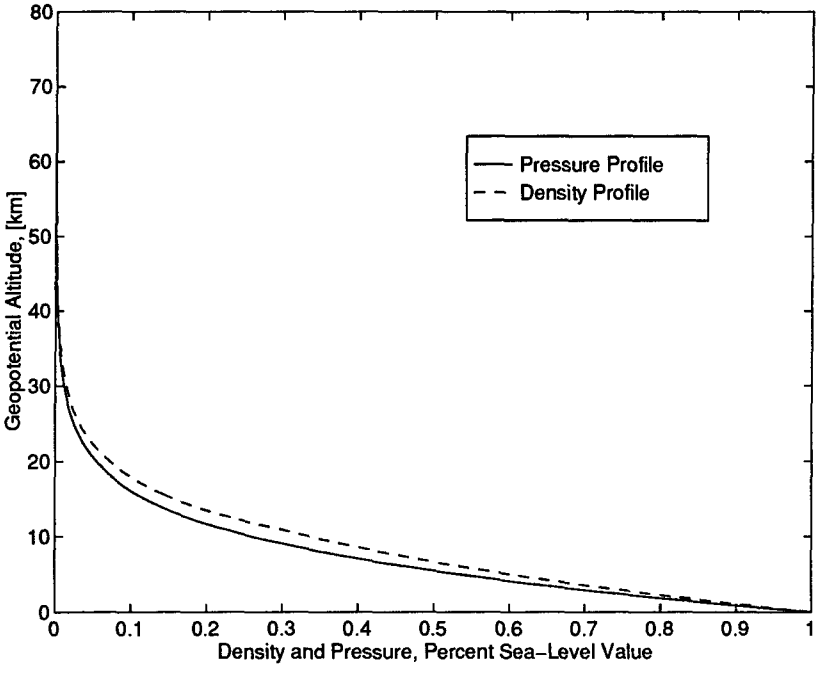

Figure 2.2 Density and Pressure as Percent of Sea Level Value

level value. Above 80 km, air begins to diffuse and the molecular weight can no longer be assumed constant.

From these quantities, the following expressions for a, the speed of sound in air, and Q_o, dynamic pressure, can be obtained:

$$a = \sqrt{\gamma_{air} R_{air} T} \tag{2.17}$$

$$Q_o = \frac{1}{2}\rho V_{air}^2. \tag{2.18}$$

γ_{air} = the the specific heat ratio of air

V_{air} = the velocity of the freestream air.

2.2 Coordinate Systems

This section describes the various coordinate systems used in the model and the necessary rotation sequences used to define the axis systems. This model is developed assuming that the earth is a flat, non-rotating reference frame. This assumption is valid given the relatively short duration of a typical flight which is on the order of one minute.

2.2.1 Inertial Axis. The inertial axis is formed by using the right hand rule with x_E and y_E forming a plane parallel to the surface of the earth, and z_E normal to the surface of the earth. Figure 2.3 depicts the earth fixed coordinate system.

2.2.2 Velocity Axis. To go from the Earth-fixed, or inertial, axis system to the velocity axis system, a rotation of angle ψ is made about the z_E axis. This forms an intermediate axis x_{E1}, y_{E1}, and z_{E1}. Figure 2.4 shows this rotation. The

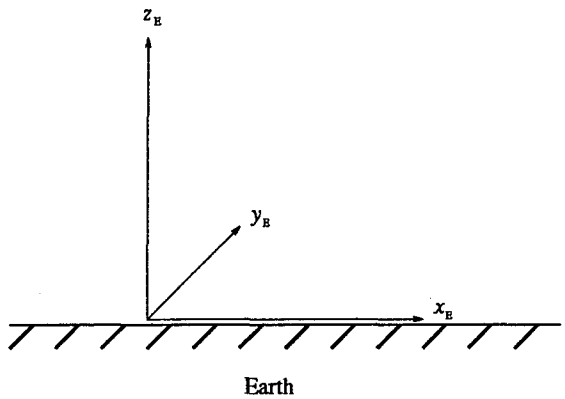

Figure 2.3 Inertial Axis System

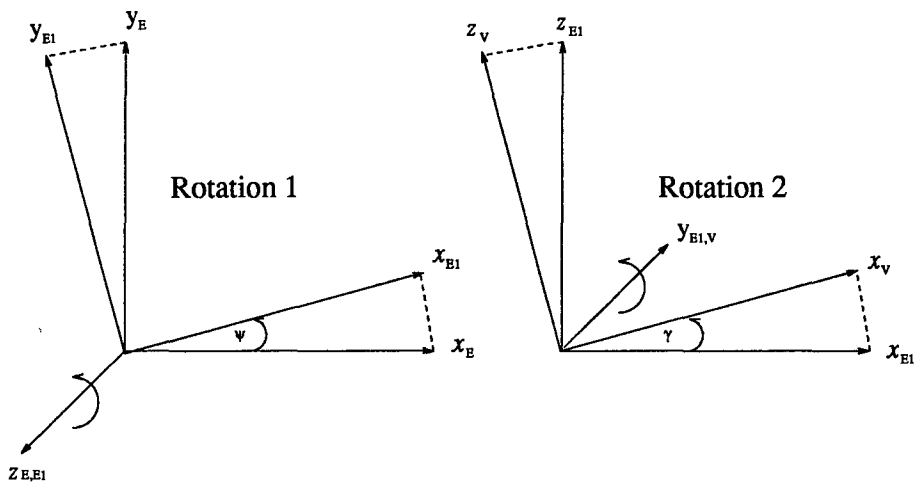

Figure 2.4 Rotation Sequence From Earth to Velocity Axis

transformation from the inertial axis to the intermediate axis is given by

$$\begin{bmatrix} x_{E1} \\ y_{E1} \\ z_{E1} \end{bmatrix} = \begin{bmatrix} \cos\psi & \sin\psi & 0 \\ -\sin\psi & \cos\psi & 0 \\ 0 & 0 & 1 \end{bmatrix} \begin{bmatrix} x_E \\ y_E \\ z_E \end{bmatrix} \tag{2.19}$$

Next, a rotation of angle γ is made about the resulting -y_{E1} axis. This is chosen so a positive γ represents climbing flight. This produces unit vectors in x_V, y_V, and z_V

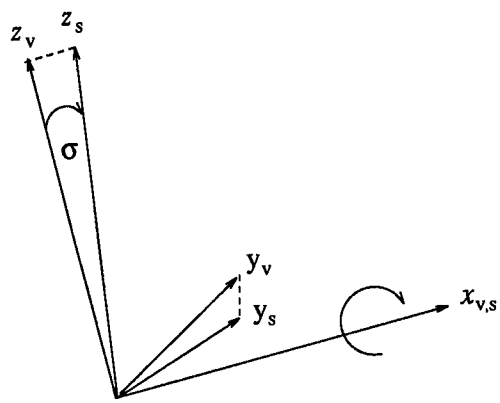

Figure 2.5 Rotation from Velocity to Stability Axis

directions with the total velocity, V, always pointed in the x_V direction.

$$\begin{bmatrix} x_V \\ y_V \\ z_V \end{bmatrix} = \begin{bmatrix} \cos\gamma & 0 & \sin\gamma \\ 0 & 1 & 0 \\ -\sin\gamma & 0 & \cos\gamma \end{bmatrix} \begin{bmatrix} x_{E1} \\ y_{E1} \\ z_{E1} \end{bmatrix} \tag{2.20}$$

Equations (2.19) and (2.20) can be combined allowing the definition of $\mathbf{T_{EV}}$ to be the rotation matrix from the earth to the velocity coordinate system.

$$\begin{bmatrix} x_V \\ y_V \\ z_V \end{bmatrix} = \begin{bmatrix} \cos\gamma & 0 & \sin\gamma \\ 0 & 1 & 0 \\ -\sin\gamma & 0 & \cos\gamma \end{bmatrix} \begin{bmatrix} \cos\psi & \sin\psi & 0 \\ -\sin\psi & \cos\psi & 0 \\ 0 & 0 & 1 \end{bmatrix} \begin{bmatrix} x_E \\ y_E \\ z_E \end{bmatrix} \tag{2.21}$$

$$= \begin{bmatrix} \cos\gamma\cos\psi & \cos\gamma\sin\psi & \sin\gamma \\ -\sin\psi & \cos\psi & 0 \\ -\sin\gamma\cos\psi & -\sin\gamma\sin\psi & \cos\gamma \end{bmatrix} \begin{bmatrix} x_E \\ y_E \\ z_E \end{bmatrix} \tag{2.22}$$

$$= \mathbf{T_{EV}} \begin{bmatrix} x_E \\ y_E \\ z_E \end{bmatrix} \tag{2.23}$$

2.2.3 Stability Axis. The stability axis is defined by a roll angle, σ, about the -x_V axis. This results in coordinates x_S, y_S, and z_S. Figure 2.5 shows the rotation sequence to the stability axis system and is given by

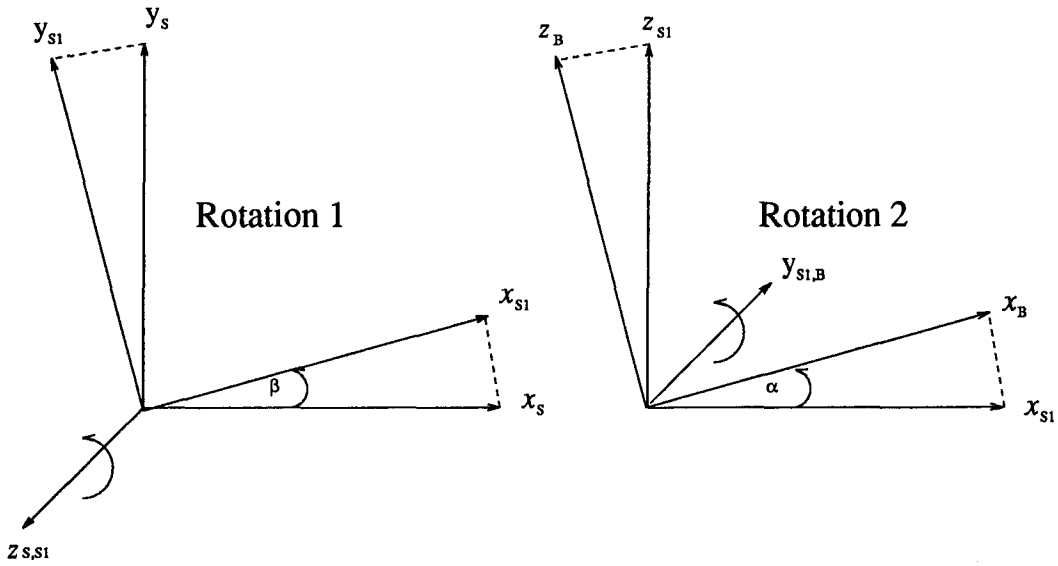

Figure 2.6 Rotation Sequence from Stability to Body Axis

$$\begin{bmatrix} x_S \\ y_S \\ z_S \end{bmatrix} = \begin{bmatrix} 1 & 0 & 0 \\ 0 & \cos\sigma & -\sin\sigma \\ 0 & \sin\sigma & \cos\sigma \end{bmatrix} \begin{bmatrix} x_V \\ y_V \\ z_V \end{bmatrix} \tag{2.24}$$

$$= \mathbf{T_{VS}} \begin{bmatrix} x_V \\ y_V \\ z_V \end{bmatrix}. \tag{2.25}$$

Equation (2.24) leads to the definition of the rotation matrix from the velocity to the stability axis system, $\mathbf{T_{VS}}$.

2.2.4 Body Axis. The body axis system is defined relative to the stability axis system by two rotations. Figure 2.6 shows the rotation sequence from the stability axis to the body axis. The first is a rotation of angle β about the z_S axis. The second rotation is an angle α about the resulting -y axis. The transformation from the stability axis to the body axis is

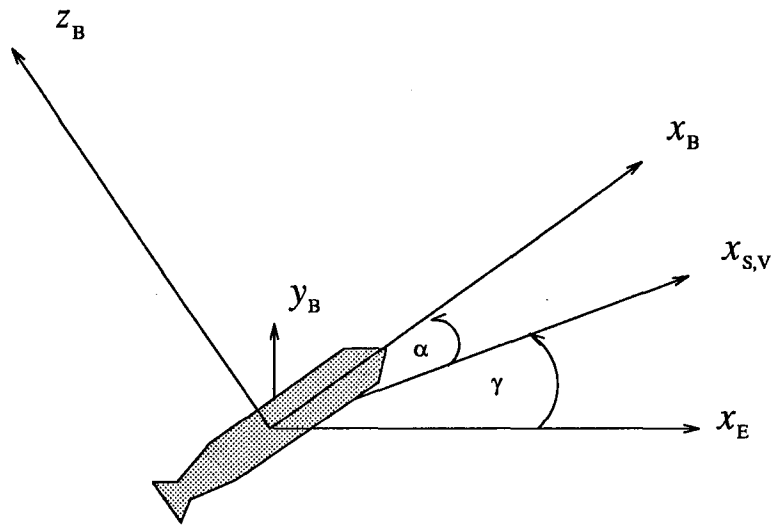

Figure 2.7 Body Fixed Axis System

$$\begin{bmatrix} x_B \\ y_B \\ z_B \end{bmatrix} = \begin{bmatrix} \cos\alpha & 0 & \sin\alpha \\ 0 & 1 & 0 \\ -\sin\alpha & 0 & \cos\alpha \end{bmatrix} \begin{bmatrix} \cos\beta & \sin\beta & 0 \\ -\sin\beta & \cos\beta & 0 \\ 0 & 0 & 1 \end{bmatrix} \begin{bmatrix} x_S \\ y_S \\ z_S \end{bmatrix} \tag{2.26}$$

$$= \begin{bmatrix} \cos\alpha\cos\beta & \cos\alpha\sin\beta & \sin\alpha \\ -\sin\beta & \cos\beta & 0 \\ -\sin\alpha\cos\beta & -\sin\alpha\sin\beta & \cos\alpha \end{bmatrix} \begin{bmatrix} x_S \\ y_S \\ z_S \end{bmatrix} \tag{2.27}$$

$$= \mathbf{T_{SB}} \begin{bmatrix} x_S \\ y_S \\ z_S \end{bmatrix}. \tag{2.28}$$

The resulting direction vectors, x_B, y_B, and z_B, are fixed to the missile with x_B out the nose, y_B out the left side of the missile and z_B out the top; see Fig 2.7. The transformation from the stability axis system to the body axis system is accomplished by $\mathbf{T_{SB}}$, which is defined by Eq. (2.28).

2.3 Force Equations

Figure 2.8 is a free body diagram of the missile in flight. The missile is assumed to be a point mass. The sum of forces produces the net acceleration of the vehicle.

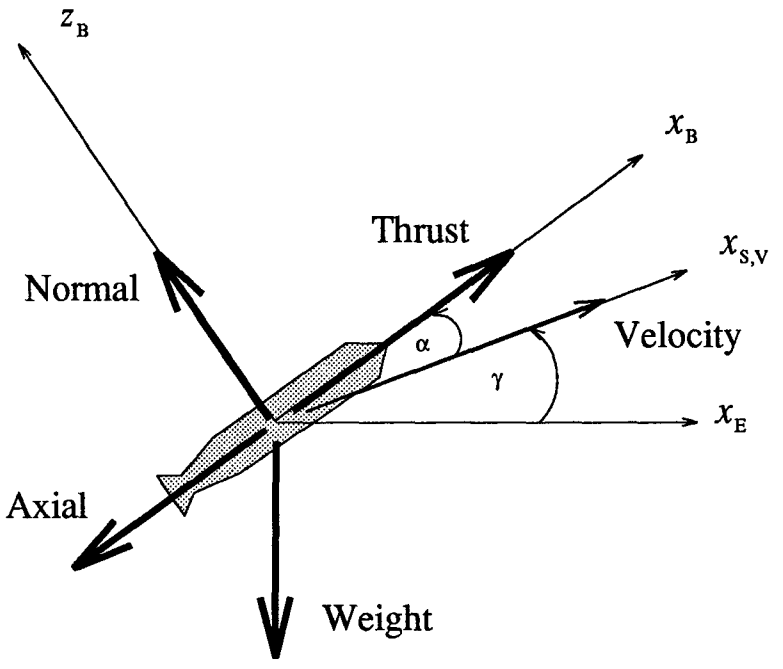

Figure 2.8 Free Body Diagram of the Missile in Flight

The acceleration terms are derived followed by a development of the force terms.

$$\begin{aligned}\sum \mathbf{F_V} &= m\mathbf{a_V} \\ &= m\left[\frac{d}{dt}(\mathbf{V_V}) + \boldsymbol{\omega}_{V/E} \times \mathbf{V_V}\right]\end{aligned} \tag{2.29}$$

where

$\mathbf{F_V} =$ the total force on the missile,

$\mathbf{a_V} =$ the total acceleration of the missile,

$\mathbf{V_V} =$ the velocity vector in the velocity frame,

$\boldsymbol{\omega}_{V/E} =$ the angular velocity vector of the velocity frame relative to the inertial frame.

The forces acting on the missile in flight are in various reference frames. Weight, W, is acting in the inertial frame and the axial, F_a, normal, F_n, lateral, F_y, and thrust, F_T, forces are in the body frame.

By definition, the velocity axis system is aligned with the velocity vector,

$$\mathbf{V_V} = \begin{bmatrix} V \\ 0 \\ 0 \end{bmatrix}. \tag{2.30}$$

The angular velocity of the velocity axis system relative to the inertial frame is known through the rotations required to go from the inertial to velocity coordinate systems.

$$\boldsymbol{\omega}_{V/E} = \dot{\psi}\hat{z}_E - \dot{\gamma}\hat{y}_{E1} \tag{2.31}$$

However, $\dot{\psi}\hat{z}_E$ and $\dot{\gamma}\hat{y}_{E1}$ must be expressed in the velocity frame, hence

$$\begin{aligned}
\dot{\boldsymbol{\psi}}_v &= \mathbf{T_{EV}} \begin{bmatrix} 0 \\ 0 \\ \dot{\psi} \end{bmatrix} \\
&= \begin{bmatrix} \cos\gamma\cos\psi & \cos\gamma\cos\psi & \sin\gamma \\ -\sin\psi & \cos\psi & 0 \\ -\sin\gamma\cos\psi & -\sin\gamma\sin\psi & \cos\gamma \end{bmatrix} \begin{bmatrix} 0 \\ 0 \\ \dot{\psi} \end{bmatrix} \\
&= \begin{bmatrix} \dot{\psi}\sin\gamma \\ 0 \\ \dot{\psi}\cos\gamma \end{bmatrix}
\end{aligned}$$

and

$$\dot{\boldsymbol{\gamma}}_v = \begin{bmatrix} \cos\gamma & 0 & \sin\gamma \\ 0 & 1 & 0 \\ -\sin\gamma & 0 & \cos\gamma \end{bmatrix} \begin{bmatrix} 0 \\ \dot{\gamma} \\ 0 \end{bmatrix} \tag{2.32}$$

$$= \begin{bmatrix} 0 \\ \dot{\gamma} \\ 0 \end{bmatrix}.$$

Therefore, $\boldsymbol{\omega}_{V/E}$ can be expressed entirely in the velocity axis system as

$$\boldsymbol{\omega}_{V/E} = \dot{\psi}\sin\gamma\hat{x}_V - \dot{\gamma}\hat{y}_V + \dot{\psi}\cos\gamma\hat{z}_V. \tag{2.33}$$

Knowing $\boldsymbol{\omega}_{V/E}$ and $\boldsymbol{V}_V$, the cross product of Eq. (2.29) becomes

$$\begin{aligned} \omega_{V/E}\times\mathbf{V_V} &= \begin{vmatrix} \hat{x}_V & \hat{y}_V & \hat{z}_V \\ \dot{\psi}\sin\gamma & -\dot{\gamma} & \dot{\psi}\cos\gamma \\ V & 0 & 0 \end{vmatrix} \\ &= \begin{bmatrix} 0 \\ V\dot{\psi}\cos\gamma \\ V\dot{\gamma} \end{bmatrix}. \end{aligned} \tag{2.34}$$

Also,

$$\begin{aligned} \frac{d}{dt}(\mathbf{V_V}) &= \begin{bmatrix} \dot{V} \\ 0 \\ 0 \end{bmatrix} \\ &= \dot{V}\hat{x}_V. \end{aligned} \tag{2.35}$$

Combining Eqs. (2.34) and (2.35) the total acceleration vector, $\mathbf{a_V}$ becomes

$$\begin{aligned} \mathbf{a_V} &= \frac{d}{dt}(\mathbf{V_V}) + \boldsymbol{\omega}_{V/E}\times\mathbf{V_V} \\ &= \begin{bmatrix} \dot{V} \\ V\dot{\psi}\cos\gamma \\ V\dot{\gamma} \end{bmatrix}. \end{aligned} \tag{2.36}$$

For completion of Eq. (2.29), the net forces in the velocity axis frame must be determined. The forces acting in the body frame are the thrust, the axial force, the normal force and the side force. The thrust force is aligned with the $\hat{x}_B$ axis. The axial force is also aligned with the $\hat{x}_B$ axis but acts in the opposite direction of the thrust force. The normal force acts normal to the $\hat{x}_B - \hat{y}_B$ plane in the $\hat{z}_B$ direction. The lateral force acts in the $\hat{y}_B$ direction. The force vector is expressed as

$$\tilde{\mathbf{F}}_{\mathbf{B}} = \begin{bmatrix} F_T - F_a \\ F_y \\ F_n \end{bmatrix}, \tag{2.37}$$

where $\tilde{\mathbf{F}}_{\mathbf{B}}$ indicates the force vector is only thrust and aerodynamic forces, and gravity is not yet included. As a first step in transforming $\tilde{\mathbf{F}}_{\mathbf{B}}$, the force vector is rotated to the stability axis,

$$\begin{aligned}
\tilde{\mathbf{F}}_{\mathbf{S}} &= \mathbf{T}_{\mathbf{BS}}\tilde{\mathbf{F}}_{\mathbf{B}} \\
&= \mathbf{T}_{\mathbf{SB}}{}^{T}\tilde{\mathbf{F}}_{\mathbf{B}} \\
&= \begin{bmatrix} \cos\alpha\cos\beta & -\sin\beta & -\sin\alpha\cos\beta \\ \cos\alpha\sin\beta & \cos\beta & -\sin\alpha\sin\beta \\ \sin\alpha & 0 & \cos\alpha \end{bmatrix} \begin{bmatrix} F_T - F_a \\ F_y \\ F_n \end{bmatrix} \\
&= \begin{bmatrix} F_T\cos\alpha\cos\beta - F_a\cos\alpha\cos\beta - F_y\sin\beta - F_n\sin\alpha\cos\beta \\ F_T\cos\alpha\sin\beta - F_a\cos\alpha\sin\beta + F_y\cos\beta - F_n\sin\alpha\sin\beta \\ F_T\sin\alpha - F_a\sin\alpha + F_n\cos\alpha \end{bmatrix}
\end{aligned} \tag{2.38}$$

Equation (2.38) represents the thrust and aerodynamic forces acting on the missile relative to the stability axis system. Drag, D, side, S and lift, L, are defined in the missile stability axis and are pictured in Fig 2.9. Lift is the total aerodynamic force acting on the missile in the stability axis in the $\hat{z}_S$ direction. Drag is the total aerodynamic force acting on the missile in the stability axis in the -$\hat{x}_S$ direction. The side force is the total aerodynamic force acting on the missile in the stability axis in

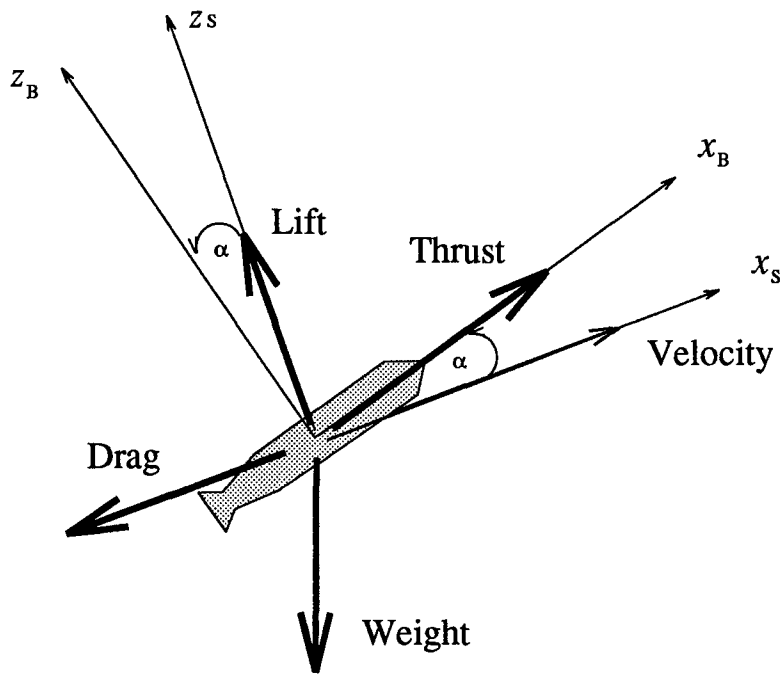

Figure 2.9 Forces on Missile in Stability Axis System

the $\hat{y}_S$ direction.

$$D \equiv F_a \cos\alpha \cos\beta + F_y \sin\beta + F_n \sin\alpha \cos\beta \tag{2.39}$$

$$S \equiv -F_a \cos\alpha \sin\beta + F_y \cos\beta - F_n \sin\alpha \sin\beta \tag{2.40}$$

$$L \equiv -F_a \sin\alpha + F_n \cos\alpha \tag{2.41}$$

The above definitions reduce Eq. (2.38) to

$$\tilde{\mathbf{F}}_{\mathbf{S}} = \begin{bmatrix} F_T \cos\alpha \cos\beta - D \\ F_T \cos\alpha \sin\beta + S \\ F_T \sin\alpha + L \end{bmatrix}. \tag{2.42}$$

The final rotation sequence from the stability axis system to the velocity axis system is accomplished by the transpose of the rotation matrix in Eq. (2.25). The result of the rotation is the thrust and the aerodynamic forces are expressed in the velocity

axis system.

$$
\begin{aligned}
\tilde{\mathbf{F}}_{\mathbf{V}} &= \mathbf{T}_{\mathbf{VS}}{}^{T}\tilde{\mathbf{F}}_{\mathbf{S}} \\
&= \begin{bmatrix} 1 & 0 & 0 \\ 0 & \cos\sigma & \sin\sigma \\ 0 & -\sin\sigma & \cos\sigma \end{bmatrix} \begin{bmatrix} F_T\cos\alpha\cos\beta - D \\ F_T\cos\alpha\sin\beta + S \\ F_T\sin\alpha + L \end{bmatrix} \\
&= \begin{bmatrix} F_T\cos\alpha\cos\beta - D \\ (F_T\sin\alpha + L)\sin\sigma + (F_T\cos\alpha\sin\beta + S)\cos\sigma \\ (F_T\sin\alpha + L)\cos\sigma - (F_T\cos\alpha\sin\beta + S)\sin\sigma \end{bmatrix}. \qquad (2.43)
\end{aligned}
$$

$\tilde{\mathbf{F}}_{\mathbf{V}}$ is the thrust and aerodynamic forces acting of the missile in the velocity reference frame. Gravity effects are now included to produce the total force vector in the velocity coordinate system, $\mathbf{F}_{\mathbf{V}}$. Gravity acts in the -$\hat{z}_E$ direction of the inertial frame. Noting the mass of the missile is m and using the relation

$$
\mathbf{W}_{\mathbf{E}} = m \begin{bmatrix} 0 \\ 0 \\ -g \end{bmatrix} \qquad (2.44)
$$

yields

$$
\mathbf{W}_{\mathbf{E}} = \begin{bmatrix} 0 \\ 0 \\ -W \end{bmatrix}.
$$

Resolving the weight vector into the the velocity axis components yields,

$$
\begin{aligned}
\mathbf{W}_{\mathbf{V}} &= \mathbf{T}_{\mathbf{EV}} \begin{bmatrix} 0 \\ 0 \\ -W \end{bmatrix} \\
&= \begin{bmatrix} \cos\gamma\cos\psi & \cos\gamma\cos\psi & \sin\gamma \\ -\sin\psi & \cos\psi & 0 \\ -\sin\gamma\cos\psi & -\sin\gamma\sin\psi & \cos\gamma \end{bmatrix} \begin{bmatrix} 0 \\ 0 \\ -W \end{bmatrix}
\end{aligned}
$$

$$= \begin{bmatrix} -W\sin\gamma \\ 0 \\ -W\cos\gamma \end{bmatrix}. \tag{2.45}$$

The thrust and aerodynamic forces, Eq. (2.43), are combined with the weight, Eq. (2.45) to denote the total forces acting on the missile in the velocity frame.

$$\begin{aligned}
\mathbf{F_V} &= \tilde{\mathbf{F}}_\mathbf{V} + \mathbf{W_V} \\
&= \begin{bmatrix} F_T\cos\alpha\cos\beta - D \\ (F_T\sin\alpha + L)\sin\sigma + (F_T\cos\alpha\sin\beta + S)\cos\sigma \\ (F_T\sin\alpha + L)\cos\sigma - (F_T\cos\alpha\sin\beta + S)\sin\sigma \end{bmatrix} + \begin{bmatrix} -W\sin\gamma \\ 0 \\ -W\cos\gamma \end{bmatrix} \\
&= \begin{bmatrix} F_T\cos\alpha\cos\beta - D - W\sin\gamma \\ (F_T\sin\alpha + L)\sin\sigma + (F_T\cos\alpha\sin\beta + S)\cos\sigma \\ (F_T\sin\alpha + L)\cos\sigma - (F_T\cos\alpha\sin\beta + S)\sin\sigma - W\cos\gamma \end{bmatrix}.
\end{aligned} \tag{2.46}$$

The expressions for the acceleration of the missile in the velocity axis and the total forces acting on the missile in the velocity axis can now be combined in Eq. (2.29) to complete the expressions for the equations of motion of the missile. Recall Eq. (2.29):

$$\sum \mathbf{F_V} = m\mathbf{a_V}$$

Substituting the expression obtained from Eq. (2.46) for $\mathbf{F_V}$ and the expression obtained from Eq. (2.36) for $\mathbf{a_V}$ yields

$$m\begin{bmatrix} \dot{V} \\ V\dot{\psi}\cos\gamma \\ V\dot{\gamma} \end{bmatrix} = \begin{bmatrix} F_T\cos\alpha\cos\beta - D - W\sin\gamma \\ (F_T\sin\alpha + L)\sin\sigma + (F_T\cos\alpha\sin\beta + S)\cos\sigma \\ (F_T\sin\alpha + L)\cos\sigma - (F_T\cos\alpha\sin\beta + S)\sin\sigma - W\cos\gamma \end{bmatrix}. \tag{2.47}$$

Dividing both sides of the equation by the mass of the missile, the above equation becomes

$$\begin{bmatrix} \dot{V} \\ V\dot{\psi}\cos\gamma \\ V\dot{\gamma} \end{bmatrix} = \frac{1}{m}\begin{bmatrix} F_T\cos\alpha\cos\beta - D - W\sin\gamma \\ (F_T\sin\alpha + L)\sin\sigma + (F_T\cos\alpha\sin\beta + S)\cos\sigma \\ (F_T\sin\alpha + L)\cos\sigma - (F_T\cos\alpha\sin\beta + S)\sin\sigma - W\cos\gamma \end{bmatrix}. \tag{2.48}$$

Substituting

$$\frac{1}{m} = \frac{g}{W} \tag{2.49}$$

into Eq. (2.48), the expression becomes

$$\begin{bmatrix} \dot{V} \\ V\dot{\psi}\cos\gamma \\ V\dot{\gamma} \end{bmatrix} = \begin{bmatrix} g\left(\frac{F_T}{W}\cos\alpha\cos\beta - \frac{D}{W} - \sin\gamma\right) \\ g\left[\left(\frac{F_T}{W}\sin\alpha + \frac{L}{W}\right)\sin\sigma + \left(\frac{F_T}{W}\cos\alpha\sin\beta + \frac{S}{W}\right)\cos\sigma\right] \\ g\left[\left(\frac{F_T}{W}\sin\alpha + \frac{L}{W}\right)\cos\sigma - \left(\frac{F_T}{W}\cos\alpha\sin\beta + \frac{S}{W}\right)\sin\sigma - \cos\gamma\right] \end{bmatrix}. \tag{2.50}$$

Rearranging the terms, expressions for $\dot{V}$, $\dot{\psi}$ and $\dot{\gamma}$ are

$$\begin{bmatrix} \dot{V} \\ \dot{\psi} \\ \dot{\gamma} \end{bmatrix} = \begin{bmatrix} g\left(\frac{F_T}{W}\cos\alpha\cos\beta - \frac{D}{W} - \sin\gamma\right) \\ \frac{g}{V\cos\gamma}\left[\left(\frac{F_T}{W}\sin\alpha + \frac{L}{W}\right)\sin\sigma + \left(\frac{F_T}{W}\cos\alpha\sin\beta + \frac{S}{W}\right)\cos\sigma\right] \\ \frac{g}{V}\left[\left(\frac{F_T}{W}\sin\alpha + \frac{L}{W}\right)\cos\sigma - \left(\frac{F_T}{W}\cos\alpha\sin\beta + \frac{S}{W}\right)\sin\sigma - \cos\gamma\right] \end{bmatrix}. \tag{2.51}$$

Noting $S = 0$ and $\beta = 0$ for this missile, the equations of motion reduce to

$$\begin{bmatrix} \dot{V} \\ \dot{\psi} \\ \dot{\gamma} \end{bmatrix} = \begin{bmatrix} g\left(\frac{F_T}{W}\cos\alpha - \frac{D}{W} - \sin\gamma\right) \\ \frac{g}{V\cos\gamma}\left(\frac{F_T}{W}\sin\alpha + \frac{L}{W}\right)\sin\sigma \\ \frac{g}{V}\left[\left(\frac{F_T}{W}\sin\alpha + \frac{L}{W}\right)\cos\sigma - \cos\gamma\right] \end{bmatrix}. \tag{2.52}$$

$\dot{x}_E$, $\dot{y}_E$, and $\dot{z}_E$ are related to the velocity vector in the velocity axis system through the transpose of Eq. (2.23)

$$\begin{bmatrix} \dot{x}_E \\ \dot{y}_E \\ \dot{z}_E \end{bmatrix} = \mathbf{T_{EV}}^T \begin{bmatrix} V \\ 0 \\ 0 \end{bmatrix}$$

$$= \begin{bmatrix} V\cos\gamma\cos\psi \\ V\cos\gamma\sin\psi \\ V\sin\gamma \end{bmatrix}. \tag{2.53}$$

Equation (2.53) gives the translational equations needed to determine the position of the missile in the inertial coordinate system and Eq. (2.52) represents the equations of motion in the velocity frame for the missile in flight. Specific expressions for F_T, L and D are developed in the following sections.

2.4 Aerodynamic Forces

The aerodynamic forces for this missile are in the form of dimensionless aerodynamic coefficients. This data is in tabular form and was generated through wind tunnel testing. There is no sideslip angle, hence there is no side force. The axial force is modeled as a function of a dimensionless axial force coefficient, C_a, based on Mach number, M, and α. A dimensionless compensation to the axial force coefficient, ΔC_a, as a function of altitude and Mach number corrects for the variations in aerodynamic effects as density and Mach number vary. The axial force, F_a, is expressed as

$$F_a = (C_a + \Delta C_a) A_{ref} Q_o \tag{2.54}$$

$$C_a = f(\alpha, M) \tag{2.55}$$

$$\Delta C_a = f(h, M) \tag{2.56}$$

where

$$A_{ref} = \text{the aerodynamic reference area of the missile.}$$

Two sets of data are required for C_a. The RAMJET requires air flow into the combustion chamber, which requires ducts to open. These ducts are not deployed during

the rocket boost phase, hence the two different axial force profiles, one corresponding to the axial coefficient during the rocket boost phase, and the other corresponding to the axial coefficient during the RAMJET boost phase.

The normal force, F_n, is modeled as a function of a dimensionless normal force coefficient, C_n, based on M and α.

$$F_n = C_n A_{ref} Q_o \tag{2.57}$$

$$C_n = f(\alpha, M) \tag{2.58}$$

2.5 Engine

The engine needs to be described during the three phases of its flight. Overall, there are two propulsion phases and one coast phase. The rocket boost phase is the first phase. The rocket booster burns at a fixed rate until the propellant is depleted. The next propulsion phase is the air-breathing boost phase. This phase is terminated when the oxidizer is depleted. Unlike the constant fuel flow rate in the rocket boost phase, the fuel flow rate is variable in the air-breathing boost phase. Separating the rocket boost phase and the air-breathing boost phase is a brief (0.2 sec) coast phase where there is no thrust developed and no fuel depletion. This phase begins when the propellant for the rocket engine is depleted and the transition time permits the opening of the RAMJET inlet. Finally, the missile returns to the coast phase if the oxidizer is depleted prior to target intercept.

2.5.1 Rocket Boost Phase. The thrust, F_T, of a rocket engine pictured in Fig. 2.10 is given by

$$F_T = T_{sl} + A_{exit}(p_{sl} - p), \tag{2.59}$$

where

T_{sl} = the thrust at sea level,

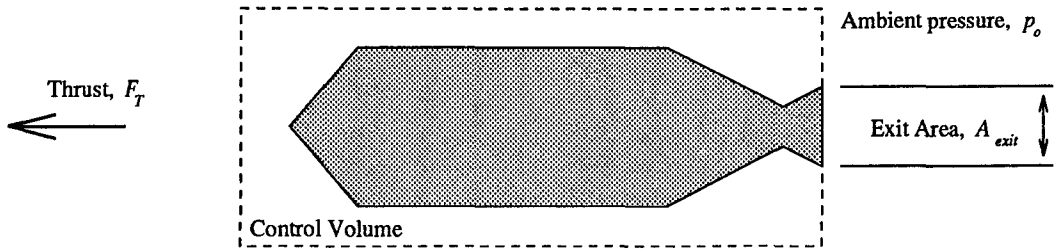

Figure 2.10 Rocket Engine Control Volume

A_{exit} = the exit area of the nozzle,

p_{sl} = the atmospheric pressure at sea level.

This equation is useful since T_{sl} is known from test data and A_{exit} is known from the geometry of the missile. The pressure, p_o, is known as a function of altitude from the atmospheric model and is given by Eq. (2.1). The weight of the missile, W_m, decreases at the rate the fuel is depleted, $\dot{w}_f$;

$$\dot{w}_f = \frac{T_{sl}}{I_{sp_{sl}}} \tag{2.60}$$

where

$I_{sp_{sl}}$ = the sea level specific impulse

and is known from test data. T_{sl} and $I_{sp_{sl}}$ are modeled as constant values which implies that $\dot{w}_f$ is constant for the rocket boost phase of flight.

2.5.2 Air-Breathing Boost Phase. A general RAMJET engine is pictured in Fig. 2.11 (11:96). Air at station 0 enters the engine at free-stream velocity, V_o, and pressure, p_o, at a rate of $\dot{w}_a$. The capture area is A_o. The velocity of the entering air is reduced and the static pressure is increased by the supersonic diffuser at station 1. The subsonic diffuser, station 2, then compresses the air further. The air flows into the combustor at station 3, which houses the burners. The air is heated by the

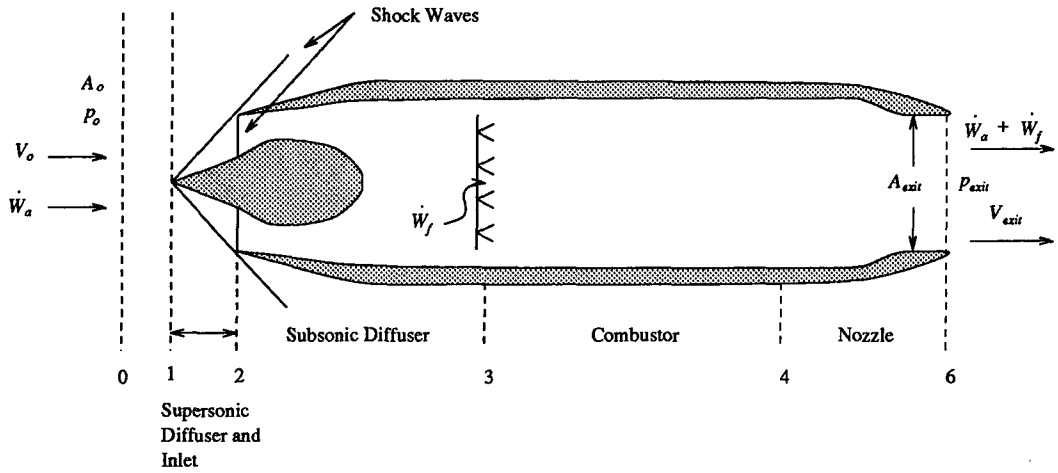

Figure 2.11 Features of the General RAMJET Engine

continuous combustion of fuel. The heated products of combustion are expanded in the nozzle, station 4, and are ejected at station 6 at a speed greater than the incoming air. The increase in momentum of the gas results in a thrust in the direction of flight.

Since this engine requires flowing air in order to build pressure for the combustion process, the engine is not able to generate thrust at zero flight speed. Hence, the RAMJET must be propelled to a minimum velocity to operate. The ABMRAAM accomplishes this through the rocket booster previously described. Once in flight, the thrust, F_T, generated by the RAMJET is given by

$$F_T = \frac{(\dot{w}_a + \dot{w}_f)}{g} V_{exit} - \frac{\dot{w}_a}{g} V_o + (p_{exit} - p_o) A_{exit}, \tag{2.61}$$

where

V_{exit} = the velocity of the gases exiting the nozzle,

p_{exit} = the pressure of the gases exiting the nozzle, and

A_{exit} = the exit area of the nozzle.

A throttle is used to control the fuel flow rate, $\dot{w}_f$, entering the combustion chamber which regulates the thrust. The throttle logic will be discussed further in the next chapter. Once $\dot{w}_f$ is determined, $\dot{w}_a$, V_{exit}, and p_{exit} in Eq. (2.61) are functions of M and α. Again, the data for this model is in tabular form.

2.5.3 Coast Phase. As previously mentioned, the coast phase can occur twice during a missile flight. The first time it occurs is between the rocket and the RAMJET boost phases. The duration is for 0.2 seconds and allows for the transition of power modes. The next time the coast phase can occur is if intercept has not happened prior to the expenditure of the fuel to sustain the RAMJET propulsion. In either situation, the drag induced by the aerodynamic effects over the inlet, D_i of the RAMJET is given by

$$D_i = C_{d_i} Q_o A_o \tag{2.62}$$

where

$$C_{d_i} = \text{the coefficient of induced drag.}$$

C_{d_i} is a function of M and α and is in tabular form for the missile model. This table was generated by wind tunnel testing.

III. Guidance and Control

3.1 Guidance

The VFDR uses a mixed guidance strategy to guide it to the target. The lateral guidance is a proportional navigation command. The horizontal guidance is a combination of a Mach command and a gravity command. The vertical guidance is a combination of a loft command, a proportional navigation command and a gravity command. This section will describe the guidance of the VFDR and derive the line of sight parameters for proportional navigation. Commands not generated by proportional navigation will then be discussed. Proportional navigation guidance results in an acceleration command in the velocity axis system proportional to the angular rate of change of the line-of sight vector, $\boldsymbol{\omega}_{LOS}$, from the missile to the target. N is called the proportional navigation constant. Therefore, the commands generated to guide the missile are proportional to the angular velocity of the missile relative to the target by a factor of N. Generally, N ranges from 2 to 6 which implies that the missile develops a lead angle on the target (9). If $N = 1$, then the resulting missile accelerations will alter the relative velocity between the missile and the target and drive the line of sight rate to zero and if $N < 1$, the missile will lag behind the target (3:262). Differentiating the velocity vector with respect to time, Eq. (3.1), yields the desired acceleration vector, $\mathbf{a_m}$, of the missile in terms of the angular velocity of line of sight vector.

$$\begin{aligned}
\mathbf{a_m} &= \left.\frac{d\mathbf{V}}{dt}\right|_E \\
&= \left.\frac{d\mathbf{V}}{dt}\right|_V + N\boldsymbol{\omega}_{LOS} \times \mathbf{V} \\
&= \dot{V}\hat{x}_V + N\boldsymbol{\omega}_{LOS} \times \mathbf{V}.
\end{aligned} \tag{3.1}$$

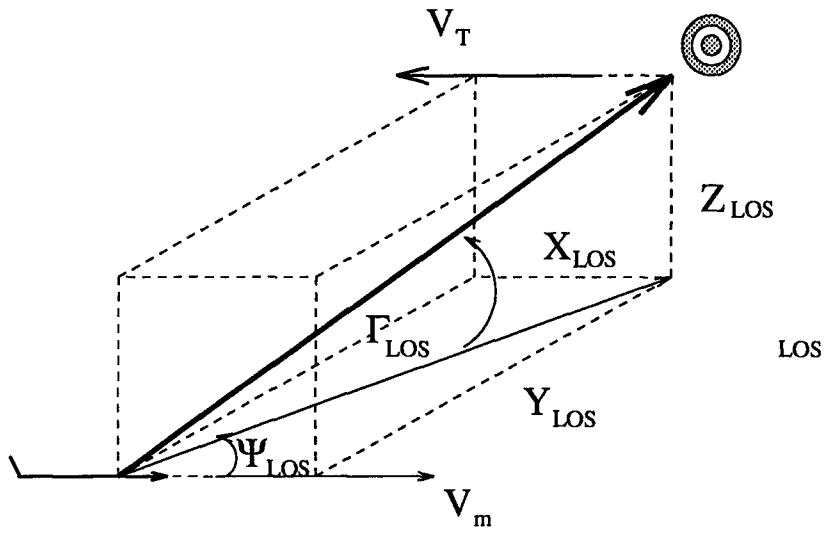

Figure 3.1 Typical Missile-Target Intercept Scenario

Taking the cross product of the final term in Eq. (3.1) yields

$$N\boldsymbol{\omega}_{LOS} \times \mathbf{V} = \begin{vmatrix} \hat{x}_V & \hat{y}_V & \hat{z}_V \\ N\omega_x & N\omega_y & N\omega_z \\ V_m & 0 & 0 \end{vmatrix} = \begin{bmatrix} 0 \\ V_m N\omega_z \\ -V_m N\omega_y \end{bmatrix}$$
$$= \dot{V}_m \hat{x}_V + V_m N\omega_z \hat{y}_V - V_m N\omega_y \hat{z}_V \tag{3.2}$$

Normalizing the acceleration vector, $\mathbf{a_m}$, with respect to gravity yields

$$\frac{\mathbf{a_m}}{g} = \mathbf{n_m}$$
$$= \frac{\dot{V}_m}{g}\hat{x}_V + \frac{V_m N\omega_z}{g}\hat{y}_V - \frac{V_m N\omega_y}{g}\hat{z}_V \tag{3.3}$$

Specific expressions for ω_y and ω_z in Eq. (3.3) are developed by examining the line of sight parameters between the missile and the target. Note that ω_x does not appear in Eq. (3.2). Figure 3.1 shows a general three-dimensional missile target game. Before expressions can be obtained for ω_y and ω_z in Eq. (3.2), some initial definitions must be made for the components of distance from the target to the missile and the

components of relative velocity from the missile to the target.

$$x_{LOS} \equiv x_T - x_m \tag{3.4}$$

$$y_{LOS} \equiv y_T - y_m \tag{3.5}$$

$$z_{LOS} \equiv h_T - h_m \tag{3.6}$$

$$V_{x_{LOS}} \equiv \dot{x}_T - V_m \cos\psi_m \cos\gamma_m \tag{3.7}$$

$$V_{y_{LOS}} \equiv \dot{y}_T - V_m \sin\psi_m \cos\gamma_m \tag{3.8}$$

$$V_{z_{LOS}} \equiv \dot{h}_T - V_m \sin\gamma_m \tag{3.9}$$

where the subscript T denotes the target and m denotes the missile. From the definitions in Eqs (3.4) through (3.9), the range along the line of sight, R_{LOS}, can be expressed as

$$\|R_{LOS}\| = \left(x_{LOS}^2 + y_{LOS}^2 + z_{LOS}^2\right)^{\frac{1}{2}}. \tag{3.10}$$

The closing velocity, V_{close} can be expressed as

$$\begin{aligned} V_{close} &= -\frac{\mathbf{R_{LOS}} \bullet \mathbf{V_{LOS}}}{\|R_{LOS}\|} \\ &= \frac{[\,x_{LOS} \quad y_{LOS} \quad z_{LOS}\,] \bullet [\,V_{x_{LOS}} \quad V_{y_{LOS}} \quad V_{z_{LOS}}\,]^T}{\|R_{LOS}\|}. \end{aligned} \tag{3.11}$$

Dividing the line of sight range by the closing velocity, an estimation for the time remaining until intercept, t_{go} is expressed as

$$t_{go} = \frac{\|R_{LOS}\|}{V_{close}}. \tag{3.12}$$

Referring to Fig 3.1, the rate of change of the position vector from the missile to the target can be described by a cross range angular velocity, $\dot{\psi}_{LOS}$, and an angular rate of change from the horizontal, $\dot{\gamma}_{LOS}$. The total angular velocity of the line of sight vector is

$$\boldsymbol{\omega}_{LOS} = \dot{\psi}_{LOS}\hat{z}_E - \dot{\gamma}_{LOS}\hat{y}_{E1}. \tag{3.13}$$

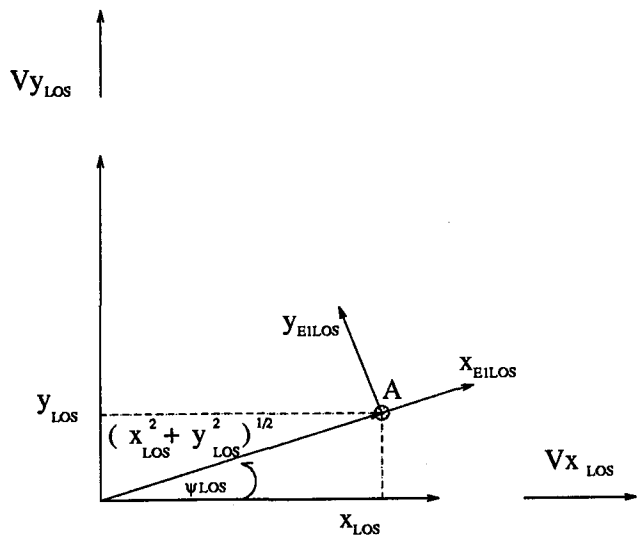

Figure 3.2 Line of Sight Geometry for the $x_{LOS} - y_{LOS}$ Plane

Specific expressions for $\dot{\psi}_{LOS}$ and $\dot{\gamma}_{LOS}$ in terms of the definitions for the line of sight parameters are required to generate the necessary guidance commands in Eq. (3.3) to intercept the target. Examining the $x_{LOS} - y_{LOS}$ plane, ψ_{LOS} is shown in Fig 3.2 along with the tangential and normal components of the line of sight velocity vector in the plane. $V_{x_{LOS}}$ and $V_{y_{LOS}}$ are the line of sight components in the x_{LOS} and y_{LOS} directions, respectively. Resolving the velocity vectors into their x_{E1} and y_{E1} components yields

$$\begin{bmatrix} V_{x_{LOS}E1} \\ V_{y_{LOS}E1} \\ V_{z_{LOS}E1} \end{bmatrix} = \begin{bmatrix} \cos\psi_{LOS} & \sin\psi_{LOS} & 0 \\ -\sin\psi_{LOS} & \cos\psi_{LOS} & 0 \\ 0 & 0 & 1 \end{bmatrix} \begin{bmatrix} V_{xLOS} \\ V_{yLOS} \\ V_{zLOS} \end{bmatrix}$$
$$= \begin{bmatrix} V_{x_{LOS}} \cos\psi_{LOS} + V_{y_{LOS}} \sin\psi_{LOS} \\ -V_{x_{LOS}} \sin\psi_{LOS} + V_{y_{LOS}} \cos\psi_{LOS} \\ V_{z_{LOS}} \end{bmatrix}. \tag{3.14}$$

The line of sight velocity component in the y_{E1} direction is the tangential velocity of point A that is being swept by the radius $(x_{LOS}^2 + y_{LOS}^2)^{\frac{1}{2}}$ with angular velocity

$\dot{\psi}_{LOS}$. Equating the two expressions for the velocity of point A yields

$$\left(x_{LOS}^2 + y_{LOS}^2\right)^{\frac{1}{2}} \dot{\psi}_{LOS} = V_{y_{LOS}} \cos\psi_{LOS} - V_{x_{LOS}} \sin\psi_{LOS}. \tag{3.15}$$

Therefore, $\dot{\psi}_{LOS}$ can be expressed as

$$\dot{\psi}_{LOS} = \frac{V_{y_{LOS}} \cos\psi_{LOS} - V_{x_{LOS}} \sin\psi_{LOS}}{(x_{LOS}^2 + y_{LOS}^2)^{\frac{1}{2}}}. \tag{3.16}$$

Noting from the geometry in Fig 3.2 that

$$\cos\psi_{LOS} = \frac{x_{LOS}}{(x_{LOS}^2 + y_{LOS}^2)^{\frac{1}{2}}}$$
$$\sin\psi_{LOS} = \frac{y_{LOS}}{(x_{LOS}^2 + y_{LOS}^2)^{\frac{1}{2}}}$$

the expression for $\dot{\psi}_{LOS}$ becomes

$$\dot{\psi}_{LOS} = \frac{V_{y_{LOS}} x_{LOS} - V_{x_{LOS}} y_{LOS}}{x_{LOS}^2 + y_{LOS}^2}. \tag{3.17}$$

The rotation due to the γ_{LOS} is shown in Fig 3.3.

$$\begin{bmatrix} V_{x_{LOS}V} \\ V_{y_{LOS}V} \\ V_{z_{LOS}V} \end{bmatrix} = \begin{bmatrix} \cos\gamma & 0 & \sin\gamma \\ 0 & 1 & 0 \\ -\sin\gamma & 0 & \cos\gamma \end{bmatrix} \begin{bmatrix} V_{x_{LOS}} \cos\psi_{LOS} + V_{y_{LOS}} \sin\psi_{LOS} \\ -V_{x_{LOS}} \sin\psi_{LOS} + V_{y_{LOS}} \cos\psi_{LOS} \\ V_{z_{LOS}} \end{bmatrix}$$
$$= \begin{bmatrix} (V_{x_{LOS}} \cos\psi_{LOS} + V_{y_{LOS}} \sin\psi_{LOS}) \cos\gamma + V_{z_{LOS}} \sin\gamma \\ -V_{x_{LOS}} \sin\psi_{LOS} + V_{y_{LOS}} \cos\psi_{LOS} \\ -(V_{x_{LOS}} \cos\psi_{LOS} + V_{y_{LOS}} \sin\psi_{LOS}) \sin\gamma + V_{z_{LOS}} \cos\gamma \end{bmatrix} \tag{3.18}$$

As before, the tangential components of velocity are equated

$$R_{LOS}\dot{\gamma}_{LOS} = V_{z_{LOS}} \cos\gamma - (V_{x_{LOS}} \cos\psi_{LOS} + V_{y_{LOS}} \sin\psi_{LOS}) \sin\gamma. \tag{3.19}$$

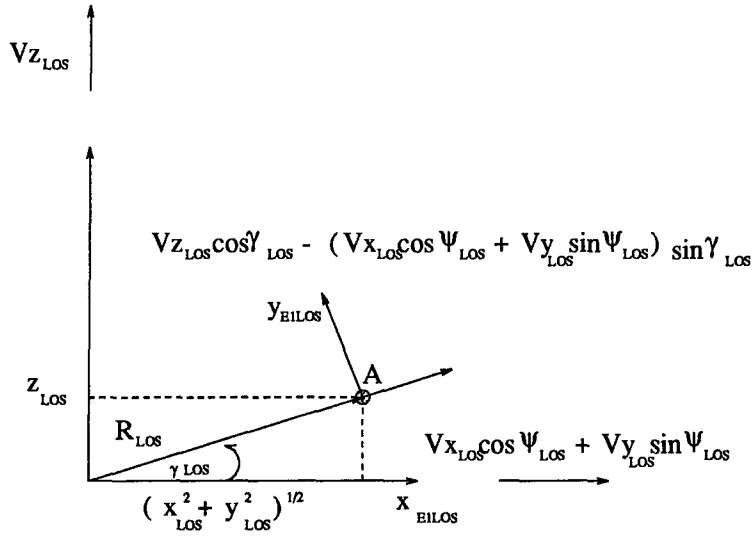

Figure 3.3 Line of Sight Geometry for the $x_{LOSE1} - z_{LOS}$ Plane

Dividing by R_{LOS}, $\dot{\gamma}_{LOS}$ is expressed as

$$\dot{\gamma}_{LOS} = \frac{V_{z_{LOS}} \cos\gamma - (V_{x_{LOS}} \cos\psi_{LOS} + V_{y_{LOS}} \sin\psi_{LOS}) \sin\gamma}{R_{LOS}}. \tag{3.20}$$

Noting from the geometry in Fig 3.3

$$\cos\gamma_{LOS} = \frac{(x_{LOS}^2 + y_{LOS}^2)^{\frac{1}{2}}}{R_{LOS}}$$
$$\sin\gamma_{LOS} = \frac{z_{LOS}}{R_{LOS}}$$

and substituting expressions for $\cos\psi_{LOS}$ and $\sin\psi_{LOS}$, $\dot{\gamma}_{LOS}$ can be expressed by

$$\begin{aligned}\dot{\gamma}_{LOS} &= \frac{V_{z_{LOS}} (x_{LOS}^2 + y_{LOS}^2)^{\frac{1}{2}}}{R_{LOS}^2} - \frac{V_{x_{LOS}} x_{LOS} z_{LOS}}{(x_{LOS}^2 + y_{LOS}^2)^{\frac{1}{2}} R_{LOS}^2} \\ &\quad - \frac{V_{y_{LOS}} y_{LOS} z_{LOS}}{(x_{LOS}^2 + y_{LOS}^2)^{\frac{1}{2}} R_{LOS}^2} \\ &= \frac{V_{z_{LOS}} (x_{LOS}^2 + y_{LOS}^2) - z_{LOS} (V_{x_{LOS}} x_{LOS} + V_{y_{LOS}} y_{LOS})}{(x_{LOS}^2 + y_{LOS}^2)^{\frac{1}{2}} R_{LOS}^2}.\end{aligned} \tag{3.21}$$

Recall the angular line of sight velocity vector

$$\boldsymbol{\omega}_{LOS} = \dot{\psi}_{LOS}\hat{z}_E - \dot{\gamma}_{LOS}\hat{y}_{E1} \tag{3.22}$$

Rotating $\dot{\psi}_{LOS}\hat{z}_E$ to the intermediate coordinate system yields

$$\begin{aligned}\begin{bmatrix}\hat{x}_{E1}\\ \hat{y}_{E1}\\ \hat{z}_{E1}\end{bmatrix} &= \begin{bmatrix}\cos\psi & \sin\psi & 0\\ -\sin\psi & \cos\psi & 0\\ 0 & 0 & 1\end{bmatrix}\begin{bmatrix}0\\ 0\\ \dot{\psi}_{LOS}\end{bmatrix}\\ &= \begin{bmatrix}0\\ 0\\ \dot{\psi}_{LOS}\end{bmatrix}.\end{aligned} \tag{3.23}$$

The line of sight angular velocity rate becomes

$$\boldsymbol{\omega}_{LOS}{}_{E1} = \dot{\psi}_{LOS}\hat{z}_{E1} - \dot{\gamma}_{LOS}\hat{y}_{E1}. \tag{3.24}$$

Rotating to the velocity axis system produces

$$\begin{aligned}\boldsymbol{\omega}_{LOS}{}_{V} &= \begin{bmatrix}\cos\gamma & 0 & \sin\gamma\\ 0 & 1 & 0\\ -\sin\gamma & 0 & \cos\gamma\end{bmatrix}\begin{bmatrix}0\\ -\dot{\gamma}_{LOS}\\ \dot{\psi}_{LOS}\end{bmatrix}\\ &= \begin{bmatrix}\dot{\psi}_{LOS}\sin\gamma\\ -\dot{\gamma}_{LOS}\\ \dot{\psi}_{LOS}\cos\gamma\end{bmatrix}\end{aligned} \tag{3.25}$$

The angular rate of change in the velocity axis of the line of sight vector is given by Eq. (3.25). Therefore,

$$\omega_y = -\dot{\gamma}_{LOS} \tag{3.26}$$

$$\omega_z = \dot{\psi}_{LOS}\cos\gamma \tag{3.27}$$

are the expressions required to generate a proportional navigation command. Recall Eq. (3.3) for the proportional navigation command vector

$$\boldsymbol{n}_m = \frac{\dot{V}_m}{g}\hat{x}_V + \frac{V_m N \omega_z}{g}\hat{y}_V - \frac{V_m N \omega_y}{g}\hat{z}_V. \tag{3.28}$$

Substituting Eqs. (3.26) and (3.27) yields

$$\boldsymbol{n}_m = \frac{\dot{V}_m}{g}\hat{x}_V + \frac{V_m N \dot{\psi}_{LOS} \cos\gamma}{g}\hat{y}_V + \frac{V_m N \dot{\gamma}_{LOS}}{g}\hat{z}_V \tag{3.29}$$

which is the dimensionless command vector. The proportional navigation command vector used is

$$\boldsymbol{g}_{cmdP/N} = \begin{bmatrix} 0 \\ \frac{V_m N \dot{\psi}_{LOS} \cos\gamma}{g} \\ \frac{V_m N \dot{\gamma}_{LOS}}{g} \end{bmatrix}. \tag{3.30}$$

Proportional navigation is not the only command used to guide the missile. The other commands employed by the VFDR will be examined. Only proportional navigation is used in the lateral, $\hat{y}_v$, direction. Therefore, the total g_{cmd_y} is given by

$$g_{cmd_y} = g_{cmdp/n_y} = \frac{V_m N \dot{\psi}_{LOS} \cos\gamma}{g} \tag{3.31}$$

where

$$g_{cmd_y} = \text{the total command in the } \hat{y}_v \text{ direction.} \tag{3.32}$$

The command in the horizontal direction is a combination of a command to control the Mach number and a command to counter the effects of gravity. The Mach command, g_{mach_x} is generated first comparing a desired Mach number to the actual Mach number of the missile;

$$M_{cmd} - M = \Delta M \tag{3.33}$$

where

$$M_{cmd} = \text{desired Mach number}$$

$$M = \text{actual Mach number}$$

$$\Delta M = \text{delta Mach number, desired - actual.}$$

The VFDR uses a fixed M_{cmd} for the desired Mach number. ΔM is multiplied by the speed of sound to obtain a delta velocity. The delta velocity is divided by a time constant and gravity to produce a dimensionless g_{mach_x}. g_{mach_x} can be expressed by

$$g_{mach_x} = (M_{cmd} - M)\frac{a}{\tau_M g} \tag{3.34}$$

where

$$a = \text{the speed of sound}$$

$$\tau_M = \text{the time constant}$$

$$g = \text{gravity}$$

The total g_{cmd_x} is a combination of g_{mach_x} and a command to counter the effects of gravity.

$$\boldsymbol{g}_V = \mathbf{T_{EV}} \begin{bmatrix} 0 \\ 0 \\ -g \end{bmatrix} \tag{3.35}$$

$$= \begin{bmatrix} -g\sin\gamma \\ 0 \\ -g\cos\gamma \end{bmatrix} \tag{3.36}$$

Making g_{Vx} dimensionless and opposite to the gravity term yields

$$g_{cmdg_x} = \sin\gamma. \tag{3.37}$$

The total command in the horizontal direction is expressed by

$$\begin{aligned} g_{cmd_x} &= g_{mach_x} + g_{cmdg_x} \\ &= (M_{cmd} - M)\frac{a}{\tau_M g} + \sin\gamma. \end{aligned} \tag{3.38}$$

ENGAGE does not use the actual value of the speed of sound in air. ENGAGE approximates the speed of sound and assumes it is constant with $a = 304.3$ m/sec (998.2 ft/sec).

The commands in the vertical direction, $\hat{z}_v$, are a combination of proportional navigation, gravity effect, and a loft command. The proportional navigation command is expressed in Eq. (3.30)

$$g_{cmdP/N_z} = \frac{VN\dot{\gamma}_{LOS}}{g}. \tag{3.39}$$

The command to counteract the effect of gravity in the $\hat{z}_v$ direction is determined by examining the $\boldsymbol{g}_V$ vector.

$$\begin{aligned} \boldsymbol{g}_V &= \mathbf{T_{EV}} \begin{bmatrix} 0 \\ 0 \\ -g \end{bmatrix} \\ &= \begin{bmatrix} -g\sin\gamma \\ 0 \\ -g\cos\gamma \end{bmatrix} \end{aligned} \tag{3.40}$$

which can be expressed as a dimensionless command by dividing by gravity

$$g_{cmdg_z} = \cos\gamma. \tag{3.41}$$

The loft command is employed to increase the altitude of the missile. g_{loft} is the control that is unknown in the formulation of the optimization problem. The total

g_{cmd_z} vector is expressed as

$$\begin{aligned} g_{cmd_z} &= g_{cmdP/N_z} + g_{cmdg_z} + g_{loft} \\ &= \frac{VN\dot{\gamma}_{LOS}}{g} + \cos\gamma + g_{loft}. \end{aligned} \tag{3.42}$$

3.2 Control

This section describes the control logic for the fuel flow rate of the RAMJET engine, the missile roll control, and the missile pitch control.

3.2.1 Fuel Flow Rate Control. The throttle logic accomplishes three things. First, it prevents the pressure inside the combustion chamber, station 3 in Fig. 2.11, from getting too large. In turn, this prevents too large a pressure at the inlet. Excessive pressure at the inlet would prevent sufficient air flow to support combustion. Second, the throttle logic maintains $\dot{w}_f$ between a minimum and maximum value. Decreasing $\dot{w}_f$ too low will cause a flame out. Increasing $\dot{w}_f$ too much will result in wasted fuel since exceeding the stoichiometric fuel air ratio will cause fuel to be exhausted without being converted to energy by the combustion process. Third, the throttle logic will prevent the missile from exceeding a maximum velocity. For sustainment of propulsion in the combustor, the air flow rate must not blow the flame out the rear of the engine. This can happen if the velocity of the air through the combustor is too large.

3.2.2 Roll Control. A block diagram of the roll control for the missile is pictured in Fig. 3.4. The control logic is simply a feedback of the actual roll angle, σ, using static gains. From the diagram,

$$\dot{\sigma} = \frac{C_\sigma}{1 + C_\sigma F_\sigma}(\sigma_{cmd} - \sigma) \tag{3.43}$$

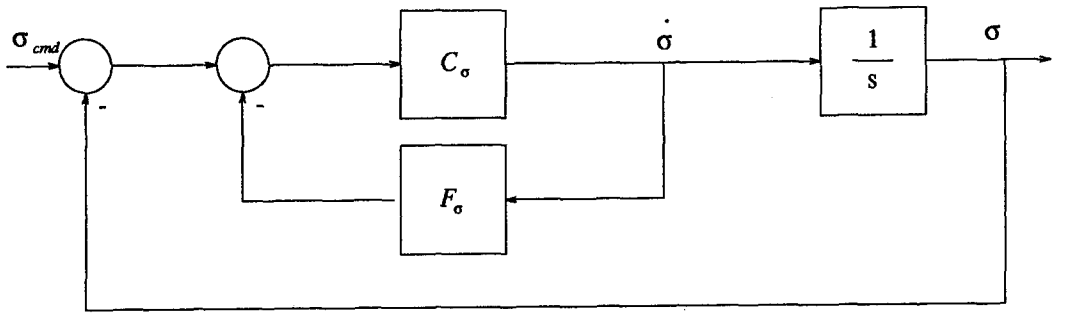

Figure 3.4 Block Diagram of Roll Control

where

$$\dot{\sigma} = \text{the roll rate of the missile,}$$

$$\sigma_{cmd} = \text{the roll command,}$$

$$C_\sigma = \text{the feedforward gain, and,}$$

$$F_\sigma = \text{the feedback gain.}$$

Defining τ_σ as

$$\frac{1}{\tau_\sigma} \equiv \frac{C_\sigma}{1 + F_\sigma C_\sigma} \tag{3.44}$$

Eq. (3.43) is reduced to

$$\dot{\sigma}(t) = \frac{1}{\tau_\sigma}\|\sigma_{cmd}\| u_{-1}(t - t_o) - \frac{1}{\tau_\sigma}\sigma(t) \tag{3.45}$$

where

$$\|\sigma_{cmd}\| = \text{the magnitude of input}$$

$$u_{-1} = \text{the unit step function}$$

where

$$u_{-1}(t-t_o) = \begin{cases} 0, t < t_o \\ 1, t > t_o \end{cases}.$$

Taking the Laplace transform of both sides yields

$$s\sigma(s) - \sigma(0) + \frac{1}{\tau_\sigma}\sigma(s) = \frac{1}{\tau_\sigma}\frac{e^{-st_o}}{s}\|\sigma_{cmd}\|. \tag{3.46}$$

Collecting terms, the expression becomes

$$\left(s + \frac{1}{\tau_\sigma}\right)\sigma(s) = \frac{1}{\tau_\sigma}\frac{e^{-st_o}}{s}\|\sigma_{cmd}\| + \sigma(0) \tag{3.47}$$

or, in terms of $\sigma(s)$

$$\sigma(s) = \frac{1}{\tau_\sigma}\frac{e^{-st_o}\|\sigma_{cmd}\|}{s\left(s+\frac{1}{\tau_\sigma}\right)} + \frac{\sigma(0)}{s+\frac{1}{\tau_\sigma}}. \tag{3.48}$$

The first term on the right side of the equation can be expanded in partial fractions to yield

$$\begin{aligned} \frac{A}{s} + \frac{B}{s+\frac{1}{\tau_\sigma}} &= \frac{A\left(s+\frac{1}{\tau_\sigma}\right) + Bs}{s\left(s+\frac{1}{\tau_\sigma}\right)} \\ &= \frac{\frac{1}{\tau_o}\|\sigma_{cmd}\|}{s\left(s+\frac{1}{\tau_\sigma}\right)} \end{aligned} \tag{3.49}$$

A and B are determined from the above expression to be

$$A = \|\sigma_{cmd}\| \tag{3.50}$$

$$B = -\|\sigma_{cmd}\|. \tag{3.51}$$

Substituting these values for A and B yields

$$\sigma(s) = \frac{\|\sigma_{cmd}\|}{s}e^{-st_o} - \frac{\|\sigma_{cmd}\|}{\left(s+\frac{1}{\tau_\sigma}\right)}e^{-st_o} + \frac{\sigma(0)}{\left(s+\frac{1}{\tau_\sigma}\right)}. \tag{3.52}$$

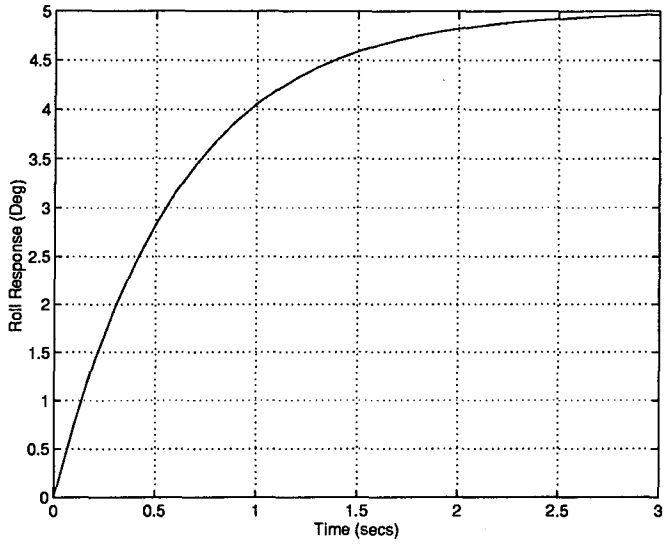

Figure 3.5 Roll Response to a 5 Degree Step Command

Inverting, σ as a function of time becomes

$$\sigma(t) = \sigma(0)e^{-\frac{1}{\tau_\sigma}t} + \|\sigma_{cmd}\|u_{-1}(t-t_o) - \|\sigma_{cmd}\|e^{-\frac{1}{\tau_\sigma}t}u_{-1}(t-t_o). \qquad (3.53)$$

The expression for $\sigma(t)$ is continuous for all time, however $\dot{\sigma}(t)$ is discontinuous at time t_o. Therefore, the commanded value of roll is achieved by a continuous change in σ rather than by a discrete step. The first two terms on the right side of the expression are the zero state solution (7:7). The final term is the zero input solution (7:8) and assumes the response is due to initial energy in the system and the input is zero. For a linear system as the roll control for the missile, the complete response is just a linear superposition of the zero input and the zero state response (7:9). The roll response for a step input of 5° is shown in Fig 3.5 assuming the input occurs at $t_o = 0$ and $\sigma_o = 0°$.

To determine σ_{cmd}, the command vector in the velocity axis is transformed to the missile body axis system.

$$\boldsymbol{g}_{cmd_B} = \boldsymbol{T}_{VB}\boldsymbol{g}_{cmd_V}$$

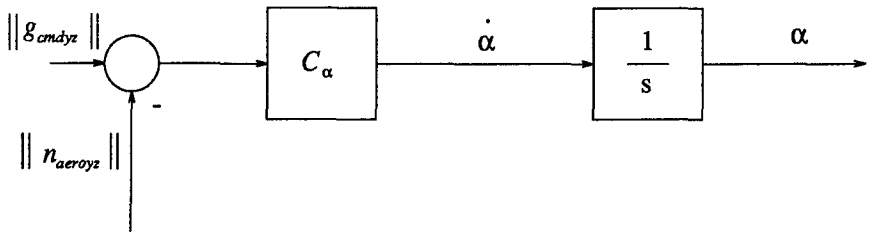

Figure 3.6 Block Diagram of Pitch Control

$$
\begin{aligned}
&= \boldsymbol{T}_{VS}\boldsymbol{T}_{SB}\boldsymbol{g}_{cmd_V} \\
&= \begin{bmatrix} g_{cmd_x}\cos\alpha + \left(g_{cmd_y}\sin\sigma + g_{cmd_z}\cos\sigma\right)\sin\alpha \\ g_{cmd_y}\cos\sigma - g_{cmd_z}\sin\sigma \\ -g_{cmd_x}\sin\alpha + \left(g_{cmd_y}\sin\sigma + g_{cmd_z}\cos\sigma\right)\cos\alpha \end{bmatrix}. \qquad (3.54)
\end{aligned}
$$

However, for a BTT missile the following must be true:

$$g_{cmd_{y_B}} = 0 = g_{cmd_y}\cos\sigma - g_{cmd_z}\sin\sigma. \qquad (3.55)$$

The expression for σ_{cmd} is therefore

$$\sigma_{cmd} = \arctan\left(\frac{g_{cmd_y}}{g_{cmd_z}}\right). \qquad (3.56)$$

3.2.3 Pitch Control. The pitch control of the VFDR is accomplished through the deflection of control surfaces on the tail. The deflections cause the rotation of the body to a new angle-of-attack and lift is generated by the wings and the body (9:18). The angle of attack of the missile changes proportionally to the difference between the magnitude of the commanded acceleration in the velocity $y_V - z_V$ plane and the actual acceleration in the velocity $y_V - z_V$ plane. A block diagram of the pitch control is pictured in Fig 3.6. Therefore,

$$\dot{\alpha} = \|g_{cmdyz}\| - \|n_{aeroyz}\|. \qquad (3.57)$$

The magnitude of g_{cmdyz} is given by

$$\|g_{cmdyz}\| = \left(g_{cmd_y}^2 + g_{cmd_z}^2\right)^{\frac{1}{2}} \tag{3.58}$$

and the magnitude of the actual acceleration is given by

$$\begin{aligned}
\|n_{aeroyz}\| &= \left[\left(\frac{F_{Vy}}{W}\right)^2 + \left(\frac{F_{Vz}}{W} + \cos\gamma\right)^2\right]^{\frac{1}{2}} \\
&= \left[\left\{\left(\frac{F_T}{W}\sin\alpha + \frac{L}{W}\right)\sin\sigma + \left(\frac{F_T}{W}\cos\alpha\sin\beta + \frac{S}{W}\right)\cos\sigma\right\}^2\right. \\
&\quad \left. + \left\{\left(\frac{F_T}{W}\sin\alpha + \frac{L}{W}\right)\cos\sigma - \left(\frac{F_T}{W}\cos\alpha\sin\beta + \frac{S}{W}\right)\sin\sigma\right\}^2\right]^{\frac{1}{2}} \qquad (3.59)
\end{aligned}$$

Recalling that $S = 0$ and $\beta = 0$ for the VFDR, the equation reduces to

$$\begin{aligned}
\|n_{aeroyz}\| &= \left[\left(\frac{T}{W}\sin\alpha + \frac{L}{W}\right)^2\left(\sin^2\sigma + \cos^2\sigma\right)\right]^{\frac{1}{2}} \\
&= \left\|\frac{T}{W}\sin\alpha + \frac{L}{W}\right\| \qquad (3.60)
\end{aligned}$$

The pitch control is an open loop system and integrates the command. A bounded input does not produce bounded output. An angle of attack response for a 1g delta command is pictured in Fig 3.7. As is the case with the roll control logic, the pitch control logic produces a continuous change in the angle of attack so discontinuities in α do not exist.

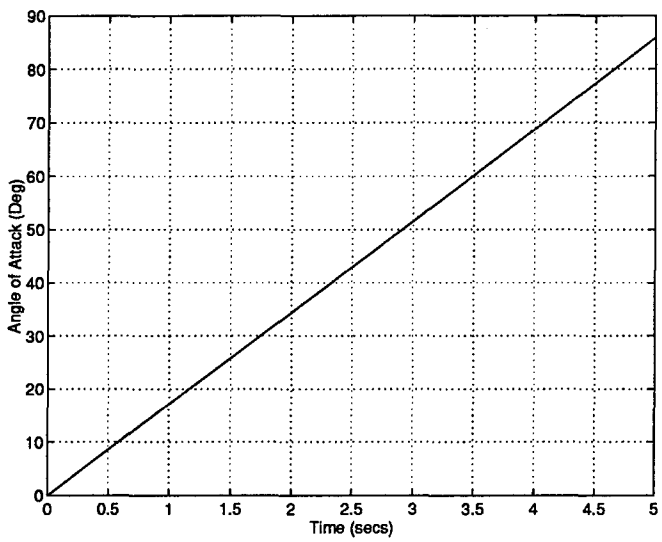

Figure 3.7 Angle of Attack Response to 1g Command

IV. Analysis of Simulation

Upon completion of the modeling, the simulation was coded into MATLAB^{TM}. Two baseline test flights were used for comparison and the results of ENGAGE were not duplicated for flight based solely on proportional navigation. For the first test flight, the missile and target are initially at the same altitude and relative cross range; the flight is in a vertical plane. Figure 4.1 depicts the scenario. The target flies a constant altitude profile and is non accelerating at an air speed of 0.9 Mach. The missile is launched with an initial speed of 0.9 Mach and is pointing directly at the target. For the second test flight, the target is at a lower altitude and a different cross range position than the missile. Table 4.1 summarizes the initial conditions and the results for the two flights. The states for the first flight are shown in Figs 4.2 and 4.3. The solid lines indicate the simulation results from the MATLAB^{TM} code and the dashed lines represent the results obtained from ENGAGE. An error exists between the two simulations. The states for the second test case are shown in Figs 4.4 and 4.5. Again, an error is noticeable.

During the course of comparing results to those obtained from ENGAGE, two errors were found in the original code of ENGAGE. The first error was in the model of the atmosphere. Recall the two expressions obtained for density depending upon

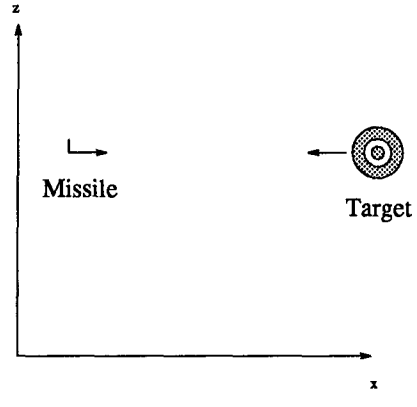

Figure 4.1 Initial Conditions of Baseline Simulation

	Flight 1		Flight 2	
	Missile	Target	Missile	Target
Down Range (km)	0	27.8	0	18.5
Cross Range (km)	0	0	0	9.26
Altitude (m)	6098	6098	6098	4573
Mach Number	0.9	0.9	0.9	0.9
Flight Path Angle (Deg)	0	0	0	0
Heading Angle (Deg)	0	-180	0	-180
Intercept Time (Sec)	24.76		21.10	
R_{LOS} (m)	2.03		0.640	

Table 4.1 Initial Conditions and Results for Baseline Simulations

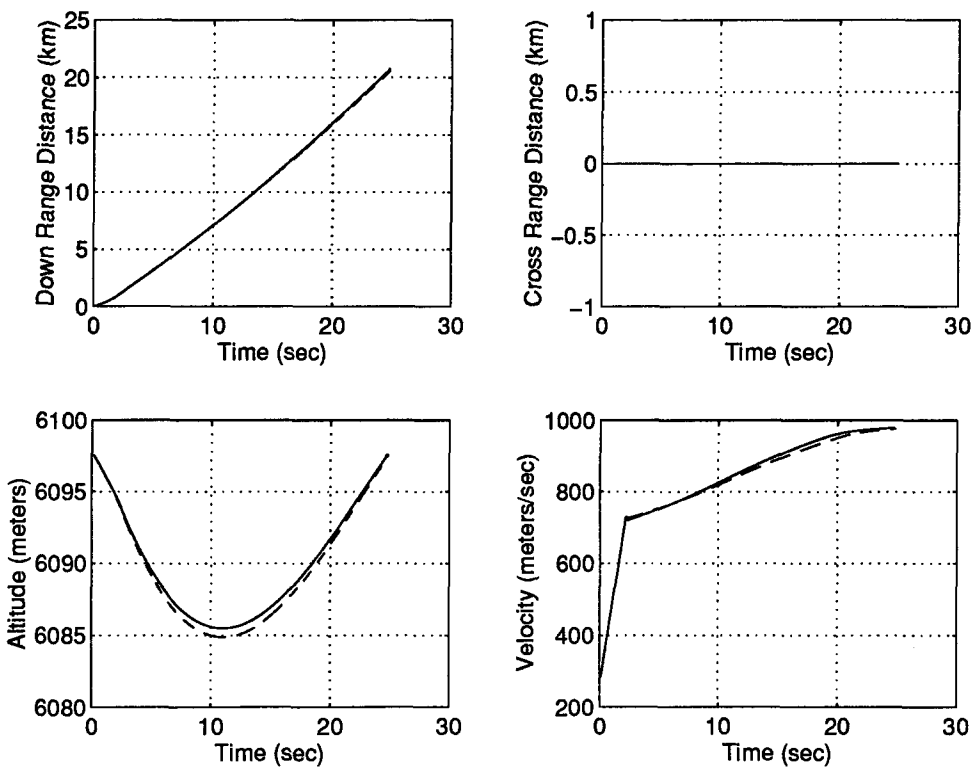

Figure 4.2 x_E, y_E, z_E and V Simulation Comparisons for Flight 1

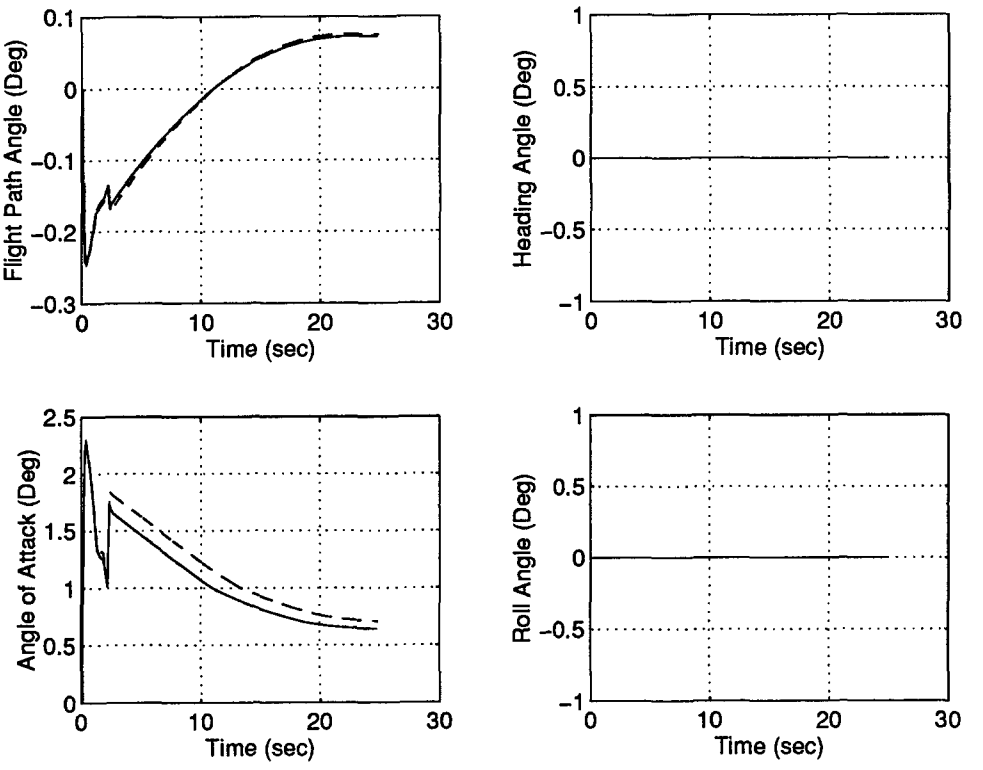

Figure 4.3 γ, ψ, α and σ Simulation Comparisons for Flight 1

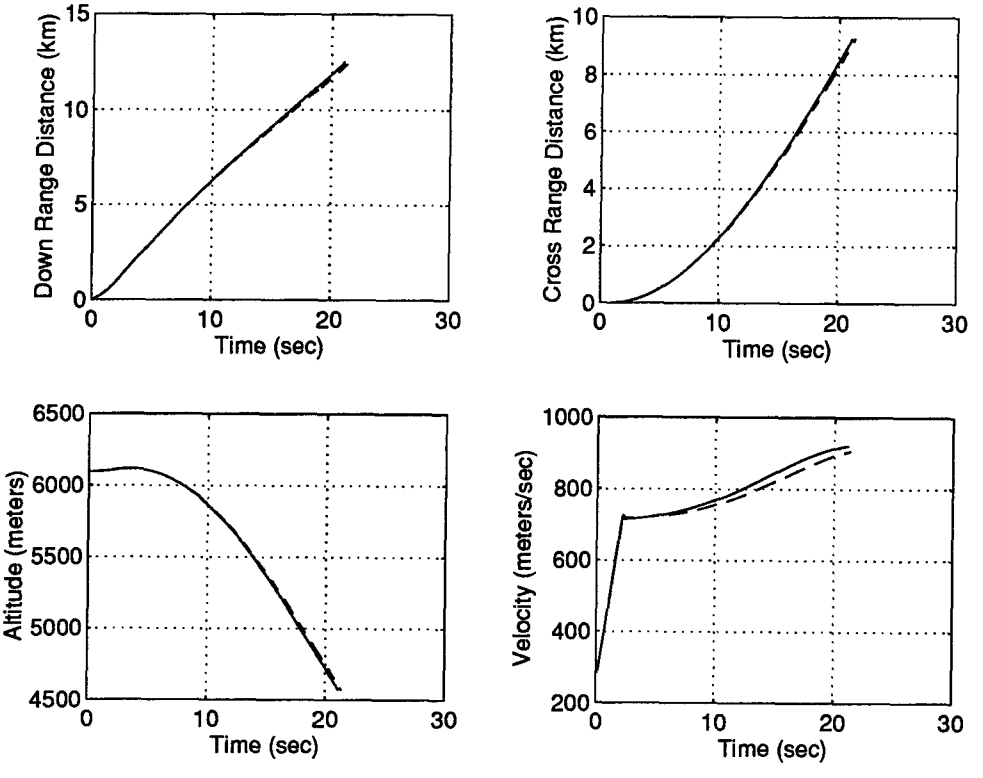

Figure 4.4 x_E, y_E, z_E and V Simulation Comparisons for Flight 2

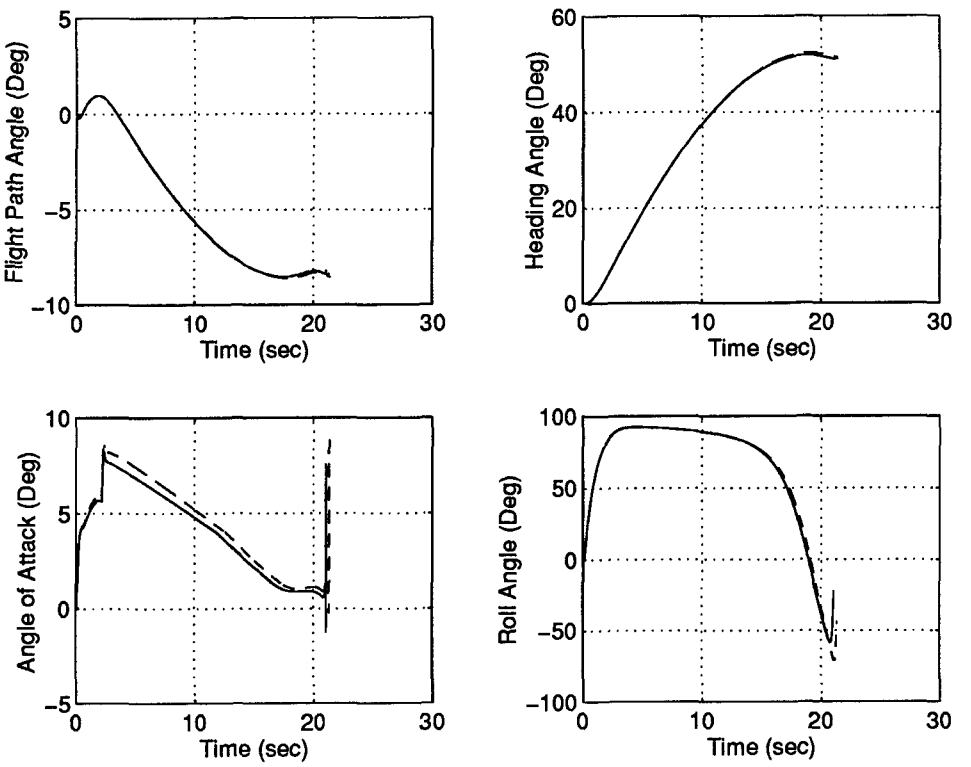

Figure 4.5 γ, ψ, α and σ Simulation Comparisons for Flight 2

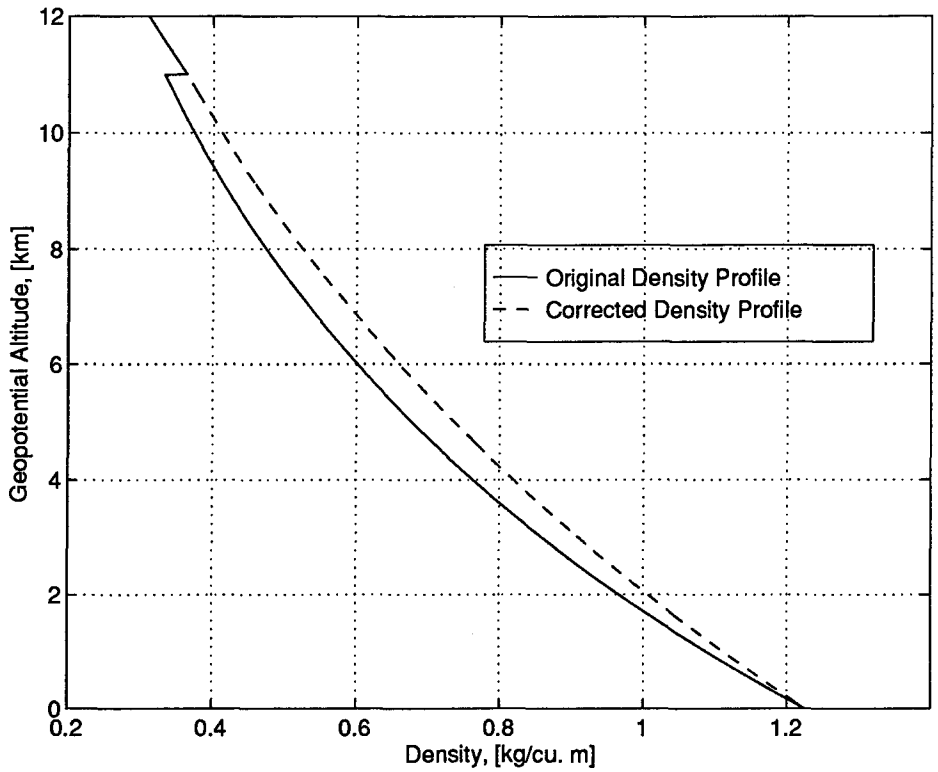

Figure 4.6 Density as a Function of Altitude

the characteristics of temperature for the local region; Eq. (2.15) and Eq. (2.16).

$$\rho_o = \rho_b \left(\frac{T_o}{T_b}\right)^{-\left(1+\frac{g}{R\zeta}\right)} \text{ for } \frac{dT}{dh_G} \neq 0, \text{ and,}$$
$$\rho_o = \rho_b e^{-\frac{g(h_G - h_b)}{RT_b}} \text{ for } \frac{dT}{dh_G} = 0.$$

The first expression is used to approximate air density in regions that temperature is characterized as varying linearly with altitude, Fig 2.1. The second expression is used within regions that temperature is constant with altitude.

ENGAGE utilizes the expression for density valid only in isothermal regions. Figure 4.6 shows the density calculated with both equations. Figure 4.7 shows the percent error between the correct expression and the incorrect expression. Notice that near the top of the gradient region the error is almost 10.0 percent. The density

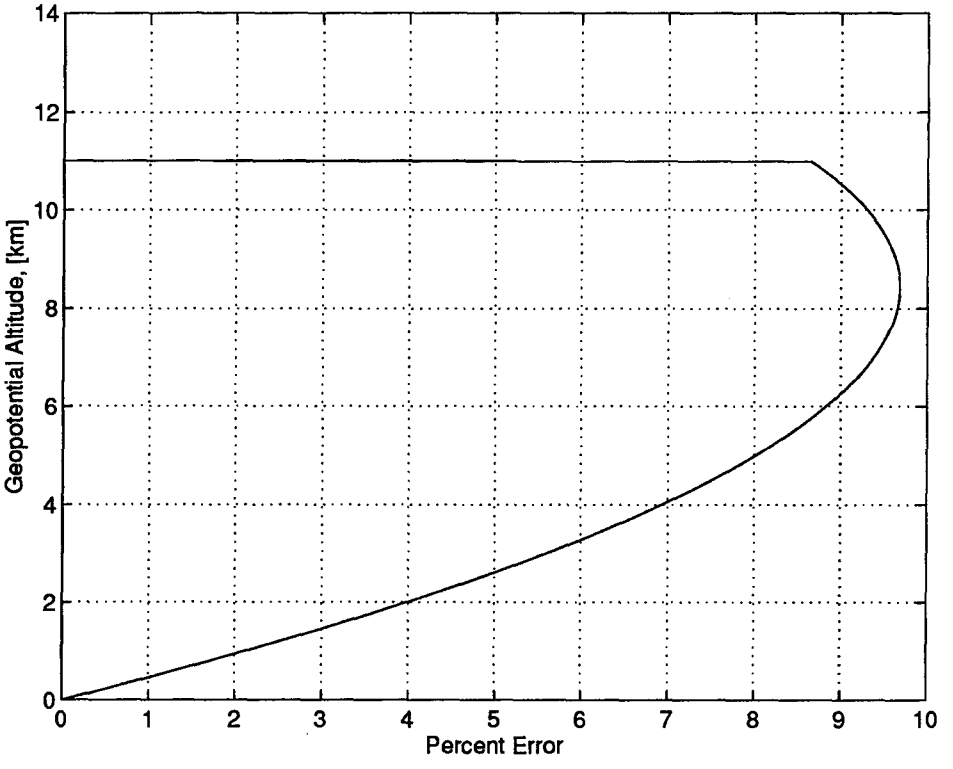

Figure 4.7 Percent Error in the Density Value

value is used to determine the aerodynamic forces acting on the missile; Eqs. (2.54) and (2.57) where

$$Q_o = \frac{1}{2}\rho V^2. \tag{4.1}$$

Hence, the aerodynamic forces acting on the missile in a region of the atmosphere that temperature is modeled as varying with altitude will be in error and this error could be a high as 9.7 percent at 8,400 m.

The throttle control logic during the RAMJET boost phase requires the density of the air in determining the maximum airflow rate through the engine. The maximum airflow rate information is then utilized in the determination of the fuelflow rate. Consequently, an incorrect density value will result in an improper thrust level.

The thrust calculated during the rocket boost phase will also have an associated error due to the density error. Recall Eq. (2.59), the thrust for the rocket boost phase,

$$F_T = T_{sl} + A_{exit}(p_{sl} - p). \tag{4.2}$$

Due to the error in the density calculation, the atmospheric pressure calculated will be lower than the actual atmospheric pressure. Hence, the thrust value calculated in ENGAGE will be too large.

A second error was discovered in the line of sight algorithm of ENGAGE. Recall from Eq. (3.21) that

$$\begin{aligned}\dot{\gamma}_{LOS} = &\frac{1}{R_{LOS}^2\left(x_{LOS}^2 + y_{LOS}^2\right)^{\frac{1}{2}}}\left\{V_{z_{LOS}}\left(x_{LOS}^2 + y_{LOS}^2\right)\right.\\ &\left.-z_{LOS}\left(V_{x_{LOS}}x_{LOS} + V_{y_{LOS}}y_{LOS}\right)\right\}.\end{aligned}$$

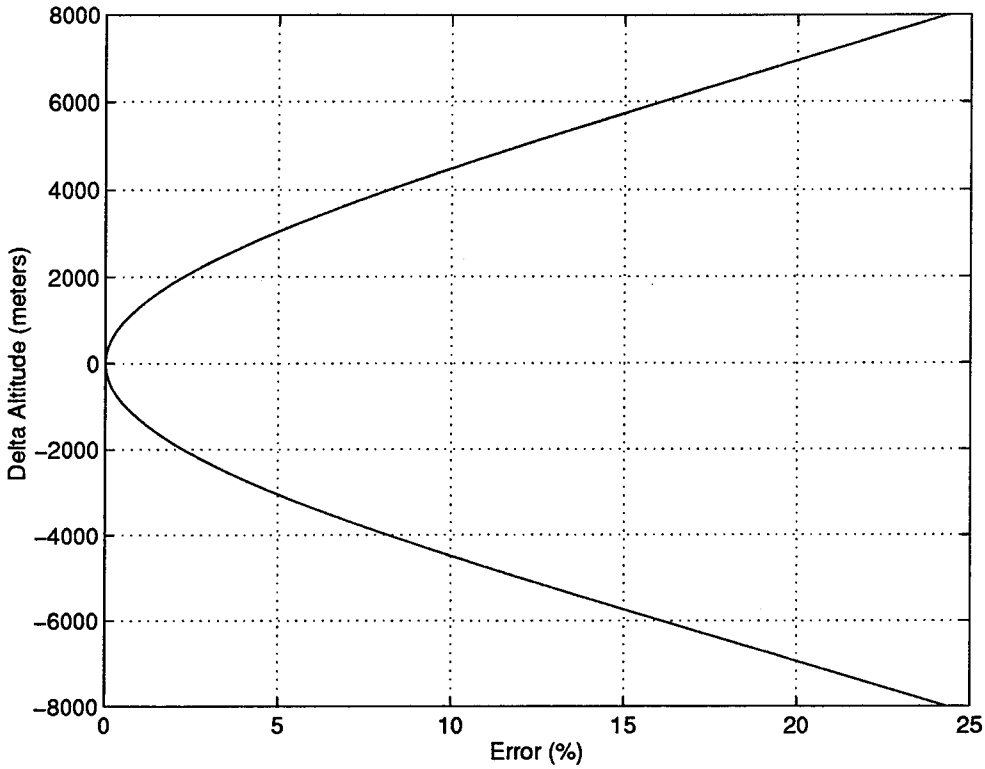

Figure 4.8 Percent Error in $\dot{\gamma}_{LOS}$

ENGAGE calculated $\dot{\gamma}_{LOS}$ as

$$\dot{\gamma}_{LOS} = \frac{1}{R_{LOS}^2 \left(x_{LOS}^2 + y_{LOS}^2 + 2z_{LOS}^2\right)^{\frac{1}{2}}} \left\{ V_{z_{LOS}} \left(x_{LOS}^2 + y_{LOS}^2\right) \right.$$
$$\left. - z_{LOS} \left(V_{x_{LOS}} x_{LOS} + V_{y_{LOS}} y_{LOS}\right) \right\}.$$

Upon inspection, an error between the two expressions for $\dot{\gamma}_{LOS}$ occurs when the target and missile are not at the same altitude. The relative error between the two expressions is shown in Fig 4.8. The x_{LOS} and y_{LOS} values were both fixed at 9.3 km and z_{LOS} was varied from -8 to 8 km. Recall the proportional navigation command in the vertical direction:

$$g_{cmd_{P/N_z}} = \frac{VN\dot{\gamma}_{LOS}}{g}.$$

The command is proportional to $\dot{\gamma}_{LOS}$. Hence, ENGAGE generated less of a vertical proportional navigation command. Figure 4.8 depicts the percentage decrease of the proportional command.

The errors noticed in Figs 4.2 through 4.5 are a combination of these two errors. Modifying the MATLAB^{TM} code to recreate the errors, the simulations agreed and the missile still intercepted the target. The MATLAB^{TM} simulation can interface with computer workstations so that numerical techniques can be employed to optimize the missile's performance.

V. The Optimal Control Problem

5.1 Necessary Conditions For a Minimum

This chapter describes the necessary conditions for the standard optimal control problem with free final time (2:71) (5:155). Consider a dynamic system described by a set of differential equations with known initial time, t_o, in the form of

$$\dot{\boldsymbol{x}} = \boldsymbol{f}(\boldsymbol{x}, \boldsymbol{u}, t) \tag{5.1}$$

where,

$$\begin{aligned} \boldsymbol{x} &= \text{ an } n \times 1 \text{ vector of the state variables,} \\ \boldsymbol{u} &= \text{ an } m \times 1 \text{ vector of control variables, and} \\ t_o, \boldsymbol{x}_o &= \text{ known.} \end{aligned}$$

The system is subject to p constraints on the terminal conditions of the state variables, q constraints on the state variables, and r constraints on the control variables, so the constraints can be expressed by

$$\Psi_i(\boldsymbol{x}_f, t_f) = 0 \text{ for } i = 1 \ldots p, \tag{5.2}$$

$$S_i(\boldsymbol{x}, t) = 0 \text{ for } i = 1 \ldots q, \text{ and} \tag{5.3}$$

$$C_i(\boldsymbol{u}, t) = 0 \text{ for } i = 1 \ldots r. \tag{5.4}$$

The problem is to determine a function $\boldsymbol{u}(t)$ which minimizes a scalar performance index, J, subject to the conditions stated in Eqs (5.1) through Eq. (5.4). The performance index is given by

$$J = \Phi(\boldsymbol{x}_f, t_f) + \int_{t_o}^{t_f} L(\boldsymbol{x}, \boldsymbol{u}, t) dt. \tag{5.5}$$

The performance index is adjoined with the system differential equations, Eq. (5.1), by introducing Lagrange multipliers, $\boldsymbol{\lambda}(t)$, as a multiplier function. Similarly, the constraints, Eqs (5.2) through (5.4), are also adjoined to the performance index with additional Lagrange multipliers, $\boldsymbol{\nu}(t)$, $\boldsymbol{\theta}(t)$, and $\boldsymbol{\mu}(t)$. Therefore, the augmented performance index, J', is given by,

$$J' = G(t_f, \boldsymbol{x}_f, \boldsymbol{\nu}) + \int_{t_o}^{t_f} \left[H\left(t, \boldsymbol{x}, \boldsymbol{u}, \boldsymbol{\lambda}, \boldsymbol{\theta}, \boldsymbol{\mu}\right) - \boldsymbol{\lambda}^T \dot{\boldsymbol{x}} \right] dt \tag{5.6}$$

where the Bolza function, G, and the variational Hamiltonian, H (5:156), are defined as

$$\begin{aligned} G(t_f, \boldsymbol{x}_f, \boldsymbol{\nu}) &= \Phi(t_f, \boldsymbol{x}_f) + \boldsymbol{\nu}^T \boldsymbol{\Psi}(t_f, \boldsymbol{x}_f), \\ H(t, \boldsymbol{x}, \boldsymbol{u}, \boldsymbol{\lambda}, \boldsymbol{\theta}, \boldsymbol{\mu}) &= L(t, \boldsymbol{x}, \boldsymbol{u}) + \boldsymbol{\lambda}^T \boldsymbol{f}(\boldsymbol{x}, t, \boldsymbol{u}) + \boldsymbol{\theta}^T \boldsymbol{S}(\boldsymbol{x}, t) + \boldsymbol{\mu}^T \boldsymbol{C}(\boldsymbol{u}, t). \end{aligned}$$

Furthermore, the constraints can be of an equality or inequality type. For inequality constraints, slack variables, $\boldsymbol{l}$, are introduced. For example, assume a control $\boldsymbol{u}$ is limited to some maximum value, $\boldsymbol{u}_{max}$. The constraint equation is,

$$\boldsymbol{u} \leq \boldsymbol{u}_{max}. \tag{5.7}$$

The new constraint equation is expressed by Eq. (5.8),

$$\boldsymbol{u} - \boldsymbol{u}_{max} + \boldsymbol{l}^2 = \boldsymbol{0} \tag{5.8}$$

The inequality constraint is now an equality constraint because any value of $\boldsymbol{u}$ greater than $\boldsymbol{u}_{max}$ will never satisfy Eq. (5.8) for real valued $\boldsymbol{l}$. When $\boldsymbol{l}$ is zero, the control is at the constraint value. When $\boldsymbol{l}$ is not zero, $\boldsymbol{\mu}$ is identically zero. A potential drawback is there exists another unknown variable. Note the Hamiltonian is now a

function of $\boldsymbol{l}$ also. Thus,

$$H(t,\boldsymbol{x},\boldsymbol{u},\boldsymbol{\lambda},\boldsymbol{\theta},\boldsymbol{\mu},\boldsymbol{l}) = L(t,\boldsymbol{x},\boldsymbol{u}) + \boldsymbol{\lambda}^T\boldsymbol{f}(\boldsymbol{x},t,\boldsymbol{u}) + \boldsymbol{\theta}^T\boldsymbol{S}(\boldsymbol{x},t) + \boldsymbol{\mu}^T\boldsymbol{C}(\boldsymbol{u},t,\boldsymbol{l}) \quad (5.9)$$

and the augmented performance index becomes

$$J' = G(t_f,\boldsymbol{x}_f,\boldsymbol{\nu}) + \int_{t_o}^{t_f}\left[H\left(t,\boldsymbol{x},\boldsymbol{u},\boldsymbol{\lambda},\boldsymbol{\theta},\boldsymbol{\mu},\boldsymbol{l}\right) - \boldsymbol{\lambda}^T\dot{\boldsymbol{x}}\right]dt. \quad (5.10)$$

The first variation of the augmented performance index is given by

$$\begin{aligned}\delta J' = {} & G_{t_f}\delta t_f + \boldsymbol{G}_{x_f}\delta\boldsymbol{x}_f + \boldsymbol{G}_\nu\delta\boldsymbol{\nu} \\ & + \int_{t_o}^{t_f}\{\boldsymbol{H}_x\tilde{\delta}\boldsymbol{x} + \boldsymbol{H}_u\tilde{\delta}\boldsymbol{u} + \boldsymbol{H}_\lambda\tilde{\delta}\boldsymbol{\lambda} + \boldsymbol{H}_\theta\tilde{\delta}\boldsymbol{\theta} + \boldsymbol{H}_\mu\tilde{\delta}\boldsymbol{\mu} + \boldsymbol{H}_l\tilde{\delta}\boldsymbol{l} - \dot{\boldsymbol{x}}^T\tilde{\delta}\boldsymbol{\lambda} - \boldsymbol{\lambda}^T\tilde{\delta}\dot{\boldsymbol{x}}\}dt \\ & +[H - \boldsymbol{\lambda}^T\dot{\boldsymbol{x}}]\delta t\,|_{t_o}^{t_f} \end{aligned} \quad (5.11)$$

where the notation implies

$$\begin{aligned} ()_y &= \frac{\partial()}{\partial y}, \\ ()_{t_f} &= \frac{\partial()}{\partial t} \text{ evaluated at } t = t_f, \\ \delta() &= \text{a time free variation}, \\ \tilde{\delta}() &= \text{a time fixed variation}. \end{aligned}$$

The last term in Eq. (5.11) can be evaluated at t_o and t_f as

$$[H - \boldsymbol{\lambda}^T\dot{\boldsymbol{x}}]\delta t\,|_{t_o}^{t_f} = (H_f - \boldsymbol{\lambda}_f^T\dot{\boldsymbol{x}}_f)\delta t_f - (H_o - \boldsymbol{\lambda}_o^T\dot{\boldsymbol{x}}_o)\delta t_o. \quad (5.12)$$

The initial time is known, hence δt_o is zero. Therefore, the final term on the right in Eq. (5.12) is eliminated. Eliminating this term, the variation of the augmented

performance index becomes

$$\delta J' = G_{t_f}\delta t_f + \boldsymbol{G}_{x_f}\delta \boldsymbol{x}_f + \boldsymbol{G}_\nu \delta \boldsymbol{\nu} + (H_f - \boldsymbol{\lambda}_f^T \dot{\boldsymbol{x}}_f)\delta t_f$$
$$+ \int_{t_o}^{t_f} \{\boldsymbol{H}_x \tilde{\delta}\boldsymbol{x} + \boldsymbol{H}_u \tilde{\delta}\boldsymbol{u} + \boldsymbol{H}_\lambda \tilde{\delta}\boldsymbol{\lambda} + \boldsymbol{H}_\theta \tilde{\delta}\boldsymbol{\theta} + \boldsymbol{H}_\mu \tilde{\delta}\boldsymbol{\mu} + \boldsymbol{H}_l \tilde{\delta}\boldsymbol{l} - \dot{\boldsymbol{x}}^T \tilde{\delta}\boldsymbol{\lambda} - \boldsymbol{\lambda}^T \tilde{\delta}\dot{\boldsymbol{x}}\} dt. \tag{5.13}$$

Recall the constraint equations given by Eqs (5.2) through (5.4). Recognizing

$$\boldsymbol{G}_\nu = \boldsymbol{\Psi}(\boldsymbol{x}_f, t_f) = 0 \tag{5.14}$$

$$\boldsymbol{H}_\theta = \boldsymbol{S}(\boldsymbol{x}, t) = 0 \tag{5.15}$$

$$\boldsymbol{H}_\mu = \boldsymbol{C}(\boldsymbol{u}, t) = 0 \tag{5.16}$$

eliminates $\boldsymbol{G}_\nu \delta \boldsymbol{\nu}$, $\boldsymbol{H}_\theta \tilde{\delta}\boldsymbol{\theta}$ and $\boldsymbol{H}_\mu \tilde{\delta}\boldsymbol{\mu}$ from Eq. (5.13). Thus, the variation of the augmented performance index is now expressed as

$$\delta J' = G_{t_f}\delta t_f + \boldsymbol{G}_{x_f}\delta \boldsymbol{x}_f + (H_f - \boldsymbol{\lambda}_f^T \dot{\boldsymbol{x}}_f)\delta t_f$$
$$+ \int_{t_o}^{t_f} \left\{\boldsymbol{H}_x \tilde{\delta}\boldsymbol{x} + \boldsymbol{H}_u \tilde{\delta}\boldsymbol{u} + \boldsymbol{H}_l \tilde{\delta}\boldsymbol{l} + (\boldsymbol{H}_\lambda - \dot{\boldsymbol{x}}^T)\tilde{\delta}\boldsymbol{\lambda} - \boldsymbol{\lambda}^T \tilde{\delta}\dot{\boldsymbol{x}}\right\} dt. \tag{5.17}$$

Noting $\boldsymbol{H}_\lambda = \boldsymbol{f}^T$ and recalling Eq. (5.1), the terms multiplied by $\tilde{\delta}\boldsymbol{\lambda}$ reduce to

$$\boldsymbol{H}_\lambda - \dot{\boldsymbol{x}}^T = \boldsymbol{f}^T - \dot{\boldsymbol{x}}^T = \dot{\boldsymbol{x}}^T - \dot{\boldsymbol{x}}^T = 0. \tag{5.18}$$

Hence, the term multiplied by $\tilde{\delta}\boldsymbol{\lambda}$ is always zero. Substituting Eq. (5.18) into Eq. (5.17) yields

$$\delta J' = G_{t_f}\delta t_f + \boldsymbol{G}_{x_f}\delta \boldsymbol{x}_f + (H_f - \boldsymbol{\lambda}_f^T \dot{\boldsymbol{x}}_f)\delta t_f$$
$$+ \int_{t_o}^{t_f} \{\boldsymbol{H}_x \tilde{\delta}\boldsymbol{x} + \boldsymbol{H}_u \tilde{\delta}\boldsymbol{u} + \boldsymbol{H}_l \tilde{\delta}\boldsymbol{l} - \boldsymbol{\lambda}^T \tilde{\delta}\dot{\boldsymbol{x}}\} dt. \tag{5.19}$$

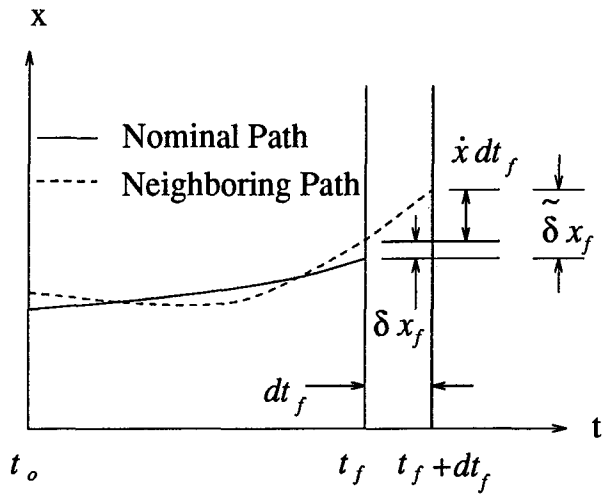

Figure 5.1 Relationship Between $\tilde{\delta}\boldsymbol{x}_f$, $\delta\boldsymbol{x}_f$, and $\dot{\boldsymbol{x}}_f\delta t$

The last term in the integral in Eq. (5.11) can be integrated by parts in the following fashion,

$$\int_{t_o}^{t_f} -\boldsymbol{\lambda}^T\tilde{\delta}\dot{\boldsymbol{x}} = -\boldsymbol{\lambda}_f^T\tilde{\delta}\boldsymbol{x}_f + \boldsymbol{\lambda}_o^T\tilde{\delta}\boldsymbol{x}_o + \int_{t_o}^{t_f} -\dot{\boldsymbol{\lambda}}^T\tilde{\delta}\boldsymbol{x}dt. \tag{5.20}$$

Therefore, substituting the above information into Eq. (5.11), $\delta J'$ can now be expressed by

$$\begin{aligned}\delta J' &= G_{t_f}\delta t_f + \boldsymbol{G}_{x_f}\delta\boldsymbol{x}_f - \boldsymbol{\lambda}_f^T\tilde{\delta}\boldsymbol{x}_f + \boldsymbol{\lambda}_o^T\tilde{\delta}\boldsymbol{x}_o \\ &+ (H_f - \boldsymbol{\lambda}_f^T\dot{\boldsymbol{x}}_f)\delta t_f + \int_{t_o}^{t_f}[(\boldsymbol{H}_x + \dot{\boldsymbol{\lambda}}^T)\tilde{\delta}\boldsymbol{x} + \boldsymbol{H}_u\tilde{\delta}\boldsymbol{u} + \boldsymbol{H}_l\tilde{\delta}\boldsymbol{l}]dt.\end{aligned} \tag{5.21}$$

The relationship between the final time free variation and the final time fixed variation is

$$\tilde{\delta}\boldsymbol{x}_f = \delta\boldsymbol{x}_f - \dot{\boldsymbol{x}}_f\delta t. \tag{5.22}$$

This relationship is presented graphically in Fig 5.1. Also, since the initial conditions are known,

$$\tilde{\delta}\boldsymbol{x}_o = 0 \Rightarrow \boldsymbol{\lambda}_o^T\tilde{\delta}\boldsymbol{x}_o = 0. \tag{5.23}$$

Substituting Eq. (5.22) and Eq. (5.23) into Eq. (5.21) yields

$$\delta J' = G_{t_f}\delta t_f + \boldsymbol{G}_{x_f}\delta \boldsymbol{x}_f + \boldsymbol{\lambda}_f^T \dot{\boldsymbol{x}}_f \delta t_f - \boldsymbol{\lambda}_f^T \delta \boldsymbol{x}_f + [H_f - \boldsymbol{\lambda}_f^T \dot{\boldsymbol{x}}_f]\delta t_f$$
$$+ \int_{t_o}^{t_f} [(\boldsymbol{H}_x + \dot{\boldsymbol{\lambda}}^T)\tilde{\delta}\boldsymbol{x} + \boldsymbol{H}_u \tilde{\delta}\boldsymbol{u} + \boldsymbol{H}_l \tilde{\delta}\boldsymbol{l}]dt.$$

Collecting terms and noting $\boldsymbol{\lambda}_f^T \dot{\boldsymbol{x}} - \boldsymbol{\lambda}_f^T \dot{\boldsymbol{x}} = 0$ yields

$$\delta J' = (G_{t_f} + H_f)\delta t_f + (\boldsymbol{G}_{x_f} - \boldsymbol{\lambda}_f^T)\delta \boldsymbol{x}_f$$
$$+ \int_{t_o}^{t_f} [(\boldsymbol{H}_x + \dot{\boldsymbol{\lambda}}^T)\tilde{\delta}\boldsymbol{x} + \boldsymbol{H}_u \tilde{\delta}\boldsymbol{u} + \boldsymbol{H}_l \tilde{\delta}\boldsymbol{l}]dt. \tag{5.24}$$

For an extremal, the variation of J' must be zero. Additionally, each variation is independent yielding the free final time necessary conditions for an extremal;

$$H_f = -G_{t_f} \tag{5.25}$$
$$\boldsymbol{\lambda}_f = \boldsymbol{G}_{x_f}^T \tag{5.26}$$
$$\dot{\boldsymbol{\lambda}} = -\boldsymbol{H}_x^T \tag{5.27}$$
$$\boldsymbol{H}_u = \boldsymbol{0} \tag{5.28}$$
$$\boldsymbol{H}_l = \boldsymbol{0} \tag{5.29}$$
$$\boldsymbol{\Psi} = \boldsymbol{S} = \boldsymbol{C} = \boldsymbol{0} \tag{5.30}$$
$$t_o = t_{os} \tag{5.31}$$
$$\boldsymbol{x}_o = \boldsymbol{x}_{os} \tag{5.32}$$
$$\dot{\boldsymbol{x}} = \boldsymbol{f}. \tag{5.33}$$

Equations (5.25) through (5.33) provide the necessary conditions for an extremal.

The Weierstrass condition and the Legendre-Clebsch condition are two sufficient conditions for a minimum (5:106). The Weierstrass condition is necessary for a strong relative minimum. This condition states that no other control can produce a lower value of the Hamiltonian than the optimal control. More precisely, the

Weierstrass condition states that for any control u_* other than the optimal control u

$$H(t, \boldsymbol{x}, u_*, \boldsymbol{\lambda}) - H(t, \boldsymbol{x}, u, \boldsymbol{\lambda}) \geq 0. \tag{5.34}$$

The Legendre-Clebsch condition is sufficient for only a weak relative minimum. The weak variation is a particular case of a strong variation and is applicable only for small variations in the control. The Legendre-Clebsch condition requires

$$\boldsymbol{H}_{uu} \geq 0. \tag{5.35}$$

When the Weierstrass condition is satisfied, the Legendre-Clebsch condition is automatically satisfied. However, the Weierstrass condition is not necessarily satisfied if the Legendre-Clebsch condition is satisfied. When the Legendre-Clebsch condition is not satisfied, the Weierstrass condition will not be satisfied.

5.2 Shooting Method

The shooting method is an algorithm that provides a numerical solution to a two-point boundary-value problem. Hence, if the optimal control problem can be converted into a two-point boundary-value problem, the shooting method can be used to provide a numerical solution. Recall the necessary conditions for the free final time problem;

$$\dot{\boldsymbol{x}} = \boldsymbol{f} \tag{5.36}$$

$$\dot{\boldsymbol{\lambda}} = -\boldsymbol{H}_x^T \tag{5.37}$$

$$t_o = t_{os} \tag{5.38}$$

$$\boldsymbol{x}_o = \boldsymbol{x}_{os} \tag{5.39}$$

$$H_f = -G_{t_f} \tag{5.40}$$

$$\mathbf{0} = \boldsymbol{H}_u \tag{5.41}$$

$$\boldsymbol{\lambda}_f = \boldsymbol{G}_{x_f}^T \tag{5.42}$$

$$\boldsymbol{H}_l = \mathbf{0} \tag{5.43}$$

$$\boldsymbol{\Psi} = \boldsymbol{S} = \boldsymbol{C} = \mathbf{0}. \tag{5.44}$$

The Lagrange multipliers adjoined to the constraints, $\boldsymbol{\nu}$, $\boldsymbol{\theta}$ and $\boldsymbol{\mu}$ and the slack variables, $\boldsymbol{l}$, are eliminated through the solutions to Eqs (5.40) through (5.44). The control, $\boldsymbol{u}$, is expressed as a function of $\boldsymbol{x}$, $\boldsymbol{\lambda}$, and t from the solution to Eq. (5.41). Hence the problem is reduced to a function of $\boldsymbol{x}$, $\boldsymbol{\lambda}$, and t. The necessary conditions become

$$\dot{\boldsymbol{x}} = \boldsymbol{F}_1\left(t, \boldsymbol{x}, \boldsymbol{\lambda}\right) \tag{5.45}$$

$$\dot{\boldsymbol{\lambda}} = \boldsymbol{F}_2\left(t, \boldsymbol{x}, \boldsymbol{\lambda}\right) \tag{5.46}$$

$$\boldsymbol{h}\left(t_f, \boldsymbol{x}_f, \boldsymbol{\lambda}_f\right) = 0 \tag{5.47}$$

$$t_o = t_{os} \tag{5.48}$$

$$\boldsymbol{x}_o = \boldsymbol{x}_{os} \tag{5.49}$$

A new vector is defined that is a combination of $\boldsymbol{x}$ and $\boldsymbol{\lambda}$

$$\boldsymbol{z} \equiv \begin{bmatrix} \boldsymbol{x} \\ \boldsymbol{\lambda} \end{bmatrix}. \tag{5.50}$$

Therefore, the necessary conditions are restated in terms of this new definition as

$$\dot{\boldsymbol{z}} = \boldsymbol{F}\left(t, \boldsymbol{z}\right) \tag{5.51}$$

$$t_o = t_{os} \tag{5.52}$$

$$\boldsymbol{z}_o = \begin{bmatrix} \boldsymbol{x}_o \\ \boldsymbol{\lambda}_o \end{bmatrix} \tag{5.53}$$

$$\boldsymbol{h}\left(t_f, \boldsymbol{z}_f\right) = \mathbf{0}. \tag{5.54}$$

$\boldsymbol{z}$ is a vector of length $2n$ where n is the number of original states. n of the initial conditions of $\boldsymbol{z}$ are known (i.e. $\boldsymbol{x}_o$). Equation (5.54) gives the $2n + 1$ terminal conditions for $\boldsymbol{z}_f$ and t_f. The conditions stated in Eqs (5.51) through (5.54) represent a standard two-point boundary-value problem. The n unknown initial $\boldsymbol{z}$ values and a final time are guessed and the shooting method iteratively updates the unknown initial $\boldsymbol{z}$ (i.e. $\boldsymbol{\lambda}_o$) and t_f until Eq. (5.54) is satisfied to within a specified tolerance. Therefore, a method is required to update the initial guesses.

Taking the first variation of Eq. (5.51) yields

$$\tilde{\delta}\dot{\boldsymbol{z}} = \boldsymbol{F}_z \tilde{\delta}\boldsymbol{z} \tag{5.55}$$

$$\frac{d}{dt}\tilde{\delta}\boldsymbol{z} = \boldsymbol{F}_z \tilde{\delta}\boldsymbol{z}. \tag{5.56}$$

Recall the definition for $\boldsymbol{z}$ and that the initial conditions for $\boldsymbol{x}$ are known. Therefore, the total variation of $\boldsymbol{z}$ at the initial time is

$$\tilde{\delta}\boldsymbol{z}_o = \begin{bmatrix} \tilde{\delta}\boldsymbol{x}_o \\ \tilde{\delta}\boldsymbol{\lambda}_o \end{bmatrix} \tag{5.57}$$

$$= \begin{bmatrix} \boldsymbol{0} \\ \tilde{\delta}\boldsymbol{\lambda}_o \end{bmatrix}. \tag{5.58}$$

Assume the initial guesses are in the neighborhood of the actual values. A state transition matrix, $\boldsymbol{\Phi}$, is introduced to relate the total variation of $\boldsymbol{z}$ at any time to the initial total variation of $\boldsymbol{z}$. Using $\boldsymbol{\Phi}$, $\tilde{\delta}\boldsymbol{z}$ is expressed by

$$\tilde{\delta}\boldsymbol{z} = \boldsymbol{\Phi}\left(t, t_o\right) \tilde{\delta}\boldsymbol{z}_o \tag{5.59}$$

and the initial condition on $\boldsymbol{\Phi}$ is

$$\boldsymbol{\Phi}\left(t_o, t_o\right) = \boldsymbol{I}. \tag{5.60}$$

Substituting Eq. (5.59) into Eq. (5.56) yields

$$\frac{d}{dt}\left[\boldsymbol{\Phi}\left(t,t_o\right)\tilde{\delta}\boldsymbol{z}_o\right] = \boldsymbol{F}_z\boldsymbol{\Phi}\left(t,t_o\right)\tilde{\delta}\boldsymbol{z}_o \tag{5.61}$$

$$\dot{\boldsymbol{\Phi}}\left(t,t_o\right)\tilde{\delta}\boldsymbol{z}_o = \boldsymbol{F}_z\boldsymbol{\Phi}\left(t,t_o\right)\tilde{\delta}\boldsymbol{z}_o. \tag{5.62}$$

Equation (5.62) reduces to another set of differential equations

$$\dot{\boldsymbol{\Phi}}\left(t,t_o\right) = \boldsymbol{F}_z\boldsymbol{\Phi}\left(t,t_o\right) \tag{5.63}$$

with the initial condition

$$\boldsymbol{\Phi}(t_o,t_o) = \boldsymbol{I}. \tag{5.64}$$

This equation is integrated from t_o to t_f to yield an expression for the final total variation of $\boldsymbol{z}$ in terms of linear combinations of the initial total variation of $\boldsymbol{z}$

$$\tilde{\delta}\boldsymbol{z}_f = \boldsymbol{\Phi}\left(t_f,t_o\right)\tilde{\delta}\boldsymbol{z}_o. \tag{5.65}$$

Applying the initial total variation of $\boldsymbol{z}$ to the above equation, the final total variation of $\boldsymbol{z}$ becomes

$$\begin{aligned}\tilde{\delta}\boldsymbol{z}_f &= \boldsymbol{\Phi}\left(t_f,t_o\right)\tilde{\delta}\boldsymbol{z}_o \\ &= \boldsymbol{\Phi}\left(t_f,t_o\right)\begin{bmatrix}\boldsymbol{0}\\ \tilde{\delta}\boldsymbol{\lambda}_o\end{bmatrix}.\end{aligned} \tag{5.66}$$

The transition matrix can be partitioned to yield

$$\tilde{\delta}\boldsymbol{z}_f = \left[\,\boldsymbol{\Phi}_1\left(t_f,t_o\right) \quad \boldsymbol{\Phi}_2\left(t_f,t_o\right)\right]\begin{bmatrix}\boldsymbol{0}\\ \tilde{\delta}\boldsymbol{\lambda}_o\end{bmatrix}. \tag{5.67}$$

Therefore, the final total variation of $\boldsymbol{z}$ is expressed solely as a total variation of the initial unknown elements of $\boldsymbol{z}$

$$\tilde{\delta}\boldsymbol{z}_f = \boldsymbol{\Phi}_2\left(t_f, t_o\right)\tilde{\delta}\boldsymbol{\lambda}_o. \tag{5.68}$$

The final boundary conditions of Eq. (5.54) are evaluated based upon the initial guess for the unknown initial variables. Assuming Eq. (5.54) is not satisfied, the initial guess of the unknown variables must be modified. To determine the modification to the guess, the time free variation of the terminal boundary condition is examined

$$\delta\boldsymbol{h} = \boldsymbol{h}_{t_f}\delta t_f + \boldsymbol{h}_{z_f}\delta\boldsymbol{z}_f. \tag{5.69}$$

The relationship between a time free variation and a total variation is

$$\delta\boldsymbol{z}_f = \tilde{\delta}\boldsymbol{z}_f + \dot{\boldsymbol{z}}_f\delta t_f. \tag{5.70}$$

Substituting Eq. (5.70) into Eq. (5.69) yields

$$\begin{aligned}\delta\boldsymbol{h} &= \boldsymbol{h}_{t_f}\delta t_f + \boldsymbol{h}_{z_f}\tilde{\delta}\boldsymbol{z}_f + \boldsymbol{h}_{z_f}\dot{\boldsymbol{z}}_f\delta t_f \\ &= \boldsymbol{h}_{z_f}\tilde{\delta}\boldsymbol{z}_f + \left(\boldsymbol{h}_{t_f} + \boldsymbol{h}_{z_f}\dot{\boldsymbol{z}}_f\right)\delta t_f.\end{aligned} \tag{5.71}$$

The total variation of the final $\boldsymbol{z}$ is known through Eq. (5.68). Making the substitution for $\tilde{\delta}\boldsymbol{z}_f$, $\delta\boldsymbol{h}$ becomes

$$\delta\boldsymbol{h} = \boldsymbol{h}_{z_f}\boldsymbol{\Phi}_2\left(t_f, t_o\right)\tilde{\delta}\boldsymbol{\lambda}_o + \left(\boldsymbol{h}_{t_f} + \boldsymbol{h}_{z_f}\dot{\boldsymbol{z}}_f\right)\delta t_f. \tag{5.72}$$

The variation of $\boldsymbol{h}$ can also be expressed as

$$\delta\boldsymbol{h} = \boldsymbol{h}_{new} - \boldsymbol{h}. \tag{5.73}$$

Recall the previous assumption of the neighboring path. With this assumption, the variation of $\boldsymbol{h}$ due to variations in $\boldsymbol{z}$ is small. Hence, the value for $\boldsymbol{h}_{new}$ is close to the old value of $\boldsymbol{h}$ and is expressed as

$$\boldsymbol{h}_{new} = \eta \boldsymbol{h} \tag{5.74}$$

$$\text{with } \eta \text{ close to } 1. \tag{5.75}$$

Substituting the expression for $\boldsymbol{h}_{new}$ into Eq. (5.73), $\delta \boldsymbol{h}$ becomes

$$\begin{aligned} \delta \boldsymbol{h} &= -(1-\eta)\,\boldsymbol{h} \\ &= -\alpha \boldsymbol{h} \end{aligned} \tag{5.76}$$

where α is defined as,

$$\alpha \equiv (1-\eta)\,. \tag{5.77}$$

Typically, α is about 0.1. Combining Eq. (5.72) and Eq. (5.76) yields

$$\left[\, \boldsymbol{h}_{z_f} \boldsymbol{\Phi}_2\,(t_f, t_o) \quad \boldsymbol{h}_{t_f} + h_{z_f} \dot{\boldsymbol{z}}_f \,\right] \begin{bmatrix} \tilde{\delta} \boldsymbol{\lambda}_o \\ \delta t_f \end{bmatrix} = -\alpha \boldsymbol{h}. \tag{5.78}$$

A means to modify the initial guess is provided by Eq. (5.78). The initial guess for λ_o and t_f is updated by

$$\lambda_{new} = \lambda_o + \tilde{\delta} \lambda_o \tag{5.79}$$

$$t_{f_{new}} = t_f + \delta t_f \tag{5.80}$$

To implement the algorithm, $\boldsymbol{\lambda}_o$ and t_f are guessed. Equations (5.51) and (5.63) are integrated from t_o to t_f. $\boldsymbol{z}_f$, $\boldsymbol{\Phi}_2(t_f, t_o)$, and $\|\boldsymbol{h}\|$ are computed. $\|\boldsymbol{h}\|$ is checked to determine if it is within a specified tolerance. α is set to 1 and $\tilde{\delta} \boldsymbol{\lambda}_o$ and δt_f are calculated and intermediate values for the initial guesses are formed. Equations (5.51) and (5.63) are integrated again from t_o to t_f using the intermediate values. $\|\boldsymbol{h}\|$ is

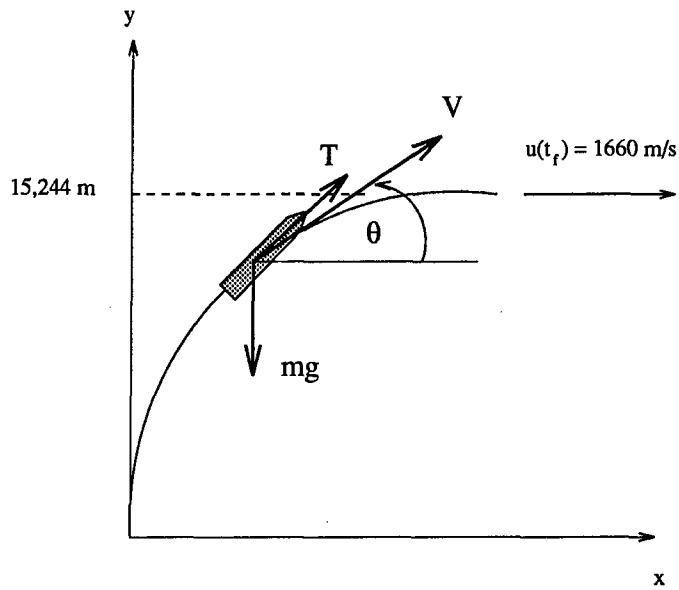

Figure 5.2 Lunar Launch Example Problem

checked again to determine if its value decreased. If not, α is reduced by half and $\tilde{\delta}\boldsymbol{\lambda}_o$ and δt_f are recomputed. If $\|\boldsymbol{h}\|$ was less than the previous value, then the intermediate values are accepted as the new $\boldsymbol{\lambda}_o$ and t_f values. This process is repeated until the specified tolerance for $\|\boldsymbol{h}\|$ is achieved.

5.3 Shooting Method Example Problem

The necessary conditions are utilized to formulate a two-point boundary-value problem for a lunar launch. The shooting method previously described is implemented to provide a numerical solution to the problem. The problem is to find the control history which minimizes the final time for a spacecraft's injection into Lunar orbit at prescribed final conditions from the surface of the moon. Figure 5.2 depicts the scenario. The problem is stated as;

$$\text{minimize } J = t_f \tag{5.81}$$

subject to the differential equations

$$\dot{x} = u \tag{5.82}$$

$$\dot{y} = v \tag{5.83}$$

$$\dot{u} = \frac{T}{m} \cos\theta \tag{5.84}$$

$$\dot{v} = \frac{T}{m} \sin\theta - g \tag{5.85}$$

with initial conditions

$$t_o = 0 \tag{5.86}$$

$$x(0) = 0 \tag{5.87}$$

$$y(0) = 0 \tag{5.88}$$

$$u(0) = 0 \tag{5.89}$$

$$v(0) = 0 \tag{5.90}$$

and the terminal conditions

$$t_f = \text{ unknown} \tag{5.91}$$

$$x\left(t_f\right) = \text{ free} \tag{5.92}$$

$$y\left(t_f\right) = 15.24 \text{ km} \tag{5.93}$$

$$u\left(t_f\right) = 1660 \text{ m/s} \tag{5.94}$$

$$v\left(t_f\right) = 0 \tag{5.95}$$

where

$u =$ the velocity component in the x direction

$v =$ the velocity component in the y direction

$$\frac{T}{m} = 6.34 \text{ m/s}^2 \text{ and is constant}$$

$$g = \text{the force of gravity, } 1.62 \text{ m/s}^2 \text{ and is constant}$$

$$\theta = \text{the control variable.}$$

Expressing the terminal constraints as functions of ψ yields

$$\Psi_y = y_f - 15,240 = 0 \tag{5.96}$$

$$\Psi_u = u_f - 1660 = 0 \tag{5.97}$$

$$\Psi_v = v_f = 0. \tag{5.98}$$

Adjoining the terminal constraints with Lagrange multipliers, $\boldsymbol{\nu}$, the Bolza function is expressed as

$$\begin{aligned} G(t_f, \boldsymbol{x}_f, \boldsymbol{\nu}) &= \phi(t_f, \boldsymbol{x}_f) + \boldsymbol{\nu}^T \boldsymbol{\Psi}(t_f, \boldsymbol{x}_f) \\ &= t_f + \nu_y (y_f - 15240) + \nu_u (u_f - 1660) + \nu_v v_f. \end{aligned} \tag{5.99}$$

Adjoining the differential equations with Lagrange multipliers, $\boldsymbol{\lambda}$, the Hamiltonian is expressed as

$$\begin{aligned} H(t, \boldsymbol{x}, \theta, \boldsymbol{\lambda}) &\equiv L(t, \boldsymbol{x}, \theta) + \boldsymbol{\lambda}^T \boldsymbol{f}(t, \boldsymbol{x}, \theta) \\ &= \lambda_x u + \lambda_y v + \lambda_u \left(\frac{T}{m} \cos\theta\right) + \lambda_v \left(\frac{T}{m} \sin\theta - g\right). \end{aligned} \tag{5.100}$$

The augmented performance index is given by

$$\begin{aligned} J' &= G(t_f, \boldsymbol{x}_f, \boldsymbol{v}) + \int_{t_o}^{t_f} \left[H(t, \boldsymbol{x}, u, \boldsymbol{\lambda}) - \boldsymbol{\lambda}^T \dot{\boldsymbol{x}}\right] dt \\ &= t_f + \nu_y (y_f - 15240) + \nu_u (u_f - 1660) + \nu_v v_f \\ &\quad + \int_{t_o}^{t_f} \left[\lambda_x u + \lambda_y v + \lambda_u \left(\frac{T}{m} \cos\theta\right)\right. \\ &\quad \left. + \lambda_v \left(\frac{T}{m} \sin\theta - g\right) - \lambda^T \dot{x}\right] dt. \end{aligned} \tag{5.101}$$

The necessary conditions for a minimum result from the first variation of the augmented performance index being set equal to zero. Hence, the differential equations for $\boldsymbol{\lambda}$ result from the necessary condition

$$\dot{\boldsymbol{\lambda}} = -\boldsymbol{H}_x^T(t, \boldsymbol{x}, \theta, \boldsymbol{\lambda}). \tag{5.102}$$

Applying Eq (5.102), the expressions for $\dot{\boldsymbol{\lambda}}$ are

$$\dot{\lambda}_x = 0 \tag{5.103}$$

$$\dot{\lambda}_y = 0 \tag{5.104}$$

$$\dot{\lambda}_u = -\lambda_x \tag{5.105}$$

$$\dot{\lambda}_v = -\lambda_y. \tag{5.106}$$

The control is eliminated by the necessary condition

$$H_\theta = 0. \tag{5.107}$$

Applying Eq. (5.107) yields

$$H_\theta = -\lambda_u \left(\frac{T}{m}\sin\theta\right) + \lambda_V \left(\frac{T}{m}\cos\theta\right) \tag{5.108}$$

$$= 0. \tag{5.109}$$

Solving for θ yields two possible control laws

$$\lambda_u \sin\theta = \lambda_v \cos\theta \tag{5.110}$$

$$\frac{\sin\theta}{\cos\theta} = \tan\theta = \frac{\lambda_v}{\lambda_u} \tag{5.111}$$

$$\theta_1 = \arctan\frac{\lambda_v}{\lambda_u} \tag{5.112}$$

$$\text{or} \qquad \theta_2 = \arctan\frac{-\lambda_v}{-\lambda_u} \tag{5.113}$$

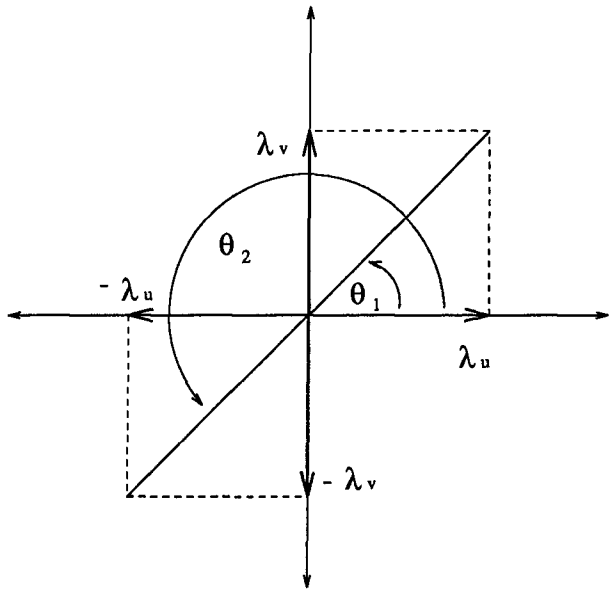

Figure 5.3 Quadrant Problem for Lunar Launch Control

The quadrant problem shown in Fig 5.3 results because of the two possible solutions for θ. Evaluating the second partial derivative of the Hamiltonian with respect to θ resolves which solution is sufficient for a local minimum. Taking the second partial derivative of H with respect to θ yields

$$\begin{aligned}\frac{\partial^2 H}{\partial \theta^2} &= -\lambda_u \frac{T}{m}\cos\theta - \lambda_v \frac{T}{m}\sin\theta \\ &= \frac{-T}{m}\left(\lambda_u \cos\theta + \lambda_v \sin\theta\right). \end{aligned} \tag{5.114}$$

Substituting θ_1 into Eq. (5.114) yields

$$\frac{\partial^2 H}{\partial \theta^2} = \frac{-T}{m}\left(\frac{\lambda_u^2}{(\lambda_v^2+\lambda_u^2)^{\frac{1}{2}}} + \frac{\lambda_v^2}{(\lambda_v^2+\lambda_u^2)^{\frac{1}{2}}}\right) \tag{5.115}$$

$$< 0. \tag{5.116}$$

θ_1 is a local maximum. Substituting θ_2 into Eq. (5.114) yields

$$\frac{\partial^2 H}{\partial \theta^2} = \frac{-T}{m}\left(\frac{-\lambda_u^2}{(\lambda_v^2+\lambda_u^2)^{\frac{1}{2}}} - \frac{\lambda_v^2}{(\lambda_v^2+\lambda_u^2)^{\frac{1}{2}}}\right) \tag{5.117}$$

$$> 0. \tag{5.118}$$

θ_2 satisfies the sufficient condition for a local minimum because it is always positive. Hence, θ is eliminated from all equations by using the relationships

$$\sin\theta = -\frac{\lambda_v}{(\lambda_v^2+\lambda_u^2)^{\frac{1}{2}}}; \qquad \cos\theta_2 = -\frac{\lambda_u}{(\lambda_v^2+\lambda_u^2)^{\frac{1}{2}}}.$$

The terminal conditions are the three constraint equations and $\lambda_x = 0$ because $x(t_f)$ is unspecified. The necessary condition H_f = -G_{t_f} provides the additional expression required to determine t_f. These conditions are expressed by

$$\begin{bmatrix} \lambda_x(t_f)\,u(t_f) + \lambda_y(t_f)\,v(t_f) - \left(\frac{T}{m}\right)\frac{\lambda_u^2(t_f)}{\Delta(t_f)} - \left(\frac{T}{m}\right)\frac{\lambda_v^2(t_f)}{\Delta(t_f)} - g\lambda_v(t_f) + 1 \\ y(t_f)/15,240 - 1 \\ u(t_f)/1660 - 1 \\ v(t_f)/1660 \\ \lambda_x(t_f) \end{bmatrix} = \begin{bmatrix} 0 \\ 0 \\ 0 \\ 0 \\ 0 \end{bmatrix}$$

where

$$\Delta \equiv \left(\lambda_v^2 + \lambda_u^2\right)^{\frac{1}{2}} \tag{5.119}$$

The problem is now in the form of a standard two-point boundary-value problem. To obtain a numerical solution to the problem using the shooting method, the lunar launch problem is formulated to coincide with the description of the shooting method provided in the previous section. Defining

$$z = [x \quad y \quad u \quad v \quad \lambda_x \quad \lambda_y \quad \lambda_u \quad \lambda_v]^T \tag{5.120}$$

the differential equations become

$$\dot{\boldsymbol{z}} = \begin{bmatrix} u \\ v \\ -\frac{T}{m}\frac{\lambda_u}{\Delta} \\ -\frac{T}{m}\frac{\lambda_v}{\Delta} - g \\ 0 \\ 0 \\ -\lambda_x \\ -\lambda_y \end{bmatrix} \tag{5.121}$$

where Δ is defined by Eq. (5.119). The initial conditions are given by

$$t_o = 0 \tag{5.122}$$

$$\boldsymbol{z}(t_o) = [0 \quad 0 \quad 0 \quad 0 \quad \lambda_{xo} \quad \lambda_{yo} \quad \lambda_{uo} \quad \lambda_{vo}]^T . \tag{5.123}$$

The terminal conditions are expressed in the form of Eq. (5.54) by

$$\boldsymbol{h}(t_f, \boldsymbol{z}_f) = \begin{bmatrix} \lambda_x(t_f)\,u(t_f) + \lambda_y(t_f)\,v(t_f) - \left(\frac{T}{m}\right)\frac{\lambda_u^2(t_f)}{\Delta(t_f)} - \left(\frac{T}{m}\right)\frac{\lambda_v^2(t_f)}{\Delta(t_f)} - g\lambda_v(t_f) + 1 \\ y(t_f)/15240 - 1 \\ u(t_f)/1660 - 1 \\ v(t_f)/1660 \\ \lambda_x(t_f) \end{bmatrix} .$$

Note some scaling has been applied to the terminal conditions for numerical conditioning. The differential equations for the state transition matrix, Eq. (5.63), require

an expression for $\boldsymbol{F}_z$ which is expressed as

$$\boldsymbol{F}_z = \begin{bmatrix} 0 & 0 & 1 & 0 & 0 & 0 & 0 & 0 \\ 0 & 0 & 0 & 1 & 0 & 0 & 0 & 0 \\ 0 & 0 & 0 & 0 & 0 & 0 & A & B \\ 0 & 0 & 0 & 0 & 0 & 0 & B & C \\ 0 & 0 & 0 & 0 & 0 & 0 & 0 & 0 \\ 0 & 0 & 0 & 0 & 0 & 0 & 0 & 0 \\ 0 & 0 & 0 & 0 & -1 & 0 & 0 & 0 \\ 0 & 0 & 0 & 0 & 0 & -1 & 0 & 0 \end{bmatrix} \tag{5.124}$$

where
$$A = \frac{T}{m}\left(\frac{-1}{\Delta} + \frac{\lambda_u^2}{\Delta^3}\right) \tag{5.125}$$
$$B = \frac{T}{m}\frac{\lambda_u \lambda_v}{\Delta^3} \tag{5.126}$$
$$C = \frac{T}{m}\left(\frac{-1}{\Delta} + \frac{\lambda_v^2}{\Delta^3}\right). \tag{5.127}$$

The update to the initial guesses requires expressions for $\boldsymbol{h}_{t_f}$ and $\boldsymbol{h}_{z_f}$ and these are expressed by

$$\boldsymbol{h}_{t_f} = [0 \quad 0 \quad 0 \quad 0 \quad 0]^T \tag{5.128}$$

$$\boldsymbol{h}_{z_f} = \begin{bmatrix} 0 & 0 & \lambda_x(t_f) & \lambda_y(t_f) & u(t_f) & v(t_f) & D(t_f) & E(t_f) \\ 0 & \frac{1}{15240} & 0 & 0 & 0 & 0 & 0 & 0 \\ 0 & 0 & \frac{1}{1660} & 0 & 0 & 0 & 0 & 0 \\ 0 & 0 & 0 & \frac{1}{1660} & 0 & 0 & 0 & 0 \\ 0 & 0 & 0 & 0 & 1 & 0 & 0 & 0 \end{bmatrix} \tag{5.129}$$

where
$$D = \frac{T}{m}\left[\frac{\lambda_u \lambda_v^2}{\Delta^3} + \frac{\lambda_u^3}{\Delta^3} - \frac{2\lambda_u}{\Delta}\right] \tag{5.130}$$
$$E = \frac{T}{m}\left[\frac{\lambda_u^2 \lambda_v}{\Delta^3} + \frac{\lambda_v^3}{\Delta^3} - \frac{2\lambda_v}{\Delta}\right] - g. \tag{5.131}$$

Applying the shooting method to the sample lunar launch problem, the minimum final time was determined to be 272.706 seconds. The tolerance for $\|\boldsymbol{h}\|$ was

Iteration	λ_x	λ_y	λ_u	λ_v
Initial	1.000×10^{-4}	-1.000×10^{-4}	-1.000×10^{-2}	-1.000×10^{-2}
1	5.150×10^{-19}	-1.483×10^{-4}	-5.370×10^{-2}	-2.668×10^{-2}
2	-1.215×10^{-21}	-8.676×10^{-5}	-4.684×10^{-2}	-2.456×10^{-2}
3	0	-7.863×10^{-5}	-4.865×10^{-2}	-2.382×10^{-2}
4	0	-7.763×10^{-5}	-4.867×10^{-2}	-2.374×10^{-2}
5	0	-7.762×10^{-5}	-4.867×10^{-2}	-2.374×10^{-2}

Table 5.1 Iteration History of $\boldsymbol{\lambda}_o$ for Shooting Method Example Problem

Iteration	t_f (Sec)	$\|\boldsymbol{h}\|$
Initial	300	9.846×10^{-1}
1	240.08	1.529×10^{-1}
2	271.45	2.311×10^{-3}
3	272.68	1.047×10^{-4}
4	272.71	5.194×10^{-7}
5	272.71	6.942×10^{-9}

Table 5.2 Iteration History of t_f and $\|\boldsymbol{h}\|$ for Shooting Method Example Problem

1 x 10^{-8} and was achieved in five iterations. Table 5.1 summarizes the iteration history of $\boldsymbol{\lambda}_o$. Table 5.2 summarizes the iteration history of t_f and $\|\boldsymbol{h}\|$. The time histories of the states are shown in Fig 5.4. Table 5.3 summarizes the prescribed final states and the numerical results for the final states. The time history of the control required to achieve the terminal conditions is shown in Fig 5.5.

$\boldsymbol{x}(t_f)$	Prescribed Value	Numerical Result
$x(t_f)$	Free	222.29723 (km)
$y(t_f)$	15.24 (km)	15.239999 (km)
$u(t_f)$	1660 (m/s)	1660.0000 (m/s)
$v(t_f)$	0	-8.86199$\times 10^{-7}$ (m/s)

Table 5.3 Summary of $\boldsymbol{x}(t_f)$ for Shooting Method Example Problem

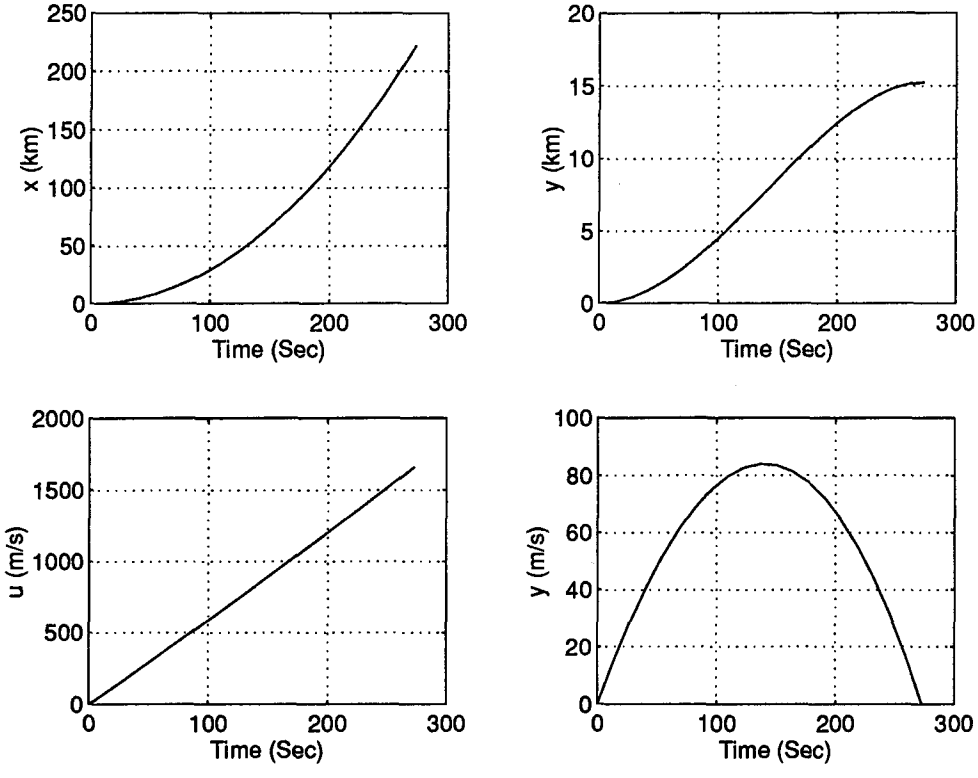

Figure 5.4 Time Histories of States for Lunar Launch

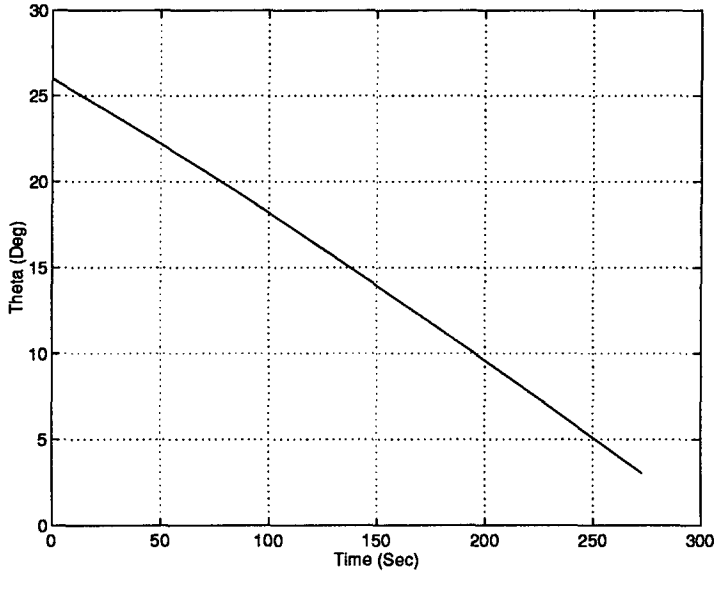

Figure 5.5 Control History for Lunar Launch

5.4 Three-Dimensional Pursuit

Consider the three-dimensional intercept scenario where the problem is to find the control $u(t)$ that minimizes the final time. The performance index is given by

$$J = t_f. \tag{5.132}$$

The differential equations described in chapters 2 and 3 are

$$\dot{x} = V\cos\gamma\cos\psi \tag{5.133}$$

$$\dot{y} = V\cos\gamma\sin\psi \tag{5.134}$$

$$\dot{h} = V\sin\gamma \tag{5.135}$$

$$\dot{V} = \frac{g}{W}(T\cos\alpha - D) - g\sin\gamma \tag{5.136}$$

$$\dot{\gamma} = \frac{g}{VW}(T\sin\alpha + L)\cos\sigma - \frac{g}{V}\cos\gamma \tag{5.137}$$

$$\dot{\psi} = \frac{g}{VW\cos\gamma}(T\sin\alpha + L)\sin\sigma \tag{5.138}$$

$$\dot{\alpha} = C_\alpha\left[\left(u^2 + g_{cmd_y}^2\right)^{\frac{1}{2}} - \frac{phase}{W}(T\sin\alpha + L)\right] \tag{5.139}$$

$$\dot{\sigma} = \frac{1}{\tau_\sigma}\left[\arctan\left(\frac{g_{cmd_y}}{u}\right) - \sigma\right] \tag{5.140}$$

$$\dot{W} = -\dot{w}_f \tag{5.141}$$

where

$$phase = \begin{cases} 1, \alpha \geq 0 \\ -1, \alpha < 0 \end{cases} \tag{5.142}$$

and the terminal constraint

$$\psi(t_f) = \left[\left(x_f - x_{T_f}\right)^2 + \left(y_f - y_{T_f}\right)^2 + \left(h_f - h_{T_f}\right)^2\right] = 0. \tag{5.143}$$

The control, u, is chosen to represent the total commanded g's in the $\hat{z}_V$ direction. Recalling Eq. (3.42), u is defined as

$$u \equiv g_{cmd_z} = g_{cmdP/N_z} + g_{cmdg_z} + g_{loft}. \tag{5.144}$$

The terminal constraint requires that the missile intercepts the target at the final time. The state constraint is given by

$$S_1 = \alpha - 20 + l_{\alpha 1}^2 = 0 \tag{5.145}$$

$$S_2 = -\alpha + l_{\alpha 2}^2 = 0 \tag{5.146}$$

which implies that the angle of attack must remain between 0° and 20°. $\boldsymbol{l}_\alpha$ is the slack variable added to the α state since the constraint is an inequality constraint. The control constraints are expressed as

$$C_1 = u - 20 + l_{u1}^2 = 0 \tag{5.147}$$

$$C_2 = -u - 20 + l_{u2}^2 = 0. \tag{5.148}$$

The control is limited to a value of -20 to 20 g's. For simplification define the state vector as $\boldsymbol{x}$

$$\boldsymbol{x} \equiv [x \quad y \quad h \quad V \quad \gamma \quad \psi \quad \alpha \quad \sigma \quad W]^T \tag{5.149}$$

then

$$\dot{\boldsymbol{x}} = \boldsymbol{f}(\boldsymbol{x}, u, t) \tag{5.150}$$

where $\boldsymbol{f}(\boldsymbol{x}, u, t)$ is the system of equations given above. The Bolza function, G, and the variational Hamiltonian, H, are expressed as

$$G(t_f, \boldsymbol{x}_f, v) = t_f + v\left[\left(x_f - x_{T_f}\right)^2 + \left(y_f - y_{T_f}\right)^2 + \left(h_f - h_{T_f}\right)^2\right]$$

$$H(t, \boldsymbol{x}, u, \boldsymbol{\lambda}, \boldsymbol{\theta}, \boldsymbol{\mu}, \boldsymbol{l}) = \lambda_x V \cos\gamma \cos\psi + \lambda_y V \cos\gamma \sin\psi + \lambda_h V \sin\gamma$$

$$
\begin{aligned}
&+\lambda_V \left[\frac{g}{W}\left(T\sin\alpha - D\right) - g\sin\gamma\right] \\
&+\lambda_\gamma \left[\frac{g}{VW}\left(T\sin\alpha + L\right)\cos\sigma - \frac{g}{V}\cos\gamma\right] \\
&+\lambda_\psi \left[\frac{g}{VW\cos\gamma}\left(T\sin\alpha + L\right)\sin\sigma\right] \\
&+\lambda_\alpha C_\alpha \left[\left(g_{cmd_y}^2 + u^2\right)^{\frac{1}{2}} - \frac{phase}{W}\left(T\sin\alpha + L\right)\right] \\
&+\frac{\lambda_\sigma}{\tau_\sigma}\left[\arctan\left(\frac{g_{cmd_y}}{u}\right) - \sigma\right] - \lambda_W \dot{w}_f \\
&+\theta_1\left(\alpha - 20 + l_{\alpha 1}^2\right) + \theta_2\left(-\alpha + l_{\alpha 2}^2\right) \\
&+\mu_1\left(u - 20 + l_{u1}^2\right) + \mu_2\left(-u - 20 - l_{u2}^2\right)
\end{aligned}
\tag{5.151}
$$

In addition to satisfying the constraints, the remaining necessary conditions are expressed as

$$
H_f = -G_{t_f} = -1 \tag{5.152}
$$

$$
\boldsymbol{\lambda}_f = \boldsymbol{G}_{x_f}^T = \begin{bmatrix} 2v\left(x_f - x_{T_f}\right) \\ 2v\left(y_f - y_{T_f}\right) \\ 2v\left(h_f - h_{T_f}\right) \\ 0 \\ 0 \\ 0 \\ 0 \\ 0 \\ 0 \end{bmatrix} \tag{5.153}
$$

$$
\dot{\lambda}_x = 0 \tag{5.154}
$$

$$
\dot{\lambda}_y = 0 \tag{5.155}
$$

$$
\dot{\lambda}_h = 0 \tag{5.156}
$$

$$
\begin{aligned}
\dot{\lambda}_v = &-\lambda_x \cos\gamma\cos\psi - \lambda_y \cos\gamma\sin\psi - \lambda_h \sin\gamma \\
&+\lambda_\gamma \left[\frac{g}{V^2 W}(T\sin\alpha + L)\cos\sigma - \frac{g}{V^2}\cos\gamma\right]
\end{aligned}
$$

$$+\lambda_\psi \left[\frac{g}{V^2 W \cos\gamma} (T \sin\alpha + L) \sin\sigma \right] \tag{5.157}$$

$$\dot{\lambda}_\gamma = \lambda_x V \sin\gamma \cos\psi + \lambda_y V \sin\gamma \sin\psi - \lambda_h V \cos\gamma$$
$$+\lambda_V g \cos\gamma - \lambda_\gamma \frac{g}{V} \sin\gamma + \lambda_\psi \left[\frac{g \sin\gamma}{VW \cos^2\gamma} (T \sin\alpha + L) \sin\sigma \right] \tag{5.158}$$

$$\dot{\lambda}_\psi = \lambda_x V \cos\gamma \sin\psi - \lambda_y V \cos\gamma \cos\psi \tag{5.159}$$

$$\dot{\lambda}_\alpha = \lambda_V \frac{g}{W} (T \sin\alpha - D) - \lambda_\gamma \frac{g}{VW} (T \cos\alpha + L) \cos\sigma$$
$$-\lambda_\psi \frac{g}{VW \cos\gamma} (T \cos\alpha + L) \sin\sigma + \lambda_\alpha C_\alpha \frac{phase}{W} (T \cos\alpha + L)$$
$$-\theta_1 + \theta_2 \tag{5.160}$$

$$\dot{\lambda}_\sigma = \lambda_\gamma \frac{g}{VW} (T \sin\alpha + L) \sin\sigma - \lambda_\psi \frac{g}{VW \cos\gamma} (T \sin\alpha + L) \cos\sigma + \frac{\lambda_\sigma}{\tau_\sigma} \tag{5.161}$$

$$\dot{\lambda}_W = \lambda_V \frac{g}{W^2} (T \cos\alpha - D) + \lambda_\gamma \frac{g}{VW^2} (T \sin\alpha + L) \cos\sigma$$
$$+\lambda_\psi \frac{g}{VW^2 \cos\gamma} (T \sin\alpha + L) \sin\sigma - \lambda_\alpha C_\alpha \frac{phase}{W^2} (T \sin\alpha + L) \tag{5.162}$$

$$\boldsymbol{H}_l = \begin{bmatrix} 2\theta_1 l_{\alpha 1} \\ 2\theta_2 l_{\alpha 2} \\ 2\mu_1 l_{u1} \\ 2\mu_2 l_{u2} \end{bmatrix} = 0 \tag{5.163}$$

$$H_u = 0 \tag{5.164}$$

Examining the optimal control law, $H_u = 0$

$$H_u = \lambda_\alpha C_\alpha \left(g_{cmd_y}^2 + u^2 \right)^{-\frac{1}{2}} u - \frac{\lambda_\sigma}{\tau_\sigma} \left(\frac{g_{cmd_y}}{g_{cmd_y}^2 + u^2} \right) + \mu_1 + \mu_2 = 0 \tag{5.165}$$

and the necessary condition $\boldsymbol{H}_l = 0$

$$\boldsymbol{H}_l = \begin{bmatrix} 2\theta_1 l_{\alpha 1} \\ 2\theta_2 l_{\alpha 2} \\ 2\mu_1 l_{u1} \\ 2\mu_2 l_{u2} \end{bmatrix} = 0. \tag{5.166}$$

three cases are required to be examined depending upon the value of u to satisfy Eqs (5.166) and (5.165).

CASE 1: $u = u_{max} = 20$. This case occurs when the constraint at u_{max} is active. Hence, μ_2 is zero because the constraint at u_{min} is inactive. l_{u1} is zero to satisfy Eq. (5.147) and $l_{u2} = \sqrt{40}$ to satisfy Eq. (5.148). An expression for μ_1 is obtained from Eq. (5.165) with the substitution $u = 20$ yielding

$$\mu_1 = -20\lambda_\alpha C_\alpha \left(g_{cmd_y}^2 + 20^2\right)^{-\frac{1}{2}} + \frac{\lambda_\sigma}{\tau_\sigma}\left(\frac{g_{cmd_y}}{g_{cmd_y}^2 + 20^2}\right). \tag{5.167}$$

CASE 2: $u = u_{min} = -20$. This case occurs when the constraint at u_{min} is active. Hence, μ_1 is zero because the constraint at u_{max} is inactive. l_{u2} is zero to satisfy Eq. (5.148) and $l_{u1} = \sqrt{40}$ to satisfy Eq. (5.147). An expression for μ_2 is obtained from Eq. (5.165) with the substitution $u = -20$ yielding

$$\mu_2 = 20\lambda_\alpha C_\alpha \left(g_{cmd_y}^2 + 20^2\right)^{-\frac{1}{2}} + \frac{\lambda_\sigma}{\tau_\sigma}\left(\frac{g_{cmd_y}}{g_{cmd_y}^2 + 20^2}\right). \tag{5.168}$$

CASE 3: $u_{min} < u < u_{max}$. This case occurs when u is between the upper and lower constraint values. Hence, $\mu_1 = \mu_2 = 0$ because both constraints are inactive. $l_{u1} = \sqrt{20 - u}$ to satisfy Eq. (5.147) and $l_{u2} = \sqrt{20 + u}$ to satisfy Eq. (5.148). Equation (5.165) is used to determine the value of u. Adding a common denominator, Eq. (5.165) becomes

$$\lambda_\alpha C_\alpha \left(g_{cmd_y}^2 + u^2\right)^{\frac{1}{2}} u = \frac{\lambda_\sigma}{\tau_\sigma} g_{cmd_y}. \tag{5.169}$$

Squaring both sides of the equation and expanding yields

$$u^4 + g_{cmd_y}^2 u^2 - K^2 g_{cmd_y}^2 = 0 \tag{5.170}$$

where

$$K = \frac{\lambda_\sigma}{\tau_\sigma \lambda_\alpha C_\alpha}. \tag{5.171}$$

Solving for u produces four possible solutions:

$$u = \begin{cases} \left\{\frac{1}{2}\left[-g_{cmd_y}^2 + \sqrt{g_{cmd_y}^4 + 4K^2 g_{cmd_y}^2}\right]\right\}^{\frac{1}{2}} \\ -\left\{\frac{1}{2}\left[-g_{cmd_y}^2 + \sqrt{g_{cmd_y}^4 + 4K^2 g_{cmd_y}^2}\right]\right\}^{\frac{1}{2}} \\ \left\{\frac{1}{2}\left[-g_{cmd_y}^2 - \sqrt{g_{cmd_y}^4 + 4K^2 g_{cmd_y}^2}\right]\right\}^{\frac{1}{2}} \\ -\left\{\frac{1}{2}\left[-g_{cmd_y}^2 - \sqrt{g_{cmd_y}^4 + 4K^2 g_{cmd_y}^2}\right]\right\}^{\frac{1}{2}} \end{cases} . \tag{5.172}$$

The last two possibilities are always imaginary and can immediately be discounted. Hence, the remaining solutions are

$$u = \begin{cases} \left\{\frac{1}{2}\left[-g_{cmd_y}^2 + \sqrt{g_{cmd_y}^4 + 4K^2 g_{cmd_y}^2}\right]\right\}^{\frac{1}{2}} \\ -\left\{\frac{1}{2}\left[-g_{cmd_y}^2 + \sqrt{g_{cmd_y}^4 + 4K^2 g_{cmd_y}^2}\right]\right\}^{\frac{1}{2}} \end{cases} . \tag{5.173}$$

An interesting problem arises when g_{cmd_y} is zero which implies flight is occurring in a vertical plane. Solving for u with $g_{cmd_y} = 0$ indicates $u = 0$. When these values are substituted back into Eq. (5.165), the result can only be evaluated in the limit as u goes to zero. Additionally, the numerical value of σ_{cmd} is either 0° or 180°, depending upon the manner in which u approaches zero. If u approaches zero from below, then σ_{cmd} is 180° and if u approaches zero from above, then σ_{cmd} is 0o. Thus, σ_{cmd} is not an explicit function of u. Therefore, Eq. (5.164) with a constant value applied for σ_{cmd} reduces to

$$\lambda_\alpha C_\alpha = 0. \tag{5.174}$$

An expression for the control is not contained in Eq. (5.174). For this third case, flight in the vertical plane is a special case and will be examined in more detail.

5.5 Two-Dimensional Pursuit

The differential equations for the two-dimensional pursuit reduce to

$$\dot{x} = V \cos\gamma \tag{5.175}$$

$$\dot{h} = V \sin\gamma \tag{5.176}$$

$$\dot{V} = \frac{g}{W}\left(T\cos\alpha - D\right) - g\sin\gamma \tag{5.177}$$

$$\dot{\gamma} = \frac{g}{VW}\left(T\sin\alpha + L\right)\Sigma - \frac{g}{V}\cos\gamma \tag{5.178}$$

$$\dot{\alpha} = C_\alpha\left[u - \frac{1}{W}\left(T\sin\alpha + L\right)\Sigma\right] \tag{5.179}$$

$$\dot{W} = -\dot{w}_f \tag{5.180}$$

where

$$\Sigma = \begin{cases} 1, u \geq 0 \\ -1, u < 0 \end{cases}. \tag{5.181}$$

Σ is representing the roll in this model. Recall the roll command for the three-dimensional intercept

$$\sigma_{cmd} = \arctan\left(\frac{g_{cmd_y}}{u}\right). \tag{5.182}$$

When g_{cmd_y} is zero and σ_{cmd} is 0° for positive u and 180° for negative u if a four quadrant *arctan* is used. The terminal constraints reduce to

$$\Psi_f = \left[\left(x_f - x_{T_f}\right)^2 + \left(h_f - h_{T_f}\right)^2\right] = 0. \tag{5.183}$$

The state and control constraints remain the same as in the three-dimensional pursuit and are given by Eqs (5.145) through (5.148). The Bolza and Hamiltonian functions are

$$G = t_f + v\left[\left(x_f - x_{T_f}\right)^2 + \left(h_f - h_{T_f}\right)^2\right] = 0 \tag{5.184}$$

$$\begin{aligned} H = {} & \lambda_x V\cos\gamma + \lambda_h V\sin\gamma + \lambda_V\left[\frac{g}{W}\left(T\cos\alpha - D\right) - g\sin\gamma\right] \\ & + \lambda_\gamma\left[\frac{g}{VW}\left(T\sin\alpha + L\right)\Sigma - \frac{g}{V}\cos\gamma\right] \\ & + \lambda_\alpha C_\alpha\left[u - \frac{1}{W}\left(T\sin\alpha + L\right)\Sigma\right] \\ & - \lambda_W\dot{w}_f + \theta_1\left(\alpha - 20 + l_{\alpha 1}^2\right) + \theta_2\left(-\alpha + l_{\alpha 2}^2\right) \\ & + \mu_1\left(u - 20 + l_{u1}^2\right) + \mu_2\left(-u - 20 + l_{u2}^2\right). \end{aligned} \tag{5.185}$$

The necessary conditions are

$$\dot{\lambda}_x = 0 \tag{5.186}$$

$$\dot{\lambda}_h = 0 \tag{5.187}$$

$$\begin{aligned}\dot{\lambda}_V = &-\lambda_x \cos\gamma - \lambda_h \sin\gamma - \lambda_V \frac{2g}{VW} D \\ &+\lambda_\gamma \left[\frac{g}{V^2 W}\left(T\sin\alpha + L\right)\Sigma - \frac{2gL}{V^2 W}\Sigma - \frac{g}{V^2}\cos\gamma\right] \\ &+\lambda_\alpha C_\alpha \frac{2L}{WV}\Sigma\end{aligned} \tag{5.188}$$

$$\dot{\lambda}_\gamma = \lambda_x V \sin\gamma - \lambda_h V \cos\gamma + \lambda_V g \cos\gamma - \lambda_\gamma \frac{g}{V}\sin\gamma \tag{5.189}$$

$$\begin{aligned}\dot{\lambda}_\alpha = &\lambda_V \frac{g}{W} T \sin\alpha - \lambda_\gamma \left(\frac{g}{VW} T \cos\alpha\right)\Sigma \\ &+\lambda_\alpha \left(C_\alpha \frac{T}{W}\cos\alpha\right)\Sigma + \theta_1 + \theta_2\end{aligned} \tag{5.190}$$

$$\begin{aligned}\dot{\lambda}_W = &\lambda_V \frac{g}{W^2}\left(T\cos\alpha - D\right) + \lambda_\gamma \frac{g}{VW^2}\left(T\sin\alpha + L\right)\Sigma \\ &-\lambda_\alpha \frac{C_\alpha}{W^2}\left(T\sin\alpha + L\right)\Sigma\end{aligned} \tag{5.191}$$

$$H_f = -1 \tag{5.192}$$

$$\boldsymbol{\lambda}_f = \boldsymbol{G}_{x_f}^T = \begin{bmatrix} 2v\left(x_f - x_{T_f}\right) \\ 2v\left(h_f - h_{T_f}\right) \\ 0 \\ 0 \\ 0 \\ 0 \end{bmatrix} \tag{5.193}$$

$$\boldsymbol{H}_l = \begin{bmatrix} 2\theta_1 l_{\alpha 1} \\ 2\theta_2 l_{\alpha 2} \\ 2\mu_1 l_{u1} \\ 2\mu_2 l_{u2} \end{bmatrix} = 0 \tag{5.194}$$

$$H_u = \lambda_\alpha C_\alpha + \mu_1 - \mu_2 = 0 \tag{5.195}$$

$$H_{uu} = 0. \tag{5.196}$$

As in the three-dimensional pursuit, three cases must be examined to satisfy Eqs (5.194) and (5.195).

CASE 1: $u = u_{max} = 20$. This case occurs when the constraint at u_{max} is active. Hence, μ_2 is zero because the constraint at u_{min} is inactive. l_{u1} is zero to satisfy Eq. (5.147) and $l_{u2} = \sqrt{40}$ to satisfy Eq. (5.148). An expression for μ_1 is obtained from Eq. (5.195) yielding

$$\mu_1 = -\lambda_\alpha C_\alpha. \tag{5.197}$$

CASE 2: $u = u_{min} = -20$. This case occurs when the constraint at u_{min} is active. Hence, μ_1 is zero because the constraint at u_{max} is inactive. l_{u2} is zero to satisfy Eq. (5.148) and $l_{u1} = \sqrt{40}$ to satisfy Eq. (5.147). An expression for μ_2 is obtained from Eq. (5.195) yielding

$$\mu_2 = \lambda_\alpha C_\alpha. \tag{5.198}$$

CASE 3: $u_{min} < u < u_{max}$. This case occurs when u is between the upper and lower constraint values. Hence, $\mu_1 = \mu_2 = 0$ because both constraints are inactive. $l_{u1} = \sqrt{20 - u}$ to satisfy Eq. (5.147) and $l_{u2} = \sqrt{20 + u}$ to satisfy Eq. (5.148). Examining Eq. (5.195) to determine the value of u yields

$$\lambda_\alpha = 0. \tag{5.199}$$

The necessary condition is satisfied when λ_α is zero. An expression for u is not contained in the optimality condition. However, since H_{uu} is singular, the extremal arc for $\lambda_\alpha = 0$ is called a singular arc (2:246). It is still possible to determine an expression for u for some finite time interval that satisfies the optimality condition. The time rate of change of the optimality condition must remain zero along the

singular arc (2:252). Hence,

$$\frac{d}{dt}(H_u) = \dot{\lambda}_\alpha C_\alpha \tag{5.200}$$

$$= C_\alpha \left[\lambda_V \frac{g}{W} T \sin\alpha - \lambda_\gamma \left(\frac{g}{VW} T \cos\alpha\right) \Sigma + \lambda_\alpha C_\alpha \left(\frac{T}{W} \cos\alpha\right) \Sigma\right] \tag{5.201}$$

$$= 0. \tag{5.202}$$

This expression still does not contain the control, so the second time derivative of H_u must be zero. The differential equations for the system can be expressed as

$$\dot{\boldsymbol{x}} = \boldsymbol{f}(\boldsymbol{x}) + \bar{\boldsymbol{g}}(\boldsymbol{x}) u \tag{5.203}$$

where

$$\boldsymbol{f} \equiv \begin{bmatrix} V\cos\gamma \\ V\sin\gamma \\ \frac{g}{W}(T\cos\alpha - D) - g\sin\gamma \\ \frac{g}{VW}(T\sin\alpha + L)\Sigma - \frac{g}{V}\cos\gamma \\ -\frac{C_\alpha}{W}(T\sin\alpha + L)\Sigma \\ -\dot{w}_f \end{bmatrix} \tag{5.204}$$

$$\bar{\boldsymbol{g}} \equiv \begin{bmatrix} 0 \\ 0 \\ 0 \\ 0 \\ C_\alpha \\ 0 \end{bmatrix}. \tag{5.205}$$

Note that Eq. (5.200) can be expressed as

$$\frac{d}{dt}(H_u) = \boldsymbol{\lambda}^T (\bar{\boldsymbol{g}}_x \boldsymbol{f} - \boldsymbol{f}_x \boldsymbol{g})$$

$$= \boldsymbol{\lambda}^T \boldsymbol{q} \tag{5.206}$$

where

$$
\begin{aligned}
\boldsymbol{q} &\equiv \bar{\boldsymbol{g}}_x \boldsymbol{f} - \boldsymbol{f}_x \boldsymbol{g} \\
&= \begin{bmatrix} 0 \\ 0 \\ C_\alpha \frac{g}{W} T \sin\alpha \\ -C_\alpha \frac{g}{VW} T \cos\alpha \Sigma \\ C_\alpha^2 \frac{T}{W} \cos\alpha \Sigma \\ 0 \end{bmatrix} u. \qquad (5.207)
\end{aligned}
$$

With the above definitions for $\boldsymbol{f}$, $\bar{\boldsymbol{g}}$, and $\boldsymbol{q}$, the second time derivative of H_u can be expressed as

$$
\begin{aligned}
\frac{d^2}{dt^2}(H_u) &= \boldsymbol{\lambda}^T \dot{\boldsymbol{q}} + \dot{\boldsymbol{\lambda}}^T \boldsymbol{q} && (5.208) \\
&= \boldsymbol{\lambda}^T \boldsymbol{q}_x (\boldsymbol{f} + \bar{\boldsymbol{g}} u) - \boldsymbol{\lambda}^T (\boldsymbol{f}_x + \bar{\boldsymbol{g}}_x u) \boldsymbol{q} && (5.209) \\
&= \boldsymbol{\lambda}^T (\boldsymbol{q}_x \boldsymbol{f} - \boldsymbol{f}_x \boldsymbol{q}) + \boldsymbol{\lambda}^T (\boldsymbol{q}_x \bar{\boldsymbol{g}} - \bar{\boldsymbol{g}}_x \boldsymbol{q}) u && (5.210) \\
&= 0 && (5.211)
\end{aligned}
$$

Noting that

$$
\bar{\boldsymbol{g}}_x = \boldsymbol{0} \qquad (5.212)
$$

$$
\boldsymbol{f} = \dot{\boldsymbol{x}} - \bar{\boldsymbol{g}} u \qquad (5.213)
$$

and recalling that λ_α is identically zero for the singular arc, an expression for u is

$$
\begin{aligned}
u &= -\frac{\boldsymbol{\lambda}^T (\boldsymbol{q}_x \boldsymbol{f} - \boldsymbol{f}_x \boldsymbol{q})}{\boldsymbol{\lambda}^T (\boldsymbol{g}_x \bar{\boldsymbol{g}})} && (5.214) \\
&= \frac{\lambda_x A + \lambda_h B - \lambda_V C - \lambda_\gamma D}{\lambda_V E + \lambda_\gamma F} && (5.215)
\end{aligned}
$$

where

$$
\begin{aligned}
A &= C_\alpha \frac{g}{W} T \left(\sin\alpha\cos\gamma + \cos\alpha\sin\gamma\Sigma\right) \\
B &= C_\alpha \frac{g}{W} T \left(\sin\alpha\sin\gamma - \cos\alpha\cos\gamma\Sigma\right) \\
C &= C_\alpha \frac{g}{W} T \left[-\frac{C_\alpha}{W}\left(T\sin\alpha + L\right)\cos\alpha\Sigma + \frac{\dot{w}_f}{W}\sin\alpha + \frac{2Dg}{VW}\sin\alpha \right. \\
&\quad \left. -\frac{g}{V}\cos\alpha\Sigma + C_\alpha\frac{T}{W}\sin\alpha\cos\alpha\Sigma\right] \\
D &= C_\alpha \frac{g}{VW}\left[\frac{g}{VW}\left(T\cos\alpha - D\right)^2\Sigma - \frac{g}{V}T\cos\alpha\sin\gamma\Sigma \right. \\
&\quad -\frac{C_\alpha}{W}T\left(T\sin\alpha + L\right)\sin\alpha - \frac{T}{W}\dot{w}_f\cos\alpha\Sigma + \frac{g}{VW}T\left(T\sin\alpha + L\right)\sin\alpha\Sigma \\
&\quad \left. -\frac{2g}{VW}LT\sin\alpha\Sigma - \frac{g}{V}T\sin\alpha\cos\gamma + \frac{g}{V}T\cos\alpha\cos\gamma\Sigma - \frac{C_\alpha}{W}T^2\cos^2\alpha\right] \\
E &= C_\alpha^2\frac{g}{W}T\cos\alpha \\
F &= C_\alpha^2\frac{g}{VW}T\sin\alpha\Sigma
\end{aligned}
$$

Having determined u for all three cases, the two-dimensional pursuit is now formulated in such a matter that the shooting method previously discussed can be used to find the optimal trajectory.

VI. Conclusions and Recommendation

The simulation was successfully recreated in MATLAB^{TM}. Errors discovered in ENGAGE were analyzed to determine the impact of the errors. The recreated simulation will permit future numerical analysis of the missile's performance. The necessary and sufficient conditions for an extremal solution to the free final time optimal control problem were presented. The shooting method was developed to provide a numerical solution to the optimal control problem posed as a two-point boundary-value problem. An example problem of a lunar lift off was formulated as a two-point boundary-value problem and then numerically solved via the shooting method. The necessary conditions for an extremal solution were applied to the three-dimensional pursuit. The vertical plane intercept scenario was determined to be an interesting case. Therefore, the two-dimensional intercept was analyzed and a two-point boundary-value problem was formulated to determine the optimal trajectory for a minimum time target intercept.

Future efforts in this project should be directed towards numerically solving the two-dimensional pursuit to analyze the behavior of the optimal loft command for various initial conditions. Efforts should then expand the problem to the three-dimensional pursuit to develop an expression for the loft control which approximates the optimal loft control.

Bibliography

1. "U.S. Standard Atmosphere, 1962." Prepared under sponsorship of NASA, USAF, and United States Weather Bureau, Dec 1962.
2. Arthur E. Bryson, Jr. and Yu-Chi Ho. *Applied Optimal Control.* New York: Hemisphere Publishing Corporation, 1975.
3. Blakelock, John H. *Automatic Control of Aircraft and Missiles.* New York: John Wiley and Sons, 1991.
4. Hill, Philip and Carl Peterson. *Mechanics and Thermodynamics of Propulsion.* Reading, Massachusetts: Addison-Wesley Publishing Company, 1992.
5. Hull, David G., "Optimal Control." Course Notes,University of Texas.
6. Paris, S. W. and others. "Application of on Advanced Trajectory Optimization Method to RAMJET Propelled Missiles," *Optimal Control Applications and Methods*, *1*:319–334 (July 1980).
7. Reid, J. Gary. *Linear System Fundamentals.* New York: McGraw Hill, 1983.
8. Shevell, Richard S. *Fundamentals of Flight.* New York: Prentice Hall, Inc., 1983.
9. Summerfield, Martin. "Test and Evaluation of the Tactical Missile." *Progress in Astronautics and Aeronautics 119*, edited by Jr. Emil J. Eichblatt, Washington DC: AIAA, 1989.
10. Watson, Kenneth A. "ENGAGE:Simulation Overview." WL/POPA.
11. Zucrow, M. J. *Aircraft and Missile Propulsion.* New York: John Wiley and Sons, 1958.

Vita

Capt Timothy Zadzora was born in Philadelphia, Pennsylvania on 26 April 1967. He graduated from Holy Ghost Preparatory School in Bensalem, Pennsylvania in 1985. He attended Lehigh University and received a Bachelor of Science in Mechanical Engineering in June 1989. He received his United States Air Force commission on 3 June 1989 and entered active duty 15 September 1989 as an engineer in support of Intercontinental Ballistic Missile (ICBM) depot maintenance at Hill Air Force Base (AFB), Utah. Capt Zadzora then served as a project engineer for the ICBM System Program Office at Hill AFB. He received a Master of Science in Aeronautical Engineering from the Air Force Institute of Technology (AFIT) on 13 December 1994. Capt Zadzora was subsequently assigned to Wright Laboratories at Wright-Patterson AFB, Ohio.

Permanent address: 7758 Clyo Road
Centerville, Ohio 45459

REPORT DOCUMENTATION PAGE

Form Approved
OMB No. 0704-0188

Public reporting burden for this collection of information is estimated to average 1 hour per response, including the time for reviewing instructions, searching existing data sources, gathering and maintaining the data needed, and completing and reviewing the collection of information. Send comments regarding this burden estimate or any other aspect of this collection of information, including suggestions for reducing this burden, to Washington Headquarters Services, Directorate for Information Operations and Reports, 1215 Jefferson Davis Highway, Suite 1204, Arlington, VA 22202-4302, and to the Office of Management and Budget, Paperwork Reduction Project (0704-0188), Washington, DC 20503.

1. AGENCY USE ONLY *(Leave blank)*

2. REPORT DATE
December 1994

3. REPORT TYPE AND DATES COVERED
Master's Thesis

4. TITLE AND SUBTITLE
FORMULATION OF THE OPTIMAL TRAJECTORY FOR AN AIR-BREATHING MEDIUM RANGE AIR-TO-AIR MISSILE

5. FUNDING NUMBERS

6. AUTHOR(S)
Timothy Zadzora
Capt, USAF

7. PERFORMING ORGANIZATION NAME(S) AND ADDRESS(ES)
Air Force Institute of Technology
Wright-Patterson AFB OH 45433-6583

8. PERFORMING ORGANIZATION REPORT NUMBER
AFIT/GA/ENY/94D-23

9. SPONSORING / MONITORING AGENCY NAME(S) AND ADDRESS(ES)
Lt Col Russell Barbero
ASC/YA
Eglin AFB, FL 32542

10. SPONSORING / MONITORING AGENCY REPORT NUMBER

11. SUPPLEMENTARY NOTES

12a. DISTRIBUTION / AVAILABILITY STATEMENT
Approved for public release; distribution unlimited

12b. DISTRIBUTION CODE

13. ABSTRACT *(Maximum 200 words)*
The Air Breathing Medium Range Air-to-Air Missile (ABMRAAM) represents developmental technology which incorporates both a rocket engine and a RAMJET engine. Such a missile uses proportional navigation guidance plus an additional trajectory loft command. This thesis examines the optimal trajectory, and hence the optimal lofting command, for an ABMRAAM. A numerical simulation of the missile is presented and the necessary conditions for the optimal trajectory are derived. From these conditions, the problem can be numerically solved for the optimal loft command.

14. SUBJECT TERMS
Trajectory Optimization, Optimal Control,
Guided Missile, Hooting Method

15. NUMBER OF PAGES
105

16. PRICE CODE

17. SECURITY CLASSIFICATION OF REPORT
UNCLASSIFIED

18. SECURITY CLASSIFICATION OF THIS PAGE
UNCLASSIFIED

19. SECURITY CLASSIFICATION OF ABSTRACT
UNCLASSIFIED

20. LIMITATION OF ABSTRACT
UL